



# UNIVERSITA' DEGLI STUDI DI PADOVA

Sede Amministrativa: Università degli Studi di Padova

Dipartimento di Ingegneria Idraulica, Marittima, Ambientale e Geotecnica

SCUOLA DI DOTTORATO DI RICERCA IN SCIENZE DELL'INGEGNERIA  
CIVILE E AMBIENTALE  
INDIRIZZO: INGEGNERIA PER L'AMBIENTE E IL TERRITORIO  
CICLO XX

## LOCAL SCOURING AT BED SILLS UNDER STEADY AND UNSTEADY CONDITIONS

**Direttore della Scuola :** Ch.mo Prof. Andrea Rinaldo

**Supervisori :** Ch.mo Prof. Andrea Marion

Ch.mo Prof. Giampaolo Di Silvlio

**Dottorando :** Matteo Tregnaghi

DATA CONSEGNA TESI  
31 gennaio 2008



---

## **Abstract**

Designers are often required to produce safe and economic structures in rivers with erodible beds, which may frequently induce scouring phenomena as they interfere with the natural stream. In CHAPTER 1, an extensive literature is illustrated on scouring by jets at high and low head structures, and predictive formulae are discussed that estimate the equilibrium scour depth of the scour hole, which are most obtained empirically from field and laboratory data. It is also discussed that different stages occur during local scour development. These stages basically include an initial rapid phase of severe scouring, followed by a stabilization phase approaching equilibrium conditions after a long time.

CHAPTER 2 describes the theoretical basis to deal with long-term local scouring at bed sills under clear-water and steady-flow conditions. In gravel bed rivers, bed sills are used to limit bed degradation. Local scouring takes place downstream of each sill in addition to the general erosion pattern, and scour hole dimensions increase with the distance between sills. While overall aggradation can be estimated by using 1D morphological models, local scouring requires a more empirical approach. In fact most scouring phenomena are induced by turbulent jets that diffuse within the scour hole, by resulting in extremely complex flow fields. Many approaches are fully empirical, being based on curve fitting of experimental data that link scour depth to hydraulic quantities and sediment properties. In the most recent attempts, a semi-empirical approach has been followed, based on the identification of appropriate dimensionless groups using dimensional analysis before employing best-fitting procedures. The theoretical derivations proposed, which are based on the assumptions of the Buckingham's  $\pi$ -theorem, are discussed by showing some further insights on the nature and role of the dimensionless parameters that ensued from dimensional analysis.

CHAPTER 3 presents the results of experimental tests carried out by the author in 2003 about the pattern of local scouring generated at the toe of bed sills. The aim of this study is to evaluate the effect of upstream sediment supply on the scour depth and shape. The experiments simulated conditions of a steady upstream sediment supply which had the same grain size composition as the sediment deposit placed on the bed of the flume. The geometric characteristics of three scour holes developed under

---

conditions of steady-flow discharge and steady upstream sediment supply were measured during 48 different tests. It is shown that the imposed sediment transport does not require the introduction of new dimensionless parameters into existing scour depth and length prediction formulae. The effects of sediment feed are shown to be incorporated in the existing dimensionless parameters. The new data set is used to recalibrate existing scour depth formula. The influence of jet erosion on scour geometry is also discussed.

Most research efforts have focused on predicting scour depth, which may affect the structure at the free overfall, as opposed to volumetric scour dimensions and sediment yield contribution due to local scour, which may affect downstream morphology and water quality as well as the structure but are much more difficult to measure in an actively eroding plunge pool. In CHAPTER 4, shape and volume of equilibrium local scour holes at bed sills in high-gradient streams are investigated by analyzing steady-flow scour profiles at the equilibrium stage. Geometric properties of the scour profile are analytically discussed and verified on the basis of new data from experimental tests described in CHAPTER 3 and data from literature. A model is presented to organize data analysis into a conceptual frame, which is based on the formal relationships for scour depth and length ensued from dimensional analysis, and on the assumption that scours exhibit definite geometric properties. Results show evidence of a universal geometric affinity of the scour. Geometric similarity is also found to occur, but only in a limited range of physical conditions. Prediction formulae are proposed which link the eroded volume to the geometric, hydraulic and sediment properties. Evidence on the scaling nature of the scour hole shapes have important implications on the prediction of the eroded volume. In turn, a correct evaluation of the eroded volume is necessary for the optimization of the design of the inter-sill distance.

The temporal development of clear-water local scour depth at bed sills in uniform gravel beds is considered in CHAPTER 5. A new experimental program has been carried out by the author, which started at the end of 2006 and was concluded in March 2007 at the Fluid Dynamics Laboratory of The University of Auckland (NZ). Experiments are presented on the development of scour holes under unsteady hydraulic conditions, with the triangular-shaped hydrographs tested being of different durations and different rates of flow variation. Preliminary observations are discussed on the

---

behavior of scour development, which is compared with the scour evolution for the steady-state case. Based on the experimental results and a theoretical framework, a method is given for the definition and prediction of the scouring process under unsteady flows in terms of a dimensionless temporal parameter. A “flash flood” is defined as an event for which the scour doesn’t attain its potential magnitude, i.e. the equilibrium value for the peak hydrograph flow rate. It is shown that this flood nature is dependent on both the characteristics of the flood event itself and the characteristics of the stream. A quantitative measure of what constitutes a flash flood is given in terms of the identified temporal parameter, which represents one of the main goal of this study.

---

---

## Sommario

Agli ingegneri idraulici viene spesso richiesto di progettare strutture sicure ed economiche in corsi d'acqua caratterizzati da letti di sedimenti, frequentemente soggetti a fenomeni di erosione localizzata per la presenza delle opere stesse che interferiscono con il flusso naturale. Nel CAPITOLO 1 viene proposta un'ampia letteratura sul fenomeno di erosione localizzata prodotto da getti bidimensionali verticali ed orizzontali. Numerose formule di previsione sono discusse, le quali permettono una stima della profondità massima di scavo in condizioni di equilibrio, e sono ottenute da indagini sperimentali con dati di campo e di laboratorio. Sono inoltre descritte le differenti fasi che si presentano durante lo sviluppo dello scavo. In generale, è possibile osservare un intenso fenomeno erosivo iniziale, seguito da un più lento processo di stabilizzazione che raggiunge una condizione finale di equilibrio dopo tempi molto lunghi rispetto alla fase iniziale.

Il CAPITOLO 2 descrive l'analisi teorica dell'erosione localizzata a valle di soglie di fondo all'equilibrio, in condizioni di acqua chiara e in regime di moto stazionario. Nei corsi d'acqua naturali, sequenze di soglie di fondo vengono utilizzate per limitare l'abbassamento generale dell'alveo fluviale. Un fenomeno erosivo localizzato si verifica a valle di ciascuna soglia e le dimensioni dello scavo crescono con l'aumentare dell'interasse tra le soglie. In generale, l'abbassamento dell'alveo può essere stimato usando modelli morfologici 1D, mentre lo scavo localizzato richiede un approccio prevalentemente empirico. In effetti, la maggior parte dei fenomeni erosivi sono indotti da getti turbolenti che originano campi di moto estremamente complessi. Molti studi presenti in letteratura presentano metodi completamente empirici, basati su curve di dati sperimentali che legano la profondità di scavo ad alcune delle grandezze idrauliche più significative ed alle proprietà dei sedimenti. Recentemente, è stato proposto un metodo semi-empirico, basato sull'identificazione di opportuni gruppi adimensionali. Le derivazioni teoriche proposte sono discusse mostrando alcune ulteriori chiarimenti sulla natura e sul ruolo di tali parametri.

Il CAPITOLO 3 presenta i risultati di prove sperimentali condotte dall'autore nel 2003 riguardanti l'erosione localizzata a valle di soglie di fondo. Lo scopo di questo studio è valutare l'effetto del trasporto solido (condizioni "sediment-supply") sulla

---

profondità e sulla forma dello scavo. Gli esperimenti sono stati svolti imponendo un'alimentazione costante di sedimenti a monte, avente la stessa composizione granulometrica del letto disposto lungo la canaletta. Le caratteristiche geometriche di tre scavi in sequenza sono state misurate durante 48 differenti test in regime di moto stazionario e con diverse condizioni di trasporto solido. I risultati mostrano che la previsione dello scavo massimo in condizioni di trasporto solido non richiede l'introduzione di nuovi parametri adimensionali nelle formule esistenti per la stima della profondità e della lunghezza di scavo. Il nuovo set di dati è usato per la taratura della formula di previsione. Inoltre viene discusso l'effetto dell'inclinazione del getto sulla geometria dello scavo.

La maggior parte dei lavori presenti in letteratura tratta il problema di stimare la massima profondità di scavo, al fine di proteggere lo scalzamento al piede dell'opera, mentre pochi studi riguardano le dimensioni volumetriche dello scavo. Queste risultano importanti se si desidera valutare l'apporto di sedimenti verso valle, che ha effetti sia sulla qualità dell'acqua sia sulla morfologia del fiume. Nel CAPITOLO 4, sono studiati la forma ed il volume di scavo a valle di soglie di fondo, analizzando i profili di scavo nella fase di equilibrio. Le proprietà geometriche del profilo sono discusse analiticamente e verificate in base sia ai dati delle prove di laboratorio descritte nel CAPITOLO 3 sia a dati di letteratura. Viene presentato un modello concettuale per l'analisi dei dati sperimentali, che è basato sulle relazioni adimensionali che legano profondità e lunghezza di scavo alle grandezze idrauliche e sedimentologiche, e sull'ipotesi che gli scavi presentino particolari proprietà geometriche. I risultati mostrano che l'affinità geometrica è una proprietà universale dei profili di scavo. La similarità geometrica risulta essere verificata soltanto in un range limitato di condizioni fisiche. Sono quindi proposte formule di previsione che legano il volume eroso alle caratteristiche geometriche e idrauliche del corso d'acqua ed alle proprietà dei sedimenti. Una valutazione corretta del volume eroso è necessaria per l'ottimizzazione della progettazione di sequenze di soglie di fondo, in cui l'unico grado di libertà è rappresentato dall'interesse tra le opere.

Lo sviluppo temporale della profondità di scavo in condizioni stazionarie e non stazionarie viene esaminato nel CAPITOLO 5. Un nuovo studio sperimentale è stato condotto dall'autore tra ottobre 2006 e marzo 2007 presso il Laboratorio di



---

Fluidodinamica dell'Università di Auckland (NZ). Gli esperimenti sono stati svolti simulando degli eventi di piena con idrogrammi di forma triangolare, variando di volta in volta la durata dell'idrogramma o la portata massima della piena. Alcune osservazioni preliminari riguardano l'andamento temporale dello sviluppo dello scavo, che viene confrontato con i risultati presenti in letteratura per il caso stazionario. Sulla base dei risultati sperimentali e dell'analisi dimensionale, viene descritto un metodo per la previsione dello scavo in regime non stazionario. Un evento "flash flood" è definito come un'onda di piena durante la quale lo scavo non raggiunge le sue dimensioni potenziali, corrispondenti al valore di equilibrio relativo alla portata di picco. In termini quantitativi, si verifica che tale definizione dipende sia dalle caratteristiche dell'evento di piena stesso sia dalle caratteristiche morfologiche del tratto di corso d'acqua. In particolare, uno degli obiettivi principali di questo studio è stato quello di fornire una misura quantitativa di cosa costituisce un evento "flash flood" in termini di un particolare parametro temporale.

---

---

<b>ABSTRACT</b>	<b>1</b>
<b>SOMMARIO</b>	<b>5</b>
<b>CHAPTER 1</b>	
<b>SCOURING AT HYDRAULIC STRUCTURES</b>	<b>13</b>
1.1 Introduction	13
1.2 General Erosion	13
1.2.1 Overall degradation	14
1.2.2 Constrictions, bends and confluences	14
1.3 Local Scouring	15
1.3.1 Scour downstream of horizontal sills	17
1.3.2 Scour due to horizontal jets	18
1.3.3 Scour due to plunging jets	23
1.3.4 Scour at abutments	28
1.3.5 Scour at bridge piers	30
1.4 Tools to Approach Local Scouring	34
1.4.1 Jet diffusion and Particle stability	35
1.4.2 Dimensional analysis	40
1.4.3 The Buckingham's $\pi$ -theorem	42
1.4.4 Self-similarity theory	45
<b>CHAPTER 2</b>	
<b>LOCAL SCOURING DOWNSTREAM OF BED SILLS</b>	<b>49</b>
2.1 Introduction	49
2.2 Grade-Control Structures	50
2.3 Maximum Scour Depth Downstream of Bed Sills	53
2.3.1 Physical definition of scouring	53
2.3.2 Dimensional approach	56
2.3.3 Froude number and jet inclination	59
2.4 Effect of Sill Spacing and Sediment Size Grading	61
2.4.1 Geometrical interference	61
2.4.2 Non-uniform sediments	67
2.4.3 Analogy between bed sills and step-and-pools	71
2.5 Similarity of Scouring in Time	73
<b>CHAPTER 3</b>	
<b>SEDIMENT SUPPLY EFFECT ON LOCAL SCOURS</b>	<b>77</b>
3.1 Summary	77
3.2 Clear-Water and Sediment-Supply Conditions	78
3.2.1 Prediction of clear-water scour depth	78

---

3.2.2	Influence of sediment supply	80
<b>3.3</b>	<b>Experimental Set-up and Procedure</b>	<b>82</b>
<b>3.4</b>	<b>Analysis of Experimental Results</b>	<b>86</b>
3.4.1	Maximum scour depth	86
3.4.2	Scour hole length	91
<b>3.5</b>	<b>Discussion</b>	<b>93</b>
3.5.1	Effect of jet inclination	93
3.5.2	Scour hole shape	95
<b>3.6</b>	<b>Conclusions</b>	<b>96</b>
<b>CHAPTER 4</b>		
<b>AFFINITY AND SIMILARITY OF SCOUR HOLES</b>		<b>99</b>
<b>4.1</b>	<b>Summary</b>	<b>99</b>
<b>4.2</b>	<b>Scour Shape and Volume</b>	<b>100</b>
<b>4.3</b>	<b>Theoretical Framework</b>	<b>102</b>
4.3.1	Similarity and affinity of scour hole profiles with uniform sediments	102
4.3.2	Similarity and affinity of scour hole profiles with non-uniform sediments	107
<b>4.4</b>	<b>Experiments and Results</b>	<b>109</b>
4.4.1	Laboratory data	109
4.4.2	Affinity of scour hole profiles	110
4.4.3	Similarity of scour hole profiles	111
<b>4.5</b>	<b>Discussion</b>	<b>115</b>
4.5.1	The physical process determining the scour shape	115
4.5.2	The effect of armoring on scour hole reduction	117
4.5.3	Choice of the distance between structures	118
<b>4.6</b>	<b>Conclusions</b>	<b>120</b>
<b>4.7</b>	<b>Appendix: non-uniform sediment formulation</b>	<b>121</b>
<b>CHAPTER 5</b>		
<b>SCOURING UNDER UNSTEADY FLOW: THE CASE OF FLASH FLOOD</b>		<b>123</b>
<b>5.1</b>	<b>Summary</b>	<b>123</b>
<b>5.2</b>	<b>Scouring, Time Evolution and Unsteady Flows</b>	<b>124</b>
<b>5.3</b>	<b>Methods and Settings</b>	<b>127</b>
<b>5.4</b>	<b>Results</b>	<b>130</b>
5.4.1	Steady flow tests	130
5.4.2	Scaling of time and scour depth for unsteady flows	132
5.4.3	Scour evolution for unsteady flows	134
<b>5.5</b>	<b>Hydrological and Morphological Time Scales</b>	<b>135</b>
5.5.1	A revised dimensional analysis	135

---

5.5.2	Statistical analysis of data	137
<b>5.6</b>	<b>Application to a case study</b>	<b>141</b>
<b>5.7</b>	<b>Conclusions</b>	<b>143</b>
	<b>NOTATIONS</b>	<b>145</b>
	<b>REFERENCES</b>	<b>151</b>

---

## **CHAPTER 1 SCOURING AT HYDRAULIC STRUCTURES**

### **1.1 INTRODUCTION**

Hydraulic structures that obstruct the flow pattern in the vicinity of the structure may cause local erosion or scour. Changes in flow characteristics (velocities or turbulence) lead to changes in the local sediment transport capacity and hence to a local disequilibrium between actual sediment transport and the capacity of the flow to transport sediment. A new equilibrium may eventually be reached as hydraulic conditions are adjusted. Scour which may occur at a structure can be divided into general scour and local scour. These possible processes have different length and time scales. As a first approximation, the scour caused by each process separately may be added linearly to obtain the resulting scour. In addition, scouring in different conditions of sediment transport can be distinguished. In general the time scale for local scour is relatively short. However, the time-dependent scour process in prototype situations may be significant.

### **1.2 GENERAL EROSION**

The time scale for general scour is generally longer than the time scale for local scour. Commonly occurring examples of general scour are the long term change in the bed level of a river, scour due to constriction, scour in a bend or scour at a confluence.

### 1.2.1 Overall degradation

Overall degradation results from modification to the stable regime conditions to which a river has become adjusted. This may be the effect of change in water or sediment flows in a river, resulting either from human interference or natural changes. Artificial interventions include flood embankment, dams for hydropower generation or flood attenuation, dredging, gravel or sand mining for industrial usage, meander cut-offs or bed canalization to make river waters navigable. Such modifications reduce the sediment yield to the downstream reaches, by resulting in increase of the sediment transport capacity of the flow. Sediments are entrained from the river bed and degradation occur until bed slope is reduced to achieve morphological conditions that equilibrate the modified capacity of the flow to transport sediments. The consequence of overall degradation at, for example, a bridge site will be the lowering of bed level, which may place the foundations at great risk. The process can affect a long reach of a river, extending over kilometers and over periods of many years [De Vries, 1975]. Commonly such process can be mitigate using a sequence of bed sills, which will be described in the next chapters. For some conditions, information on possible river bed changes can be obtained from 1D morphological models. Besides mathematical models of various degree of sophistication, some analytical models which provide insight into the nature of morphological processes are also available. More information concerning the prediction of morphological changes in rivers due to natural causes or human interferences can be found in *Julien* [1998].

### 1.2.2 Constrictions, bends and confluences

Constriction scour occurs in confined cross-sections of a river and results in lowering of the bed level across the width of the river. Bend scour depends on local parameters (bend curvature, flow depth and grain size) and upstream conditions (flow and sediment transport redistribution). In the outer part of bends excess scour occurs as a result of spiral flows. Scour downstream of a confluence is mainly related to the sediment properties, the average flow depth of the two branches and the angle between the two upstream branches. More information concerning the prediction of scouring at these locations can be found in the specific literature on this topic [*Struiksmā et al.*, 1985; *Breusers and Raudkivi*, 1991].



### 1.3 LOCAL SCOURING

Local scouring results directly from the impact of the structure on the flow. Physical model testing and prototype experience have permitted the development of methods for predicting and preventing scour at different types of structures. Information with respect to scour can be obtained by testing physical models and this approach may be particularly appropriate for unusual structures not covered by existing formulae or for field measurements of scour at existing structures. A basic feature of scour holes is the generation of a mixing layer. A mixing layer occurs between two streams that move at different speeds in the same general direction. Such a surface of discontinuity in the flow is unstable if the Reynolds number is large enough, and give rise to a zone of turbulent mixing downstream of the point where the two streams meet. According to *Breusers* [1967], the development of the scour process depends on the flow velocity and turbulence intensity at the transition between the fixed and the erodible bed. By applying this concept, the scour prediction can be restricted to one computation; no information is needed concerning the near bed velocities and bed turbulence in the scour hole.

When dealing with local scour problems, often only the maximum scour depth in the equilibrium phase is relevant. This is especially true for isolated structures such as bridge piers, spur dikes, abutments and other permanent structures (sills, weirs, final closure works). However, there are cases in which the time factor is important particularly. From model tests on different scales and with different bed materials, relationships were derived between the time scale and the scales for velocity, flow depth, and material density [*Breusers*, 1967; *Van der Meulen and Vinjé*, 1975]. The main conclusions were that the shape of the scour hole is independent of bed material and flow velocity. The scour process as function of time can be given with reasonable accuracy, provided the prediction of the equilibrium scour depth is satisfactory:

$$\frac{y_s(t)}{y_s} = 1 - \exp \left[ \ln \left( 1 - \frac{y_\xi}{y_s} \right) \cdot \left( \frac{t}{t_\xi} \right)^\xi \right] \quad (1.1)$$

where  $y_s(t)$  is the maximum scour depth at the time  $t$ ;  $y_s$  the maximum scour depth at the equilibrium stage;  $y_\xi$  a characteristic length scale;  $t_\xi$  the characteristic time at which  $y_s(t) = y_\xi$ ;  $\xi$  a calibration coefficient. In the development phase (i.e. when  $t < t_\xi$ ) Eq. (1.1) can be approximated with the scour relation originally given by *Breusers* [1967]:

$$\frac{y_s(t)}{y_\xi} = \left( \frac{t}{t_\xi} \right)^\xi \quad (1.2)$$

Values of  $\xi$  range from 0.2 to 0.4 for two-dimensional flows. Many definitions of characteristic length scales can be found in the literature including, for example, the Kolmogorov length scale which represents the micro-turbulent eddies. The size of these eddies is in the range of 0.1 to 1 mm. The largest eddies play an important part in any turbulent flow. In shallow water conditions, the size of the largest eddies is in the order of the flow depth dimension, which can be used as the characteristic length scale  $y_\xi$ . For deep water conditions the dimensions of these macro-turbulent eddies are nearly equal to those of the hydraulic structure (e.g. bridge pier width).

Depending on the structure affected by scouring, at least three phases can be distinguished in the evolution of a scour hole: a development phase, in which the erosion capacity is most severe and the scour depth increases considerably; a stabilization phase, in which the rate of development of the maximum scour depth decreases and the dimensions of the scour hole increase more in the longitudinal direction than in the vertical direction; an equilibrium phase, in which the dimensions of the scour hole do no longer change significantly.

Scouring is affected by conditions of transport. Clear-water scour occurs when no upstream sediment is present, that is when the bed material in the natural flow upstream of the scour hole is at rest or when the bed upstream of the scour hole is fixed. If the scour is caused by flow that is not transporting sediment (bed load and suspended load), the depth of scour should approach a limit asymptotically. Live-bed scour is characterized by sediment transport over the upstream undisturbed bed. Sediment particles which are continuously transported by the flow enter the scour hole. In such cases, the equilibrium scour depth is smaller than that in clear-water conditions. In general, for the live-bed case, the scour increases rapidly with time and then fluctuates

about a mean value in response to the bed features which are being passed (see Figure 1.1).

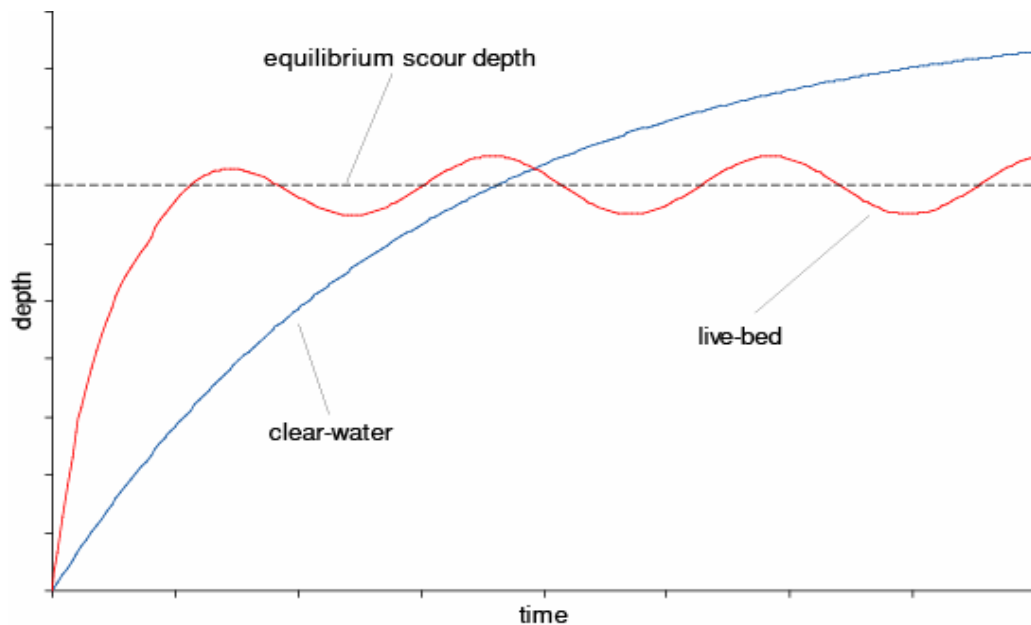
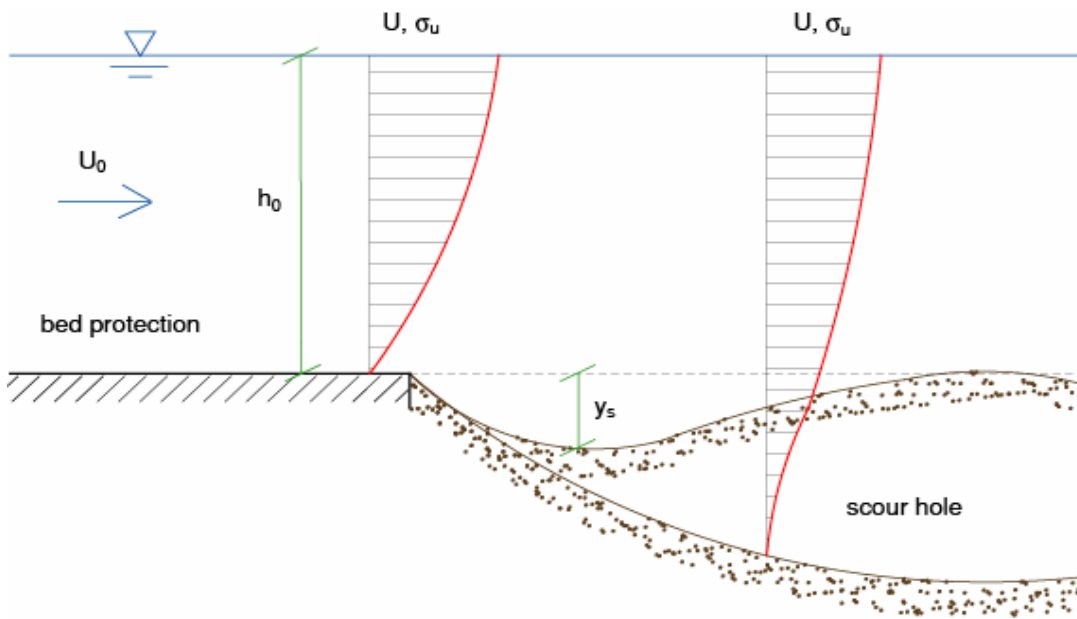


Figure 1.1 - Schematic of the scour development with time in clear-water and live-bed conditions.

### 1.3.1 Scour downstream of horizontal sills

In an estuary or a river, a sill may be the initial foundation or the lower part of a structure that has to be constructed on a bed of alluvial material. Sometimes a sill is used to reduce the mixing of different types of water in an estuary. In rivers, for example, a sill may be used as part of a scheme to maintain a minimum water level. The bed in the direct neighborhood of hydraulic structures is generally protected against current, waves and eddies (see Figure 1.2). The length of the bed protection depends on the permissible maximum scour depth and the geotechnical conditions of the soil involved. When the length of the bed protection increases, the scour process is less intense due to the decay of turbulence energy and the adaptation of the velocity profile downstream of the hydraulic structure.

Based on an extensive analysis of the measured bed levels at which the maximum scour depth was about half of the flow depth, *Breusers* [1967] reported that for two-dimensional scours the averaged value of the coefficient  $\gamma$  amounted to 0.38. For small scour depths the exponential function given by Eq. (1.2) gave a good fit if  $\xi$  values



**Figure 1.2 - Scour hole downstream of a horizontal sill.**

larger than 0.38 were used. To obtain equilibrium conditions, a relatively long period of time is needed, especially for experiments with no upstream sediment supply (clear-water scour). The equilibrium scour depth was approximated by the following expression:

$$\frac{y_s}{h_0} = \frac{\omega U_0 - U_c}{U_c} \quad (1.3)$$

where  $U_0$  and  $U_c$  are the mean flow velocity and the critical flow velocity, respectively;  $h_0$  the undisturbed flow depth;  $\omega = (1+3\sigma_u/U_0)$  a coefficient taking into account the relative turbulence intensity, being  $\sigma_u$  the standard deviation of the vertical distribution of velocities.

### 1.3.2 Scour due to horizontal jets

The study of scour downstream of hydraulic structures such as large dams, stilling basins, diversion works, underflow gates, and culverts constitutes an important field of research due to its frequent occurrence in engineering applications. The flows over and through these structures often occur in the form of jets. In general, a jet lifts the sediment particles and transports those particles downstream of the impacted area. The jet impact area is transformed into an energy dissipator and a scour hole is formed.

Several forms of jets can be found in literature including plunging jets, submerged jets, horizontal and vertical jets, and two- and three-dimensional jets. A literature review of empirical relations is given by *Whittaker and Schleiss* [1984], *Mason and Arumugam* [1985], *Breusers and Raudkivi* [1991]. To date, however, no universal scour formula is capable of handling the different flows downstream of hydraulic structures, since the erosion process is quite complex and depends upon the interaction of hydraulic and morphological factors.

Horizontal two-dimensional flows are considered to be flows under barriers or gates that are wide compared to the jet thickness. The flows in these cases are two-dimensional along the width of the barrier and usually have a considerable potential for scour. Downstream of spillways the flow is generally supercritical and is followed by a hydraulic jump in the energy dissipator with baffle blocks and possibly dentate sills, and is subcritical at the end of this section. The form of the scour depends on a number of factors, such as the submergence and the degree of dissipation of the jet energy. Several researchers have investigated the scour caused by a submerged horizontal jet over an erodible bed without bed protection.

A typical case of scouring due to two-dimensional jets is the scour below a spillway. *Farhodi and Smith* [1982, 1985] carried out an extensive study on this topic. A hydraulic jump was formed owing to a supercritical flow directed over a crest (see Figure 1.3). A plain apron was used as bed protection. The length of the apron was about equal to the length of the hydraulic jump. Three tailwater conditions were tested: a submerged hydraulic jump a balanced hydraulic jump and a downstream-moved hydraulic jump. The results on time development were in general agreement with Breusers' work, leading to the following calibration coefficient  $\xi = 0.22$ . Direct observations of the scouring process showed a geometric similarity in the progress of the scour hole. Similarity of scour profiles was established by plotting the coordinates of the profiles scaled with the maximum scour depth at any time,  $y_{s,t}$ . This result first demonstrated that the scour hole profile could be described and the volume of sediment removed out of the scour hole could be predicted, provided the corresponding maximum depth of scour,  $y_s$ , is known. The authors also showed that the shape of the profile was independent of sediment properties, although strongly influenced by geometry and intensity of the flow, which led to different tailwater conditions.

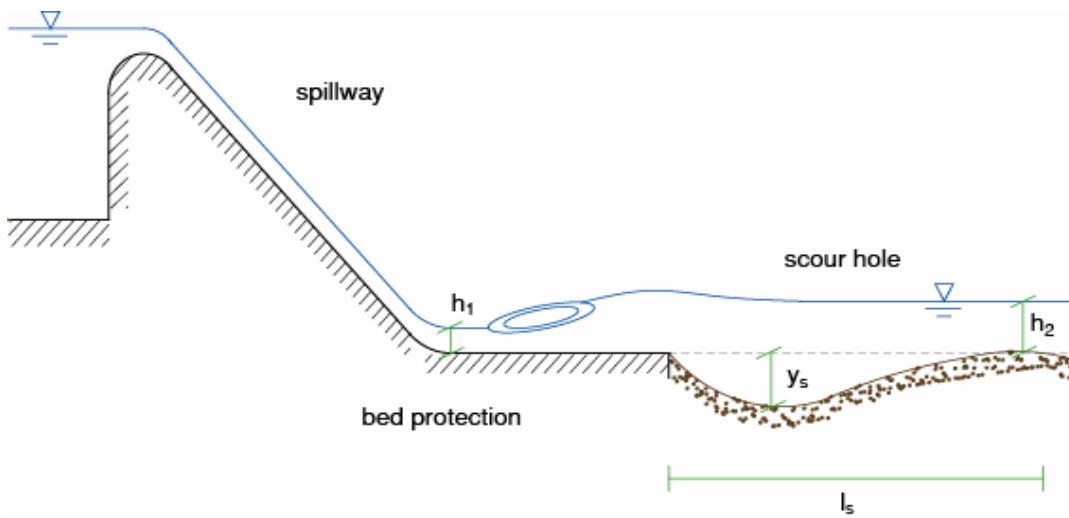


**Figure 1.3 - Local scour below a spillway.**

Another type of scouring by horizontal jets is the scour downstream of an apron due to a horizontal flow issuing from a sluice opening (Figure 1.4). This scour process was experimentally studied, among others, by *Chatterjee and Ghosh* [1980], *Hassan and Narayanan* [1985], *Chatterjee et al.* [1994], *Dey and Westrich* [2003], and *Sarkar and Dey* [2005]. A number of empirical and semi-empirical relationships have been developed for predicting the scour resulting from two-dimensional jets. *Altinbilek and Basmaci* [1973] proposed a method for computing the equilibrium scour depth under vertical gates in cohesionless bed under the action of horizontal submerged jets, leading to the following dimensionless expression:

$$\frac{y_s}{h_{jet}} = \left( \frac{h_{jet}}{D} \tan \varphi_{sed} \right)^{1/2} \left( \frac{F_{R,jet}}{\sqrt{\Delta}} \right)^{3/2} \quad (1.4)$$

where  $h_{jet}$  is the thickness of the jet at the sluice opening;  $F_{R,jet} = U_{jet}/(gh_{jet})^{0.5}$  the Froude number relevant to the jet characteristics, being  $U_{jet}$  the velocity of the jet at the sluice opening and  $g$  the acceleration due to gravity;  $\Delta$  is the relative submerged density;  $D$  a characteristic sediment size;  $\varphi_{sed}$  the angle of repose of sediments.

*Breusers and Raudkivi* [1991] used the main characteristics for fully developed jet flow to describe the dimensions of the scour hole. Based on flume experiments collected from the literature, they found the following relationship for submerged horizontal jets:

$$\frac{y_s}{h_{jet}} = 0.008 \cdot \left( \frac{U_{jet}}{u_c^*} \right)^2 \quad (1.5)$$

where  $u_c^*$  is the critical shear velocity relevant to the sediment bed. The relation can only be used to estimate scour depth for submerged horizontal jets. For unsubmerged jets, when the tailwater depth,  $h_0$ , is about equal to the jet thickness,  $h_{jet}$ , the computational results of Eq. (1.5) were poor.

*Hoffmans* [1998] applied Newton's second law to a control volume in the horizontal direction (see Figure 1.4) and found the following expression for the equilibrium scour depth:

$$\frac{y_s}{h_{jet}} = c_H \cdot \left( 1 - \frac{U_{jet}}{U_0} \right) \quad \text{with } c_H = 50 / k_c \quad (1.6)$$

where  $U_0$  is the undisturbed flow velocity, and  $k_c$  a coefficient depending on the material properties forming the scour hole (see Figure 1.5). For horizontal jets the

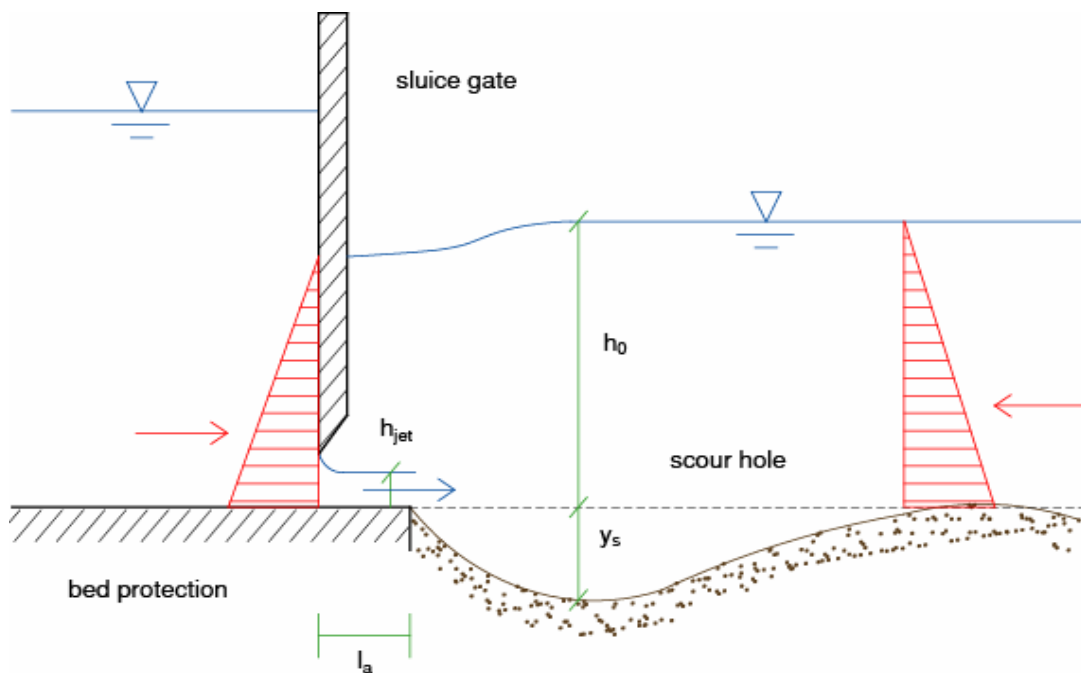


Figure 1.4 - Local scour downstream of a sluice gate opening.

hydrostatic force at Section 1 is assumed to be equal to the hydrostatic force at Section 2. This is only a fair assumption if the flow depth downstream of the hydraulic structure equals approximately the tailwater depth. When the jump is unstable, i.e. when the jump is receding to a point far downstream of the outlet, the assumption  $F_1 = F_2$  cannot be applied, and the above relationship is not valid.

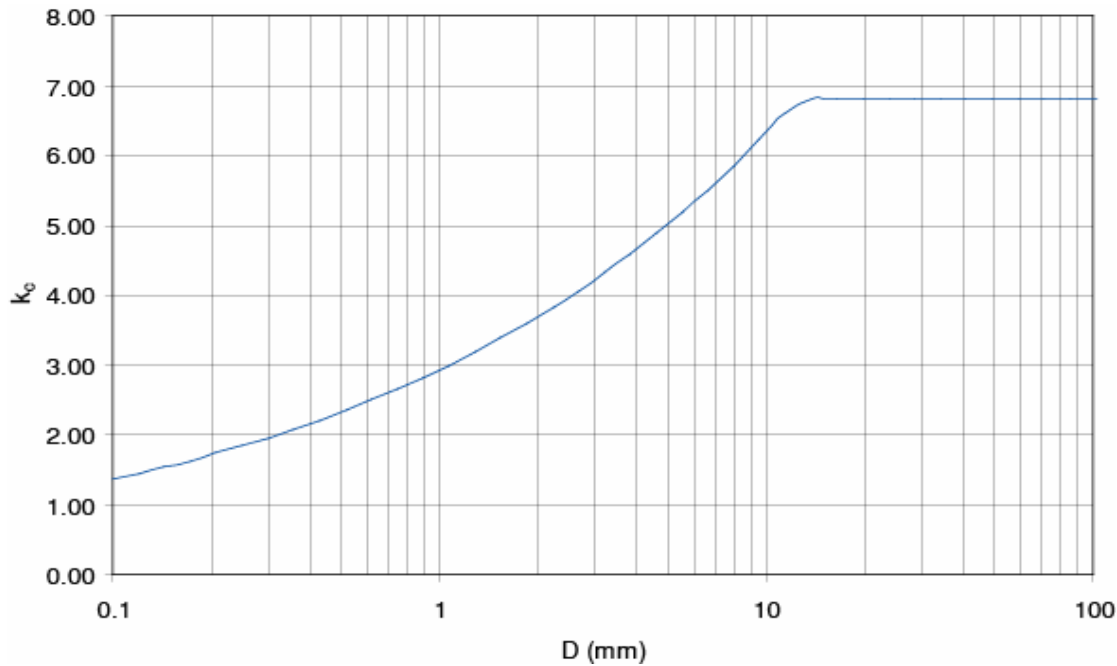


Figure 1.5 - Scour coefficient for Eqs. (1.6) and (1.13). Modified after Hoffmans [1997].

Recently, *Dey and Sarkar* [2007] showed that scouring due to horizontal jets depended on a variety of parameters. Equilibrium scour depth was found to decrease with increase in sediment size, sluice opening and apron length. On the other hand, the equilibrium scour depth increased with increase in densimetric Froude number. The variation of equilibrium scour depth with tailwater depth indicated a critical tailwater depth corresponding to a minimum equilibrium scour depth. The effect of sediment gradation on scour depth was pronounced for non-uniform sediments, which reduced scour depth significantly due to formation of an armor layer. On the base of an experimental investigation on scour of non-cohesive sediment beds (uniform and non-uniform sediments) they proposed the following dimensionless relationship:



$$\frac{y_s}{h_{jet}} = 2.59 \cdot (F_{R,jet}^*)^{0.94} \left( \frac{h_0}{h_{jet}} \right)^{0.16} \left( \frac{l_a}{h_{jet}} \right)^{-0.37} \left( \frac{D}{h_{jet}} \right)^{0.25} \quad (1.7)$$

where  $l_a$  is the length of the apron, and  $F_{R,jet}^* = U_{jet}/(g\Delta D)^{0.5}$  the densimetric Froude number relevant to the jet characteristics.

A comprehensive list of such relationships was presented by *Whittaker & Schleiss* [1984], *Breusers & Raudkivi* [1991], and *Sarkar and Dey* [2004]. It is finally noticed that in many studies [*Hassan and Narayanan*, 1985; *Chatterjee et al.*, 1994; *Dey and Sarkar*, 2007] the scour profiles (including dune in the downstream of scour hole) were observed to follow a particular geometric similarity at different times and, once properly scaled, profiles could be expressed by a combination of polynomials.

### 1.3.3 Scour due to plunging jets

In recent years, the need to dissipate the energy of flood waters passing over dams has been characterized by the use of free trajectory jets. These can take the form of free overfalls over the crests of concrete dams, direct discharges from pressure gates set in the dam wall or flows deflected from some point below the crest. At the ends of long chutes and tunnels, buckets can be used to deflect the flow in a similar manner. These structures are compact and economical compared to the stilling basins which would otherwise be required. At the point of impact with the riverbed downstream, the vertical jet will dissipate energy by excavating a scour hole. Vertical jets are also named “plunging jets”. The term refers to jets of water that impinge on the free surface due to the discharge from an outlet above the free surface or overflow through an opening. *Bennett et al.* [2000] observed that a jet separates from the overfall and diffuses downstream of the structure. This jet splits into two wall jets forming two counter-rotating eddies (rollers), upstream and downstream of the diffuse jet, eroding and shaping the scour hole. The upstream roller is captive between the overfall and the impinging jet. The circulation within the downstream roller causes a region of significant upwelling and sediment deposition occurs as the flow directs toward the water surface.

One of the earliest relations defining the scour depth was proposed by *Schoklitsch* [1932], based on hundreds of flume experiments. *Mason and Arumugam* [1985]

performed a comprehensive analysis of formulas for scouring under free-falling jets using model and prototype data. Most formulas derived from empirical analysis, with no organization of variables into dimensionless groups, and expressed the maximum scour depth,  $y_s$ , in terms of power laws increasing with the head drop from upstream to downstream water levels,  $a_H$ , and the unit discharge of the jet at the point of impact,  $q$ , and, in some cases, decreasing with the characteristic particle size of the bed material,  $D$ . The majority of authors have adopted the  $D_{90}$  size on the basis that smaller particles will be scoured most readily and the ultimate size of hole being governed by the larger particles available in the bed, while others have considered the mean  $D_m$  size as sufficiently representative. The schematic of scouring under plunging jets and relevant parameters is shown in Figure 1.6. Mason and Arumugam found this type of relationship to be most satisfactory for estimating depth of scour under a jet while retaining the benefit of simplicity, but they stated that the inclusion of tailwater depth  $h_0$  as an additional factor could enhance accuracy of prediction. They showed that the most accurate expression for calculating scour depth on both models and prototypes was:

$$y_s = (6.42 - 3.10a_H^{0.10}) \frac{q^{0.60 - \frac{a_H}{600}} \cdot a_H^{0.15 + \frac{a_H}{200}} \cdot h_0^{0.15}}{g^{0.30} \cdot D^{0.10}} \quad (1.8)$$

According to the suggestions of Yen [1987], Eq. (1.8) could be rewritten in the following dimensionless form:

$$\frac{y_s}{H_s} = \frac{2}{3} \cdot (6.42 - 3.10a_H^{0.10}) \cdot g^{\frac{a_H}{600}} \cdot \left( \frac{3}{2} \cdot \frac{a_H}{H_s} \right)^{0.20 + \frac{a_H}{200}} \cdot \left( \frac{a_H}{D} \right)^{0.10} \cdot \left( \frac{a_H}{h_0} \right)^{-0.15} \quad (1.9)$$

where  $H_s = 1.5(q^2/g)^{1/3}$  is the critical specific energy of the flow, which is introduced here instead of  $q$ , and approximates the specific flow energy at the edge of the structure. Recently, *D'Agostino and Ferro* [2004] applied dimensional analysis and incomplete self-similarity theory (see section 1.4.2) for deducing some physically based dimensionless groups controlling the geometric pattern of the scour profile downstream

of grade control structures. Neglecting the effects due to jet contraction and grain size distribution, the proposed relationship can be expressed as follows:

$$\frac{y_s}{H_s} = 0.54 \cdot \left( \frac{a_D^2}{H_s \Delta D} \right)^{1/4} \cdot \left( \frac{a_H}{h_0} \right)^{1/8} \quad (1.10)$$

where  $a_D$  is the difference in height between the crest of the grade-control structure and the bottom of the downstream undisturbed bed level. Some correspondence can be retrieved with Eq. (1.9) if  $a_D \approx a_H$ .

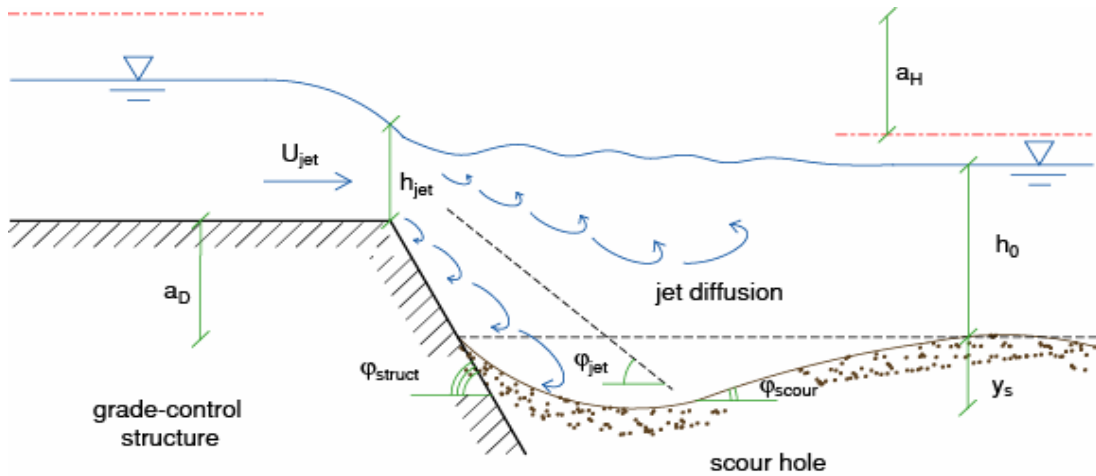


Figure 1.6 - Schematic of scouring under plunging jets.

A large-scale model research carried out by *Bormann and Julien* [1991] enabled the calibration of an equilibrium equation based on jet diffusion and particle stability, leading to its validation in a wide range of conditions: vertical jets, wall jets, free overfall jets, submerged jets and flow over large-scale grade-control structures. According to the results of the authors, the relationship for estimating had the following form:

$$y_s + a_D = C_d^2 \cdot \left[ \frac{\sin \varphi_{sed}}{\sin(\varphi_{sed} + \varphi_{scour})} \right]^{0.80} \cdot \frac{q^{0.60} U_{jet} \sin \varphi_{jet}}{(2g\Delta)^{0.80} D^{0.40}} \quad (1.11)$$

where  $U_{jet}$  the jet entering velocity;  $\varphi_{jet}$  the jet deflection angle;  $\varphi_{sed}$  the angle of repose (friction angle) of sediment;  $\varphi_{scour}$  the maximum side angle of scour hole (downstream face). The jet diffusion coefficient  $C_d$  depends on inlet conditions and remains nearly independent of the jet orientation. Values of  $C_d$  suggested by *Albertson et al.* [1950], *Beltaos and Rajaratnam* (1973), and *Yuen* [1984] ranged from 2.0 to 2.4 for well-formed jets. *Bormann and Julien* [1991] used the value  $C_d = 1.8$  for their calibration. Analysis of the free-jet data from *Yuen* [1984] showed that the angle  $\varphi_{jet}$  could be approximated by the impinging jet angle. From the investigations of *Rajaratnam* [1981], *Yuen* [1984], and *Akashi and Saitou* [1986], analysis of the scour hole geometry suggested that the downstream face slope angle,  $\varphi_{scour}$ , was also approximately equal to the jet angle, and thus  $\varphi_{scour} = \varphi_{jet}$  served as a first approximation for the downstream face slope of the scour hole as long as it did not exceed the limiting value given by the angle of repose of sediment. A dimensional analysis by *Bormann and Julien* [1991] of the jet deflection angle,  $\varphi_{jet}$ , for submerged jets yielded the following dimensionless parameters:

$$\varphi_{jet} = f \left( \varphi_{struct}, \frac{a_D}{h_{jet}}, \frac{h_{jet}}{h_0}, F_{R,jet} \right) \quad (1.12)$$

in which  $\varphi_{struct}$  is the downstream face angle of the grade-control structure. It is observed that, for partially submerged jets, the entering jet velocity and thickness can be approximated with the flow velocity and the water depth at the crest, respectively.

In analogy with the approach used to compute the practical equilibrium scour process caused by horizontal jets, *Hoffmans* [1998] applied Newton's second law of motion to a mass of particles of fluid to derive relations for the maximum scour depth caused by plunging jets in the equilibrium phase. The final expression was proposed in the following form:

$$y_s + h_0 = c_V \cdot \sqrt{\frac{q U_{jet} \sin \varphi_{jet}}{g}} \quad \text{with } c_V = 20 / k_c \quad (1.13)$$

where the value of  $k_c$  can be obtained from graph in Figure 1.5. The relationship  $c_V = 20/k_c$  is an approximation based on experimental calibration. In general many physical

factors influence the resistance of bed particles to motion, i.e. the particle diameter, the size distribution, the grain shape, the density of the sediment, the cohesion of material, and the turbulence level near the bed. From Eq. (1.13) the following conclusions can be drawn. The scour depth is significantly reduced by a substantial decrease in both the jet velocities and the discharge, while a reduction of the scour depth is obtained when the tailwater depth increases. The influence of the angle of impact on the equilibrium scour depth is marginal for  $\pi/3 < \varphi_{jet} < \pi/2$ , being  $[\sin(\pi/3)/\sin(\pi/2)]^{0.5} = 0.93$ .

There is more to evaluate, although the available scour relationships do predict a value in the right order of magnitude. Variations in the forms of equations and coefficients occur. For example, for plunging jets *Breusers and Raudkivi* [1991] showed that the exponents of the drop height vary from 0.05 to 0.5. Most relationships are not based on theoretical backgrounds, but calibrated by using a small number of experiments in which the range of hydraulic conditions was restricted. Generally, this gives satisfactory results for the range investigated. However, when different data are used to verify these relationships, the predictability is significantly reduced. The advantage of using relationships presented in this brief review is that they have been tested with large data sets. Part of the relatively large scatter can be ascribed to lack of definition of the equilibrium phase, since usually little information concerning the duration of the experiments is given and researchers terminate their experiments when the scour rate slows down (stabilization phase), not when a stable scour hole is achieved (equilibrium phase). The relationship proposed by Mason and Arumugam in the form of *Yen* [1987] shows the relative significance of different dimensionless parameters, although obtained from purely empirical considerations. Moreover, though the choice of exponents satisfies Froude similitude law, scaling errors may arise since dimensional exponents leads to dimensionally incompatible equations, as discussed in the following sections. With regard to this matter the relationship given by D'Agostino and Ferro is more consistent. Although they performed a proper dimensional analysis, the choice of the most meaningful dimensionless groups was not obvious, thus leading them to propose also a much more simplified predictive formula for practical purposes. The relationships proposed by Bormann and Julien, and Hoffman, respectively, are based on more theoretical backgrounds, but some difficulties arise when trying to define some parameters concerning jet inclination, jet diffusion, scour geometry, sediment properties

and near bed turbulence, leading to some simplifications which need empirical calibrations again.

#### 1.3.4 Scour at abutments

Abutments are part of the valley side against which dams are constructed or of the approach embankment in case of bridges. Spur dikes are usually designed to protect the banks or to provide enough flow depth for navigation purposes. These structures, alternatively named groynes, spurs or transverse dikes, can be classified according to type, e.g. T-headed or L-headed abutments. In addition, they can be classified according to construction materials (impermeable or permeable), and on the height of the abutment below high water, e.g. submerged or unsubmerged. Abutments can be placed on one bank or symmetrically on both banks of a waterway. The bed between two abutments is assumed to be horizontal. Often, in practice, the design includes a combination of abutments with a sill. An abutment can be protected by an adjacent bed protection to prevent the formation of a scour hole in the direct vicinity of the abutment. Abutments are obstacles placed in a flow, in such a way that they result in a horizontal constriction with a three-dimensional flow. Unlike horizontal sills which produce vertical constrictions in a two-dimensional flow, abutments result in horizontal constrictions mainly.

The geometry of abutments in rivers or estuaries can be schematized to define some basic types of geometries: wing-wall abutments, spill-through abutments and vertical-wall abutments. A wing-wall abutment along the bank of a canal, a river or a tidal channel can be depicted by the following geometric parameters: length,  $l_A$ , width,  $b_A$ , angle of the upstream wing-wall,  $\alpha_{A,u}$ , and angle of the downstream wing-wall,  $\alpha_{A,d}$  (see Figure 1.7). Geometry and shape of spill-through abutments can be characterized by the geometric parameters described for wing-wall abutments. Besides these parameters, the angle of the side slope,  $\beta_{A,s}$ , and the angle of the slope at the nose of the abutment,  $\beta_{A,n}$ , are also representative. The crests of abutments in a river have a gentle slope of 1:100 to 1:200 along the abutment axis to divert the overflowing flow from the bank to the centre of the flow. However, in an estuary horizontal crests are often used. The shape of the edges between the side wall and the wing-wall may be sharp or rounded. In scale models a vertical-wall abutment is sometimes schematized as a vertical plate with a vertical head. In the experiments, the thickness,  $l_A$ , of the plate is

generally small compared to the width,  $b_A$ , of the abutment normal to the flow direction ( $b_A/l_A > 5$ ). Such geometries can be considered as sharp-nosed, so therefore these structures will be found in the prototype only in exceptional cases.

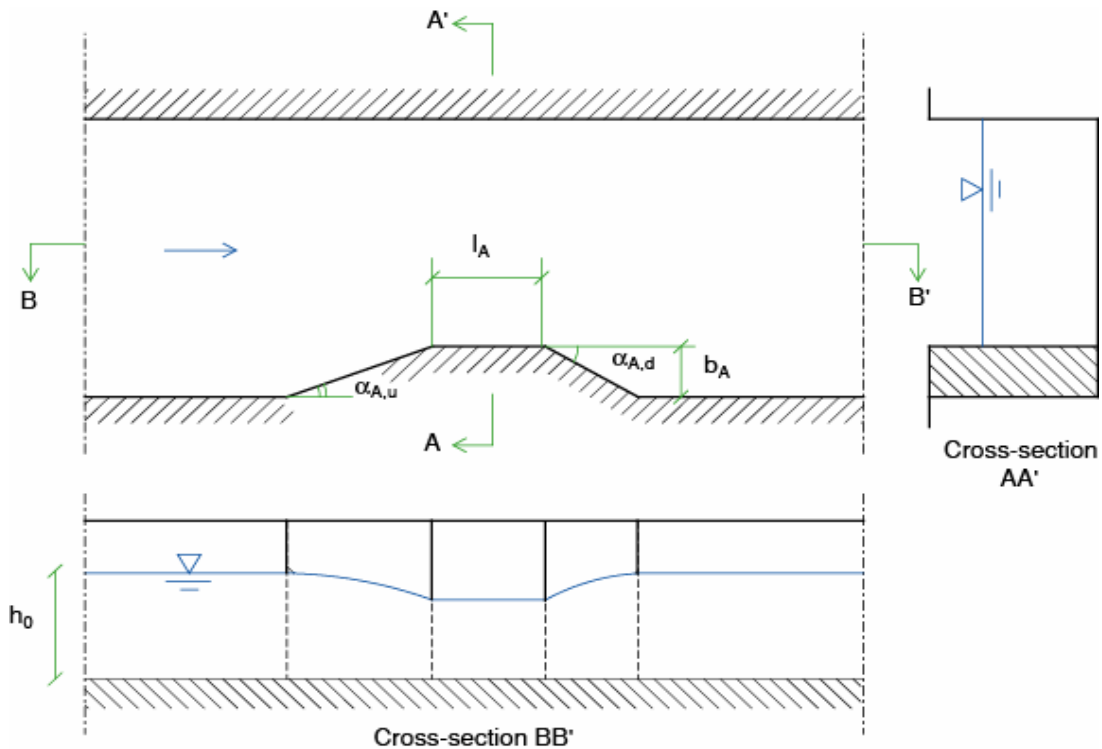


Figure 1.7 - Geometrical sketch for wing-wall abutments.

An analogy between the mechanisms of local scouring at bridge piers and abutments has long been recognized [Melville, 1997]. The flow structure and associated scour process at an abutment are considered to be similar to that at a pier of shape equivalent to the abutment and its mirror image in the channel wall. The scour depth at the abutment is acknowledged to be less than that at the analogous pier due to the channel wall effects on retarding the flow. Many studies generally confirm the similarity of the flow in and around the scour hole at piers and abutments, particularly where the abutment extends only a short distance into the channel in relation to the depth of flow, i.e. at a relatively short abutment. Thus, the dominant flow component at shorter abutments closely resembles one side of the horseshoe vortex and associated downflow, which are important in the development of scour at bridge piers. At piers, the deepest scour occurs on the line of symmetry, while the scour depth along the upstream face of shorter abutments is reasonably uniform and therefore similar to that at piers.

For this reason the methodology for predicting local scouring at abutment will be discussed in the next section in analogy with scouring at bridge piers.

### 1.3.5 Scour at bridge piers

Bridge piers in a flow cause a horizontal constriction of the flow. The local scour around bridge piers depends strongly on the geometry of the pier. Local scour around a bridge pier is usually a relatively rapid process, therefore, most investigators are interested in the maximum scour depth in the equilibrium phase. The flow pattern near a pier is rather complicated (see Figure 1.8) and this complex flow pattern in the scour hole has been described in detail by several authors, e.g. *Breusers & Raudkivi* [1991], *Melville* [1997]. The main parts are the wake vortices and the horseshoe vortices combined with the downflow. The axis of the horseshoe vortex is horizontal, and wraps around the base of the pier in the shape of a horseshoe. The wake-vortex system has vertical axes, which are commonly seen as eddies. The geometry of the pier significantly influences scour depth because it reflects the strength of the horseshoe vortex at the base of the pier.

Many parameters affect the flow pattern and the process of local scour around bridge foundations (either piers or abutments). The influence of the fluid properties (fluid density,  $\rho_w$ , kinematic viscosity,  $\nu$ , acceleration due to gravity,  $g$ ) on the scour process is generally much less important than that of the flow characteristics (flow depth,  $h_0$ , mean flow velocity,  $U_0$ , resistance coefficient, e.g. Chèzy coefficient). In addition, the size of bed material in the sand size range has little effect on scour depth. Larger size bed material that will be moved by the flow, will not affect the equilibrium scour depth, but will affect the time it takes to reach equilibrium. However, there are laboratory studies which indicate that larger size particles in the bed material armor the scour hole and decrease scour depths, e.g. *Breusers and Raudkivi* [1991]. The width of the structure,  $b_P$ , has a direct affect on the depth of scour, provided  $b_P/h_0 < 1$ . With an increase in  $b_P$ , there is an increase in scour depth. The flow depth only has a direct affect on scour depth if  $b_P/h_0 > 1$ . In fact, for deep flows compared to the pier or abutment size, the scour depth increases proportionately with  $b_P$  (or  $b_A$  in case of abutments), and is independent of  $h_0$ . Many authors [e.g. *Raudkivi*, 1986; *Melville and Sutherland*, 1988] explained that for shallow flows, the surface roller that forms ahead



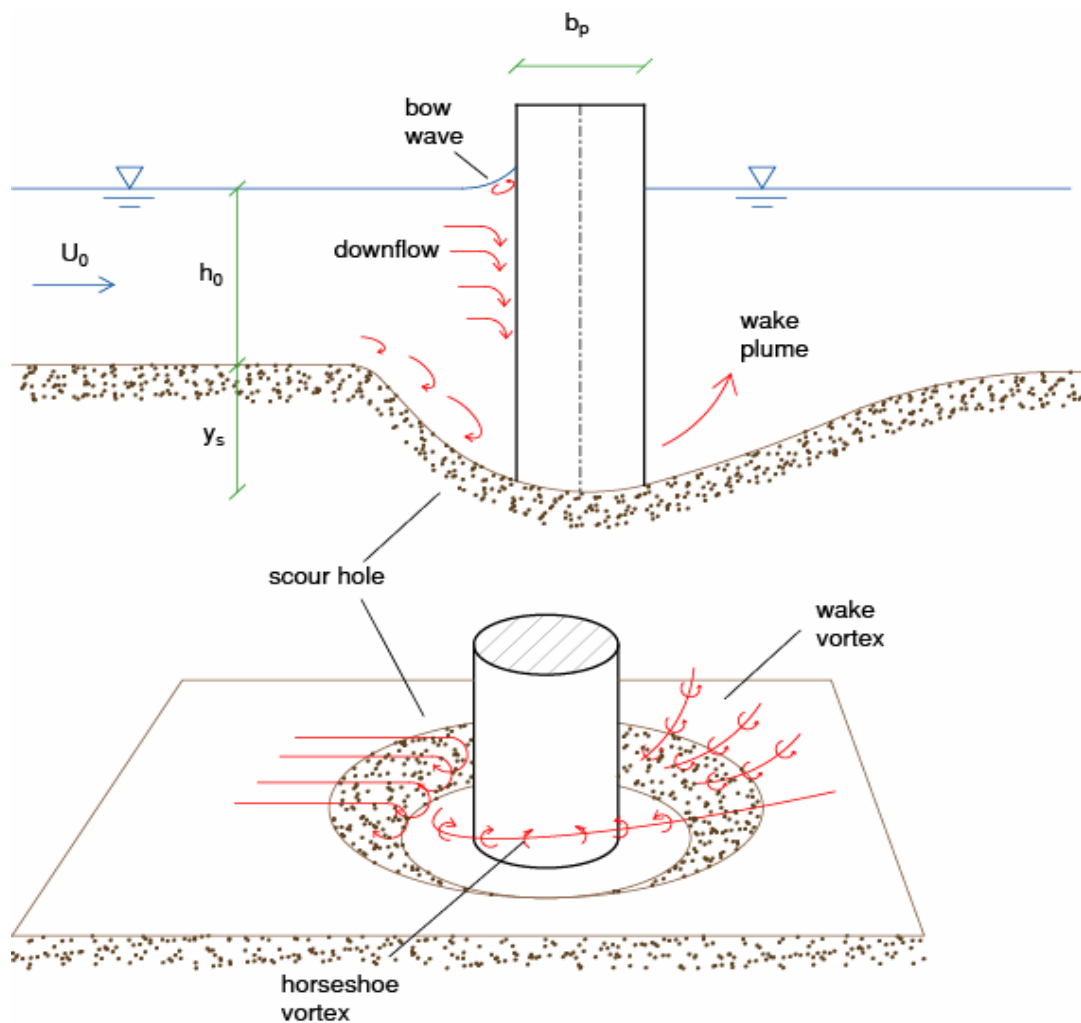


Figure 1.8 - Schematic of flow pattern and scour hole at bridge piers.

of the bridge pier interferes with the scour action of the horseshoe vortex because the two have opposite senses of rotation. With increasing flow depth, the interference reduces and eventually becomes insignificant. For shallow flows compared to the pier or abutment size, the scour depth increases proportionately with  $h_0$ , but is independent of  $b_p$ , while for intermediate flow depths  $y_s$  depends on both  $h_0$  and  $b_p$ . In rivers, bed forms which lead to bed roughness are developed. This determines the flow depth and the form of the vertical velocity profile. The velocity of the approach flow influences the scour process. The higher the velocity, the deeper the scour depth. For live-bed conditions (scour with sediment motion) the scour depth does not increase significantly with velocity. In such cases there is a dynamic equilibrium between transport out of the scour hole and the supply. Most studies have focused on local scour near circular prismatic piers in a non-cohesive sand bed. In the experiments, local scour was

generally caused by a steady flow. This situation is a reference case for other geometries. The length of the pier has no appreciable affect on the scour depth as long as the pier is aligned with the flow. If the pier (e.g. rectangular pier) is at an angle to the flow, the length influences the scour process significantly. The foundation of a prismatic pier is normally a continuation of the pier for at least a few pier-diameters into the subsoil. If the pier has a large diameter compared to its height it can be regarded as a caisson.

The temporal maximum scour depth (for a given set of conditions) is termed the equilibrium depth of scour. At equilibrium, the local scour depth at a bridge foundation can be described in so-called  $K$ -factors, i.e. empirical expressions accounting for the various influences on scour depth, as follows [Melville, 1992]:

$$y_s = K_{h-b} \cdot K_q \cdot K_D \cdot K_S \cdot K_A \cdot K_C \quad (1.14)$$

where  $K_{h-b}$  takes into account the relative size of flow depth and pier width (or abutment width) and it is the only dimensional factor other than  $y_s$ ;  $K_q$  considers the flow intensity;  $K_D$  the sediment size;  $K_S$  the pier or abutment shape;  $K_A$  the pier or abutment alignment; and  $K_C$  the channel geometry.  $K_q$  is sometime formulated to include sediment gradation effects as well as flow velocity effects. Eq. (1.14) applies to local scour and is restricted to bridge crossings where the contraction effects, as represented by the ratio of the widths of the bridge opening and channel, are insignificant, and can be alternatively expressed as [Cardoso and Bettess, 1999]:

$$\frac{y_s}{y_{se}} = K_q \left( \frac{U_0}{U_c} \right) \cdot K_D \left( \frac{b_p}{D} \right) \cdot K_S \cdot K_A \cdot K_C \quad (1.15)$$

where  $y_{se}$  is the scour depth occurring at standard-geometry structures, either thin wall abutments that protrude at right angle from the sidewall or circular bridge piers, for which  $K_S = K_A = 1$ , placed in rectangular bed channels ( $K_C = 1$ ) with fine sediment ( $K_D = 1$ ) and flow conditions close to the threshold for grain instability ( $K_q = 1$ ). The flow intensity and the sediment size factors are function of the ratio  $U_0/U_c$  and the relative depth  $b_p/D$  (or  $b_A/D$  for abutments), respectively, while  $y_{se} = K_{h-b}$ . Melville [1997] proposed the following relationships for  $y_{se}$ , which depends only on  $h_0$  and  $l_p$ :

$$y_{se} = 4.5h_0 \quad \text{for } h_0/b_p < 0.20 \quad (1.16a)$$

$$y_{se} = 2\sqrt{h_0b_p} \quad \text{for } 0.20 < h_0/b_p < 1.43 \quad (1.16b)$$

$$y_{se} = 2.4b_p \quad \text{for } h_0/b_p > 1.43 \quad (1.16c)$$

which are valid for scours at bridge piers, while the following expressions can be used at abutments:

$$y_{se} = 10h_0 \quad \text{for } h_0/b_A < 0.04 \quad (1.17a)$$

$$y_{se} = 2\sqrt{h_0b_A} \quad \text{for } 0.04 < h_0/b_A < 1 \quad (1.17b)$$

$$y_{se} = 2b_A \quad \text{for } h_0/b_A > 1 \quad (1.17c)$$

The ratio  $y_s/y_{se}$  was found to depend linearly by the flow intensity for  $U_0/U_c < 1$ , while it did not further increase for  $U_0/U_c > 1$ . In turns, Eq. (1.15) may be rewritten as follows:

$$\frac{y_s}{y_{se}} = \frac{U_0}{U_c} \cdot K_D \left( \frac{b_p}{D} \right) \cdot K_S \cdot K_A \cdot K_C \quad \text{for clear-water} \quad (1.18a)$$

$$\frac{y_s}{y_{se}} = K_D \left( \frac{b_p}{D} \right) \cdot K_S \cdot K_A \cdot K_C \quad \text{for live-bed} \quad (1.18b)$$

Sediment size factor can be expressed as follows:

$$K_D = 0.57 \log \left( 2.24 \frac{b_p}{D} \right) \quad \text{for } b_p/D < 25 \quad (1.19a)$$

$$K_D = 1 \quad \text{for } b_p/D > 25 \quad (1.19b)$$

The influence of the shape factor,  $K_S$ , and the alignment of piers to the flow,  $K_A$  are presented in Table 1.1 and Figure 1.9, respectively, according to the results of many authors. Channel geometry effects are unimportant at bridge piers, as long as the velocity and flow depth used represent the flow approaching the pier under consideration. Thus, the channel geometry factor for piers is taken as  $K_C = 1.0$ . A

**Table 1.1 - Shape factor  $K_s$  for scouring at bridge piers and abutments [after Hoffmans, 1997]**

Form of cross section	$K_s$
Lenticular	0.70 ÷ 0.80
Elliptic	0.60 ÷ 0.80
Circular	1.00
Rectangular	1.00 ÷ 1.20
Rectangular with semi-circular nose	0.90
Rectangular with chamfered corners	1.01
Rectangular nose with wedge-shaped tail	0.85
Pyramid-like (narrowing upwards)	0.75
Inverted pyramid (broadening upwards)	1.20

systematic investigation of the effect of approach channel geometry on the scour at an abutment sited in a compound channel comprising flood and main channels is presented by *Melville* [1995]. The study is limited to the case of an abutment spanning the flood channel and extending into the main channel.  $K_C$  is defined as the ratio of the depth of scour at the given abutment sited in the compound channel to that at the same abutment sited in a rectangular channel of the same width and depth equal to the main channel depth, termed the corresponding rectangular channel.

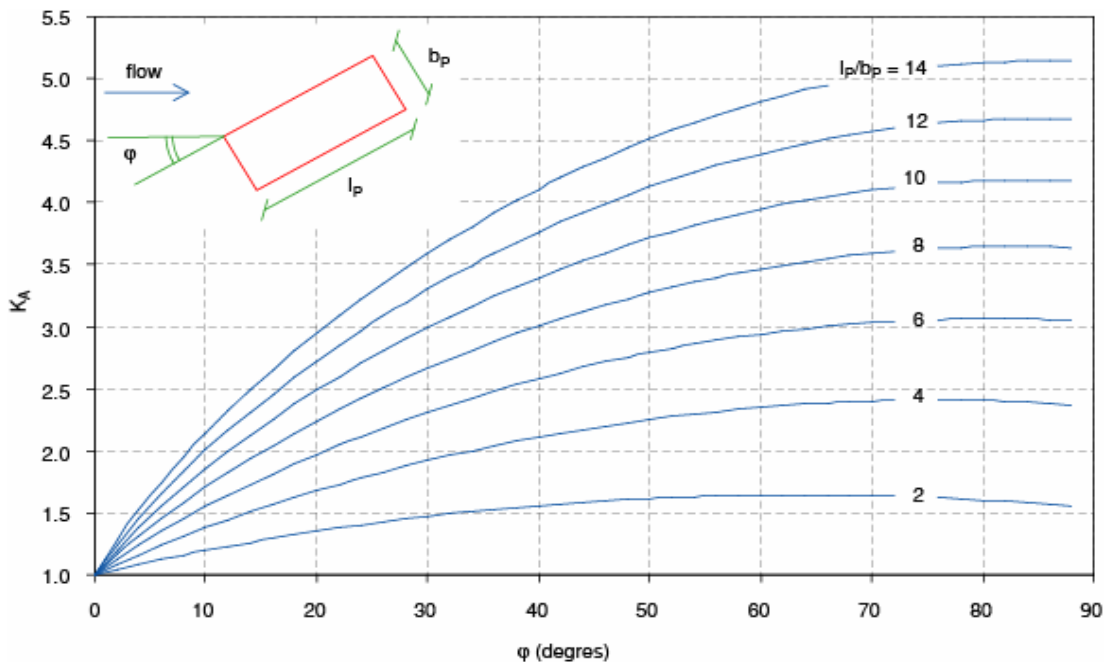


**Figure 1.9 - Influence of the alignment of the pier to the flow.**

## **1.4 TOOLS TO APPROACH LOCAL SCOURING**

There are many physical processes that are pertinent to the erosion of loose sediment beds by jet impingement. These include the strength of the jet-induced fluid turbulence, the pressure and shear stress distribution exerted on the bed, the density and size of the particles and the angle of repose of the granular material comprising the bed. The coupling between the shape of the scour hole and the characteristics of the jet flow renders this problem highly complex. As stated in the previous sections, most studies have attempted to model erosion with purely empirical instruments. Although no universal formula is capable of handling scour processes due to different flows downstream of hydraulic structures, during the past decades more theoretical attempts were made to predict maximum scour depths at different structures. Most commonly they involve concepts relevant to either jet diffusion and particle stability or dimensional analysis and self-similarity theory. Using the former approach implies that the derived equations are more physically based, though sometime it requires strong simplifications, thus reducing the applicability of the results to a limited number of physical problems. The latter is a more general approach and it can be applied in most physical cases. It does not require any particular theoretical formulation, but final relationships are not merely the result of laboratory or numerical experimentation. Dimensional analysis by itself leads to definitive solution of the original problem only in few special cases, however when associated to self-similarity concepts it may “reveal” the real nature of even very complex phenomena. Specially for those cases where no theoretical framework is available, the researcher should have a good knowledge of the physics underlying natural processes in order to identify the variables that are actually involved in a specific phenomenon.

### **1.4.1 Jet diffusion and Particle stability**

Jets impinging water depths give rise to a zone of turbulent mixing downstream of the point of impingement. The width of this mixing layer increases in the downstream direction. The jet flow can be divided into two distinct regions [*Albertson et al.*, 1950]: a zone of flow establishment, also named potential core [*Rajaratnam*, 1976], and a zone of established flow, also named fully developed flow region (see Figure 1.10). The zone

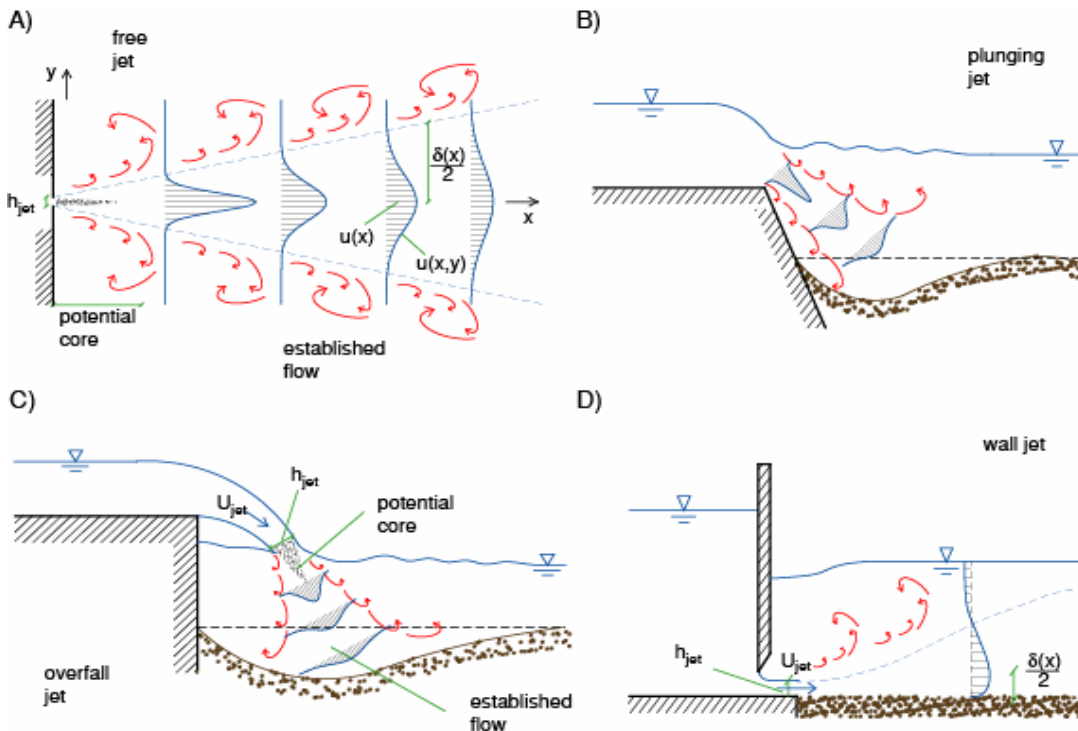


Figure 1.10 - Schematic of jet diffusion for 2D flows: potential core and established flow. A) free jet; B) partially submerged plunging jet; C) free overfall jet; D) wall jet over rough boundary.

of flow establishment is a wedge-like region in which the flow velocity equals the efflux velocity. In the zone of established flow the velocities in the central part of the jet decrease. In numerous textbooks [e.g. *Schlichting*, 1979] the theoretical relations are discussed that predict the flow velocity both in circular jets and in 2D and 3D wall jets. For 2D free jets the following relationships holds:

$$\frac{u(x)}{U_{jet}} \sim \left( \frac{h_{jet}}{x} \right)^{1/2} \quad (1.20a)$$

$$\frac{\delta(x)}{h_{jet}} \sim \left( \frac{x}{h_{jet}} \right) \quad (1.20b)$$

where  $u(x)$  and  $\delta(x)$  are the maximum jet velocity and jet thickness, respectively, along the streamwise direction,  $x$ . These are the scaling of a two-dimensional free jet sufficiently far downstream of the jet source, about six to ten times the thickness of the jet entering the flow depth,  $h_{jet}$ , which is the potential core length. They arise from the

hypotheses that molecular viscosity does not play a role in the evolution of the jet (i.e. the Reynolds number based on jet width is large) and the streamwise momentum flux is constant. Neither of these assumptions is valid for a wall jet. The boundary shear stress given by the streamwise rate of change of the momentum flux is not negligible. Hence the momentum flux is not constant. For 2D wall jets, *Wyganski et al.* [1992] and *Hogg et al.* [1997] proposed the following relationships for smooth and rough boundaries, respectively:

$$\frac{u(x)}{U_{jet}} \sim \left( \frac{h_{jet}}{x} \right)^{\zeta/2} \cdot R_{wall}^{1-\zeta} \quad (1.21a)$$

$$\frac{\delta(x)}{h_{jet}} \sim \left( \frac{x}{h_{jet}} \right)^{\eta} \cdot R_{wall}^{2(\eta-1)} \quad (1.21b)$$

where  $R_{wall} = R_{E,jet} = U_{jet}h_{jet}/\nu$  is the Reynolds number relevant to jet width and velocity, being  $\nu$  the kinematic viscosity; and  $R_{wall} = D/h_{jet}$  is relative boundary roughness;  $\zeta$  and  $\eta$  are calibration coefficients, whose values differ for the two cases. Hence the effect of both molecular viscosity and turbulent viscosity (or relative roughness) is to reduce the rate of decay of the jet velocity and the rate of jet diffusion. Presumably the exponents  $\zeta$  and  $\eta$  are functions of either the Reynolds number,  $R_{E,jet}$ , or the relative roughness,  $D/h_{jet}$ , so that  $\zeta$  and  $\eta$  approach 1 as either  $R_{E,jet} \rightarrow \infty$  or  $D/h_{jet} \rightarrow 0$ , thus retrieving scales relevant to the free jets.

Eqs. (1.20a) and (1.20b) can be applied for plunging jets, if the length of the zone of flow establishment is relatively small compared to the tailwater depth,  $h_0$ . In their theoretical investigation on local scour downstream of grade-control structures *Bormann and Julien* [1991] developed a scour depth predictive formula based on two-dimensional jet diffusion and particle stability. Critical conditions for incipient particle motion were identified by calculating the moments of the forces which drive and resist particle motion. The forces leading to particle motion on the bed surface were identified with the shear stress exerted by the jet flow, whereas the particle weight resists motion. This a rough approximation for jet flow that impinge upon the bed. Such an impingement leads to a surface pressure distribution and a seepage flow within the bed. In this case the mobilizing force is a more complex function of the surface pressure, bed

shear stress and bed permeability [Kobus *et al.*, 1979]. Borman and Julien expressed the shear stress exerted by diffusive jets as follows:

$$\tau_{jet} = C_D \cdot \rho_w \left[ u(x = l_{jet}) \right]^2 \quad (1.22)$$

where  $C_D$  is a friction (drag) coefficient;  $\rho_w$  the density of water;  $l_{jet}$  the diffusion length of jets at the equilibrium stage. Allowing for longitudinal gradients, i.e. for scour hole slope, the equilibrium condition reduces to:

$$\tau_{jet} = \tau_c \cdot \frac{\sin(\varphi_{sed} + \varphi_{scour})}{\sin(\varphi_{sed})} \quad (1.23)$$

where  $\tau_c = \theta_c \cdot \gamma_w \Delta D$  is the critical shear stress for flat beds, being  $\theta_c$  the critical Shields' mobility parameter and  $\gamma_w$  the specific weight of water. If scaling rules given in the form of Eqs. (1.20a) and (1.20b) are assumed, taking into account Eqs. (1.22) and (1.23) leads to the relationship given in Eq. (1.11), once  $l_{jet}$  is made explicit (see Appendix for complete derivation), as follows:

$$y_s + a_D = l_{jet} \cdot \sin \varphi_{jet} \quad (1.24a)$$

$$y_s + h_0 = l_{jet} \cdot \sin \varphi_{jet} \quad (1.24b)$$

which are valid for partially submerged plunging jets and free overfall jets, respectively.

Hogg *et al.* [1997] developed an analytical framework to model the progressive erosion of an initially flat sediment bed by a 2D turbulent wall jet. In this case, assuming that the shear stress is the driving force mobilizing bed particles is a more consistent assumption, as jet diffuses almost parallel to the bed surface, if the aspect ratio, i.e. the ratio of depth to streamwise extent of the scour hole, is small. The authors expressed the shear stress exerted by diffusive jets by integrating the momentum equation for 1D flows on the assumption that hydrostatic pressure holds and streamwise variations of normal stress are negligible. This led to streamwise rate of change of the momentum flux:



$$\tau_{jet} = -\frac{d}{dx} \int_0^\infty \rho_w [u(x,y)]^2 dy \sim \rho_w [u(x)]^2 \cdot \delta(x) \quad (1.25)$$

where  $u(x,y)$  represents the jet velocity varying along longitudinal and vertical directions. It is observed that, by using the current notation,  $u(x,y) = u(x)$  for  $y = \delta(x)/2$ . Hogg et al. further assumed that scaling laws for wall jet diffusion over a fixed boundary, i.e. Eqs. (1.21a) and (1.21b), can be used for jet diffusion over an erodible rough boundary. This requires that the aspect ratio of the eroded profile is small, as stated above, and that the mean flow does not separate from the boundary at any downstream location to avoid the need to introduce models allowing for flow recirculation. The profile of the scour hole was calculated by equating the shear stress distribution along the bed surface to the critical shear stress for incipient motion. Taking into account Eq. (1.23), Eq. (1.25) and the scaling for wall jet diffusion over rough boundary, the following ordinary differential equation was proposed that describes the scour hole profile at the equilibrium stage:

$$\psi \cdot \frac{\rho_w U_{jet}^2 (x/h_{jet})^{\chi-1} (h_{jet}/D)^{2\chi} G(y_s, x)}{\theta_c \cdot \gamma_w \Delta D} = \left( \frac{1}{\tan \varphi_{sed}} + \frac{dy_s}{dx} \right) \left[ 1 + \left( \frac{dy_s}{dx} \right)^2 \right]^{-1/2} \quad (1.26)$$

where  $\chi = (\eta - \zeta)$ ;  $\psi$  is a global coefficient allowing for all coefficients that are understood in Eqs. (1.21a), (1.21b) and (1.25);  $G(y_s, x)$  is a shape function describing the shear stress for non horizontal boundary;  $dy_s/dx = \tan(\varphi_{scour})$  is the local gradient of the bed, where  $y_s$  is defined here as the equilibrium scour depth along the longitudinal direction and it is a function of  $x$ .

The discussion above illustrates few examples of purely theoretical derivations used to deal with local scouring. Although this approach looks attractive, it was shown that many assumptions were required, which can not always be applied to specific physical problems. Moreover, empirical relationships and calibration coefficients were introduced into such derivations and used to take into account physical processes that develop at small spatial scales (grain scale or even molecular scale) and affect bed morphology at larger scales. In the next section, a different methodology is discussed,

which is widely used by scientists to deal with phenomena that can be hardly described by purely theoretical approaches, such as local scouring.

#### 1.4.2 Dimensional analysis

Dimensional analysis is a theoretical tool often applied in physics, chemistry, and engineering to understand phenomena involving a number of different physical quantities. It is often used by physical scientists and engineers to check the consistency of derived equations and computations, and to form reasonable hypotheses about complex physical problems. In many research fields, dimensional analysis is practically used to derive general relationships that are then completely determined through laboratory or numerical experimentation. The basics of this method is shortly described below.

To measure physical quantities a consistent system of units is required, such as the SI system, in which the basic (or fundamental) units are meter, kilogram, second, ampere, Kelvin, mole, and candela (relevant notation is m, kg, s, A, K mol, cd). The unit of a physical quantity and its dimension are related, but not precisely matching concepts. Units are defined by standard conventions; e.g. length may have meters, feet, inches, miles or micrometers as units, but any length always has a dimension [L], which is independent of the unit used to measure it. This leads to the definition of a *class of system of units*, which is a set of systems of units that differ only in magnitude, not in the physical nature. Two different systems of units of the same physical quantities (e.g. either m-Kg-s or cm-g-h) are members of the same class but have conversion factors between them, i.e. they have different magnitudes. Moreover, units are divided into two categories: fundamental and derived units. In mechanics, which represents a particular class of phenomena, dimensions of any physical quantity can be expressed in terms of mass [M], length [L] and time [T], which form a particular class of system of units, and define the relevant fundamental units. Once the fundamental units have been decided upon, derived units are obtained from the fundamental units using the definition of the physical quantities involved. The class given by mass, length and time is not the only possible class, but it is the one most commonly used. For example, one might choose force [F], length [L] and time [T] as the base dimensions. The choice of the base set of dimensions (or class) is thus partly a convention. However, a set of fundamental units (depending upon the class that has been chosen) represents a consistent system of units

only if it sufficient for measuring the properties of a given class of phenomena (e.g. kinematics, mechanics, etc.).

In the most primitive form, dimensional analysis may be used to check the consistency of physical equations: the two sides of any equation must be commensurable, i.e. the equation must be dimensionally homogeneous. As a corollary to this requirement, it follows that in a physically meaningful expression, only quantities of the same dimension can be added or subtracted. Scalar arguments to exponential, trigonometric, logarithmic, and other transcendental functions must be dimensionless quantities. This constraint is clear when one takes the Taylor expansion of these functions, which turns out to be dimensionally incompatible. The value of a dimensional physical quantity,  $z_i$ , is written as the product of a unit within the dimension,  $\omega_i$ , and a dimensionless numerical factor,  $\rho(z_i)$ . Strictly, when like dimensioned quantities are added or subtracted or compared, these dimensioned quantities must be expressed in consistent units so that the numerical values of these quantities may be directly added or subtracted. But, conceptually, there is no problem adding quantities of the same dimension expressed in different units. For example, 1 meter added to 1 foot is a length, but it would not be correct to add 1 to 1 to get the result. A conversion factor, which is a ratio of like dimensioned quantities and is equal to the dimensionless unity, is needed. Only in this manner it is meaningful to speak of adding like dimensioned quantities of differing units. Ultimately, it can be seen that the requirement for physical equations to be dimensionally homogeneous reflects the idea that the laws of physics are independent of the units employed to measure the physical variables.

What has been lastly stated represents the *covariance principle* of physics upon which dimensional analysis is based: all physical laws can be represented in a form equally valid for all observers. An important conclusion can be drawn from this simple idea, using the following argument: the functions that express physical laws must possess a certain fundamental property, which in mathematics is called generalized homogeneity or symmetry. This property allows the number of arguments in these functions to be reduced making it simpler to obtain them. Such demonstration is given in the Buckingham's  $\pi$  theorem, which is discussed in the next section. Despite the simplicity of this statement, even remarkable results have sometime been obtained in

many fields (among others Reynolds and Kolmogorov are cited for their contribute in fluid dynamic turbulence). Some very simple idealized physical problems, such as the period of small oscillation of a pendulum or the resistance force that a gas exerts on the uniform motion of a sphere, can be fully solved by applying dimensional analysis and carrying out one single experiment, with no regard to the knowledge of physics underlying such phenomena other than for the governing variables that have to be included. More complex phenomena can be approached in a similar way if the number of dimensionless parameters is reasonably small. In this regard, self-similarity theory may be helpful, as it allows to reduce the parameters involved if few requirements are satisfied.

### 1.4.3 The Buckingham's $\pi$ -theorem

The Buckingham's  $\pi$ -theorem is a key theorem in dimensional analysis. The theorem loosely states that a physically meaningful equation involving a certain number,  $s$ , of physical variables  $z_i$ :

$$f_z(z_1, z_2, \dots, z_s) = 0 \quad (1.27)$$

where the variables are expressed in terms of  $r$  independent fundamental physical dimensions, is equivalent to an equation involving a set of  $p = (s - r)$  dimensionless parameters,  $\pi_i$ , derived from the original variables:

$$f_\pi(\pi_1, \pi_2, \dots, \pi_p) = 0 \quad (1.28)$$

This provides a method for computing sets of dimensionless parameters from the given original variables, even if the form of the equation is still unknown. However, the choice of dimensionless parameters is not unique: Buckingham's theorem only provides a way of generating sets of dimensionless parameters, and will not choose the most "physically meaningful" ones. The use of  $\pi_i$  notation as dimensionless parameter was first introduced by Buckingham (1914) in his work on the subject from which the theorem draws its name.

By allowing for the space of fundamental and derived physical units,  $\omega_i$ , as a vector space, being the fundamental units the basis vector  $(\Omega_1, \dots, \Omega_r)^T$ , and considering physical unit multiplication as the “vector addition” operation and raising to powers as the “scalar multiplication” operation, a dimensional variable is represented as the set of exponents needed for the fundamental units (with a power of zero if the particular fundamental unit is not present), as follows:

$$z_j = \rho(z_j) \omega_j = \rho(z_j) \prod_{i=1}^r \Omega_i^{\alpha_{i,j}} \quad \Rightarrow \quad z_j \Leftrightarrow \alpha_{1,j}, \dots, \alpha_{r,j} \quad (1.29)$$

where  $\rho(z_i)$  is a real number, units are expressed as linear combinations of the basis vector, and the exponents  $\alpha_{1,j}, \dots, \alpha_{r,j}$  are rational numbers. It is noted that the fundamental units are independent in the sense that:

$$\prod_{i=1}^r \Omega_i^{\beta_i} = 1 \quad \Rightarrow \quad \beta_i = 0 \quad \forall i = 1, \dots, r \quad (1.30)$$

The set of physical variables can be expressed by the so-called dimension matrix:

$$A = \begin{pmatrix} \alpha_{11} & \dots & \alpha_{1s} \\ \vdots & \ddots & \vdots \\ \alpha_{r1} & \dots & \alpha_{rs} \end{pmatrix} \quad (1.31)$$

A combination of these variables is defined as a product of powers, whose dimension can be expressed by using the fundamental units and Eq. (1.29), as follows:

$$Z = z_1^{\lambda_1} \cdot z_2^{\lambda_2} \cdot \dots \cdot z_s^{\lambda_s} \quad (1.32a)$$

$$= \prod_{j=1}^s \rho^{\lambda_j}(z_j) \cdot \omega_j^{\lambda_j} \quad (1.32b)$$

$$= \prod_{j=1}^s \left[ \rho^{\lambda_j}(z_j) \cdot \left( \prod_{i=1}^k \Omega_i^{\alpha_{i,j}} \right)^{\lambda_j} \right] \quad (1.32c)$$

$$= \prod_{j=1}^s \rho^{\lambda_j}(z_j) \cdot \prod_{j=1}^s \prod_{i=1}^r \Omega_i^{\alpha_{i,j} \cdot \lambda_j} \quad (1.32d)$$

$$= \rho(Z) \cdot \prod_{i=1}^r \Omega_i^{(\alpha_{i,1} \cdot \lambda_1 + \dots + \alpha_{i,s} \cdot \lambda_s)} \quad (1.32e)$$

Such combination is defined dimensionless if the unit  $\omega_Z = Z/\rho(Z) = 1$ . This result is equivalent to the matrix equation  $A\boldsymbol{\lambda} = 0$ , where  $\boldsymbol{\lambda} = (\lambda_1, \dots, \lambda_s)^T$ , which states that a biunique correspondence holds between the null space  $N(A)$ , named *Kernel* of  $A$ , and the set of dimensionless combinations of the variables. More formally, the number of independent dimensionless terms that can be formed,  $p$ , is equal to the nullity of the dimension matrix, and  $r$  is the rank of  $A$ . By the rank-nullity theorem, a system of  $s$  vectors in  $r$  independent dimensions satisfies a  $p$ -dimensional space of relations. Any choice of basis will have  $p$  elements, any linear combination of which will give the dimensionless variables.

For practical purposes the problem can be reduced to a problem of linear algebra, using the dimension matrix as a convenient way to summarize the dimensions. Solving  $A\boldsymbol{\lambda} = 0$  leads to:

$$\lambda_j = \sum_{i=1}^p k_{r+i,j} \cdot \lambda_{r+i} \quad \forall j = 1, \dots, r \quad (1.33)$$

where  $k_{1,j}, \dots, k_{p,j}$  are function of the coefficients  $\alpha_{i,j}$ , and  $\boldsymbol{\lambda}_{r+1} = (0, \dots, \lambda_{r+1}, \dots, 0)^T, \dots, \boldsymbol{\lambda}_s = (0, \dots, \lambda_s)^T$  have been chosen as basis for the nullity of the dimension matrix,  $N(A)$ . This represents a proper choice only if the first  $r$  columns of  $A$  are linearly independent, i.e.  $z_1, \dots, z_r$  are dimensionally independent in the sense that their only dimensionless combination is the trivial one ( $\lambda_1 = \dots = \lambda_r = 0$ ). In the language of dimensional analysis,  $z_1, \dots, z_r$  are named ‘‘repeating variables’’. The following dimensionless parameters are thus obtained:

$$\pi_j = z_{r+j} \cdot \prod_{i=1}^r z_i^{k_{r+i,j}} \quad \forall j = 1, \dots, p \quad (1.34)$$

where  $\lambda_{r+j} = 1$ , and  $\lambda_{r+i} = 0$  for each  $i \neq j$ , which represents the easiest choice according to the above definition of the basis of  $N(A)$ .

A proper dimensional analysis and application of Buckingham  $\pi$ -theorem may lead to great simplification of the original dimensional problem, specially in those cases where a deterministic approach seems unrealistic to be applied (e.g. highly turbulent phenomena in hydraulics, such as local scouring). It can sometimes yield strong statements about the irrelevance of some quantities in a problem, or the need for additional parameters. Although in mathematical terms different combinations of dimensionless parameters are equivalent, for the purposes of the experimenter some of them may turn out most representative for the physical process. The relationships expressed by the general dimensionless equations, given in the form of Eq. (1.28), may come from a more detailed analysis of the underlying physics, and sometime arise from integrating differential equations. Dimensional analysis itself has little to say about these relationships, but it is useful to know that the most significant parameters very often are in the same order of magnitude, which does not much differ from unity. This can allow one to judge whether some parameters can be neglected. However the last statement should be considered very carefully, since it is not always possible neglecting dimensionless parameters even if they assume very high or low values, as will become clearer in the next section.

#### **1.4.4 Self-similarity theory**

The concepts here reported are extracted from the fundamental book of *Barenblatt* [1996] on self-similarity. The definition of self-similarity, given by Barenblatt, is that “a phenomenon is called self-similar if the spatial distribution of its properties at various moments of time can be obtained from one another by a similarity transformation”. This definition can obviously been extended to phenomena that do not involve spatial or temporal variables, considering generic spaces of physical quantities at different scales of observation. In a general context, there are several reasons for considering similarity solutions. First, they describe the intermediate asymptotes of a problem: they hold at times when the precise initial conditions are no longer important, but before the system has reached its final steady state. They are also much simpler than the full solutions and so should be easier to understand and study in different regions of parameter space. A final reason for studying them is that, in case the problem deal with differential

equations, they are solutions of a system of ordinary differential equations and hence do not suffer the extra inherent numerical problems of the full partial differential equations.

The dimensionless quantities  $\pi_1, \pi_2, \dots, \pi_n$  are also called similarity parameters, and physical phenomena are termed similar if the dimensionless parameters  $\pi_1, \pi_2, \dots, \pi_n$  are identical. Such a concept is very frequent in experimentation on physical models. The definition of similarity among physical phenomena can be applied to the case of a single phenomenon. Hence, according to the present meaning of similarity and self-similarity, a phenomenon is called self-similar if the distributions of its properties are characterized by transformations for which similarity parameters remain constant. It can be drawn that the nature of the relationships that arise from dimensional analysis is strictly linked to the concept of self-similarity. Self-similar solutions always correspond to idealized problems in which the parameters of the problem that have the dimension of the independent variables (a characteristic length, time, etc.) are equal to zero or infinity. In the non-idealized case, the arguments would include the ratios of the independent variables to these parameters, and there would be no self-similarity. This means that upon the passage from the non-idealized problem statement, corresponding to finite values of the parameter,  $z_n$ , to the idealized one, the dimensionless group,  $\pi_n$ , can tend to zero (or infinity). But what will occur if the dimensionless parameter,  $\pi_n$ , corresponding to the dimensional parameter  $z_n$  is small but finite (or large but finite)? This question is important not only in self-similarity but in every physical investigation, because in mathematical modeling certain factors considered as inessential are often dropped.

In mathematical terms, a phenomenon is defined self-similar in a given dimensionless group,  $\pi_n$ , when the functional relationship  $\pi_0 = f_\pi(\pi_1, \pi_2, \dots, \pi_n)$  representing the physical phenomenon is independent of  $\pi_n$ . The self-similarity solutions of a problem are searched for boundary conditions, i.e. the behavior of  $f_\pi$  is studied for  $\pi_n \rightarrow \infty$  or  $\pi_n \rightarrow 0$ . When the function  $f_\pi$  tends to a finite limit and is different from zero, for  $\pi_n$  approaching zero or infinity, the phenomenon is not influenced by  $\pi_n$ , and it is expressed by the functional relationship  $\pi_0 = f_\pi(\pi_1, \pi_2, \dots, \pi_{n-1})$ . In this case, the self-similarity is named complete self-similarity (CSS) or similarity of the first kind in a given dimensionless group,  $\pi_n$ . In turn, if a complete self-similarity holds, that is:



$$\pi_0 = f_\pi(\pi_1, \pi_2, \dots, \pi_n) \neq 0 \quad (1.35a)$$

is limited for  $\pi_n \rightarrow \infty$  or  $\pi_n \rightarrow 0$ , then

$$\pi_0 = f_{\pi,1}(\pi_1, \pi_2, \dots, \pi_{n-1}) \quad (1.35b)$$

where Eq. (1.35b) represents a self-similar transformation. When the function  $f_\pi$  has a limit equal to zero or is unbounded for  $\pi_n \rightarrow \infty$  or  $\pi_n \rightarrow 0$ , the quantity  $z_n$  remains essential no matter how small or large it becomes. There is however an important exception which leads to an expression formally equal to Eq. (1.35b). Namely, suppose that the function  $f_\pi$  has a power-type asymptotic representation as  $\pi_n$  tends to zero or infinity, then the phenomenon is expressed by the following functional relationship:

$$\pi_0 = \pi_n^\alpha \cdot f_{\pi,1}(\pi_1, \pi_2, \dots, \pi_{n-1}) + o(\pi_n^\alpha) \quad (1.36a)$$

or

$$\pi_0^* = \frac{\pi_0}{\pi_n^\alpha} \cong f_{\pi,1}(\pi_1, \pi_2, \dots, \pi_{n-1}) \quad (1.36b)$$

where

$$\alpha = \alpha(\pi_1, \pi_2, \dots, \pi_{n-1}) \quad (1.36c)$$

Eq. (1.36b) is formally equal to Eq. (1.35b). However,  $\alpha(\pi_1, \pi_2, \dots, \pi_{n-1})$  and, consequently, the dimensionless parameter  $\pi_0^*$  can no longer be obtained from consideration of dimensional analysis alone. Also, the parameter  $\pi_n$  appears in Eq. (1.36b) and hence  $z_n$  does not cease to influence the phenomenon. This instance is named incomplete self-similarity (ISS) or similarity of the second kind in the parameter  $\pi_n$ . If no limit for  $f_\pi$  exists of the above forms, self-similarity may then not exist. The real difficulty is that similarity methods usually apply when the solution of the complete problem is unknown. Hence, a priori, it is not possible to state which type of self-similarity may hold, unless physical considerations allow to formulate some hypotheses in this regard.

Finally, it is observed that in order to determine the functional dependence of some quantity  $z_0$  on each of the physical variables,  $z_1, \dots, z_s$ , it is necessary to either measure or calculate the function  $f_z$  for  $N$  values of each governing parameter. Then it is necessary to carry out a total of  $N^{(r+p)}$  measurements or calculations, where  $p$ ,  $r$  and  $s$  are defined according to section 1.4.3. After applying dimensional analysis, the problem is reduced to one of determining a function  $f_\pi$  of  $p$  dimensionless parameters,  $\pi_1, \pi_2, \dots, \pi_p$ , thus reducing the number of required experiments of a factor  $N^{(r)}$ . If the problem has an explicit mathematical formulation, the independent variables and the constant parameters that appear in the equations, boundary conditions and initially conditions, etc., are adopted as governing parameters. If an explicit mathematical formulation is unknown, the governing parameters are chosen on the basis of a qualitative model of the phenomenon, which each investigator may construct using his/her own experience and intuition, as well as an analysis of previous studies. Once an appropriate class of system of units is chosen, the dimensional problem can be reduced to an equivalent dimensionless functional relationship. Again, it is stressed that, though the sets of resulting parameters are equivalent from a mathematical point of view, still some of them may turn out to be more “physically meaningful”. On the basis of the values and the nature of the similarity parameters, some hypotheses can be formulated in terms of either complete or incomplete self-similarity, in order to either reduce the number of independent variables, or, at least, retrieve some more practical relations.

## **CHAPTER 2 LOCAL SCOURING DOWNSTREAM OF BED SILLS**

### **2.1 INTRODUCTION**

Designers are often required to produce safe and economic structures in rivers with erodible beds, which may frequently induce scouring phenomena as they interfere with the natural stream. As shown in CHAPTER 1, an extensive literature can be found on scouring by jets at high and low head structures, and predictive formulae are given that estimate the equilibrium scour depth of the scour hole, which are most obtained empirically from field and laboratory data. It was discussed that different stages occur during local scour development. These stages basically include an initial rapid phase of severe scouring, followed by a stabilization phase approaching equilibrium conditions after a long time. CHAPTER 2 describes the theoretical basis to deal with long-term local scouring at bed sills under clear-water and steady-flow conditions.

In gravel bed rivers, bed sills are used to limit bed degradation. Local scouring takes place downstream of each sill in addition to the general erosion pattern, and scour hole dimensions increase with the distance between sills. While overall aggradation can be estimated by using 1D morphological models, local scouring requires a more empirical approach. In fact, as previously discussed, most scouring phenomena are induced by turbulent jets that diffuse within the scour hole, by resulting in extremely complex flow fields. Many approaches are fully empirical, being based on curve fitting of experimental data that link scour depth to hydraulic quantities and sediment properties. In the most recent attempts, a semi-empirical approach has been followed, based on the identification of appropriate dimensionless groups using dimensional

analysis before employing best-fitting procedures. A part from the work by *Whittaker* [1987], who first observed the behavior of sills placed in a sequence and proposed an empirical relationship implicitly accounting for the inter-sill distance, all literature on local scouring concerned scours due to drops at single structures. Although useful in many circumstances, these formulae have one key shortcoming. Specifically, formulae obtained for isolated structures neglect the effect of the downstream boundary condition, either by assuming it to be so far downstream as not to influence the scouring process, or by replacing it with another condition, like the water depth downstream of the step. However, it has been shown that the downstream boundary condition cannot be neglected when sequences of steps are considered, as the step height is proportional to the structure spacing. Up to the work by *Gaudio et al.* [2000], no framework could be found to compute the maximum scour depth downstream of bed sills nor to evaluate the influence of the distance between them on the dimensions of the scour hole, due to the lack of specific knowledge on such structures. The theoretical derivations proposed in that work, based on the assumptions of the Buckingham's  $\pi$ -theorem, are discussed in section 2.3, by showing some further insights on the nature and role of the dimensionless parameters that ensued from dimensional analysis. The following section 2.4 revises in terms of self-similarity theory the formal relationships proposed by *Marion et al.* [2004], which account for the effect of the closeness of sills and the gradation of sediments. The analogy is also discussed between artificial sequences of structures and natural step-and-pool sequences. In the last section, preliminary concepts on time development of scouring downstream of bed sills are given, which will be widely described in CHAPTER 5, and which highlight the self-similar nature of scouring in time. Next section presents a brief overview of the use of bed sills and check dams in hydraulic engineering.

### 2.2 GRADE-CONTROL STRUCTURES

Mountain areas experience intense morphological changes in the event of extreme floods. Large water discharges may sometimes be associated to bulky sediment releases, such as triggering of mass movements on catchment sides (e.g. landslides, mudflows). Deposition occurs when sediment yield exceeds the sediment transport capacity of the stream. In order to limit sediment delivery to the downstream reaches, which may cause

flooding of populated areas, sequences of artificial storage volumes are often created using check dams. Various types of full body and permeable (size selective) check dams are encountered in mountain regions. In contrast, mountain rivers that experience sediment transport capacities exceeding the supply from slope erosion are prone to channel incision, and sediments can therefore be entrained from the bed. In such cases there is no need to create storage, but only to inhibit extensive erosion of the bed. A commonly applied measure to control excessive erosion involves the construction of sequences of grade-control transverse structures, forcing the longitudinal profile of the stream to follow a stair-like pattern. These are either check dams if they rise above the original bed level, or bed sills if they are buried into the sediment bulk and the crest rises just at the bed elevation (see Figure 1.1). Traditionally, the prevention of channel erosion is achieved by reducing the mean longitudinal bed slope to a lower value between the works, named final or equilibrium bed slope, which represents a dynamic equilibrium between general scouring and aggradation. Check dams are generally preferred when the river bed elevation is to be raised to reduce bank instability. In a river reach stabilized with check dams, equilibrium is reached through deposition upstream of the body of the structure. As for bed sills a milder slope is reached by rotating the longitudinal profile around the fixed point at the top of the sill. A new equilibrium configuration is obtained by the removal of “wedges” of sediments between the sills. The overall eroded sediment volume is much less than the eroded volume required to obtain the same equilibrium energy slope along the whole reach length. The overall eroded volume is much less than the volume necessary to erode the whole reach down to the equilibrium slope. The ultimate result of both check dams and bed sills is the formation of sequences of steps followed by reaches at a milder slope than the original channel gradient. In order to control the volumes of sediment that can be eroded, artificial steps are normally placed far apart (several tens of meters) in low-gradient channels (slope less than 1%), but close together (a few tens of meters) in high-gradient streams.

Even though the initial dynamics is different for check dams and bed sills, prevailing sedimentation in the former case and erosion in the latter, the overall hydraulic functioning approaches identical patterns at the equilibrium stage. Plunging

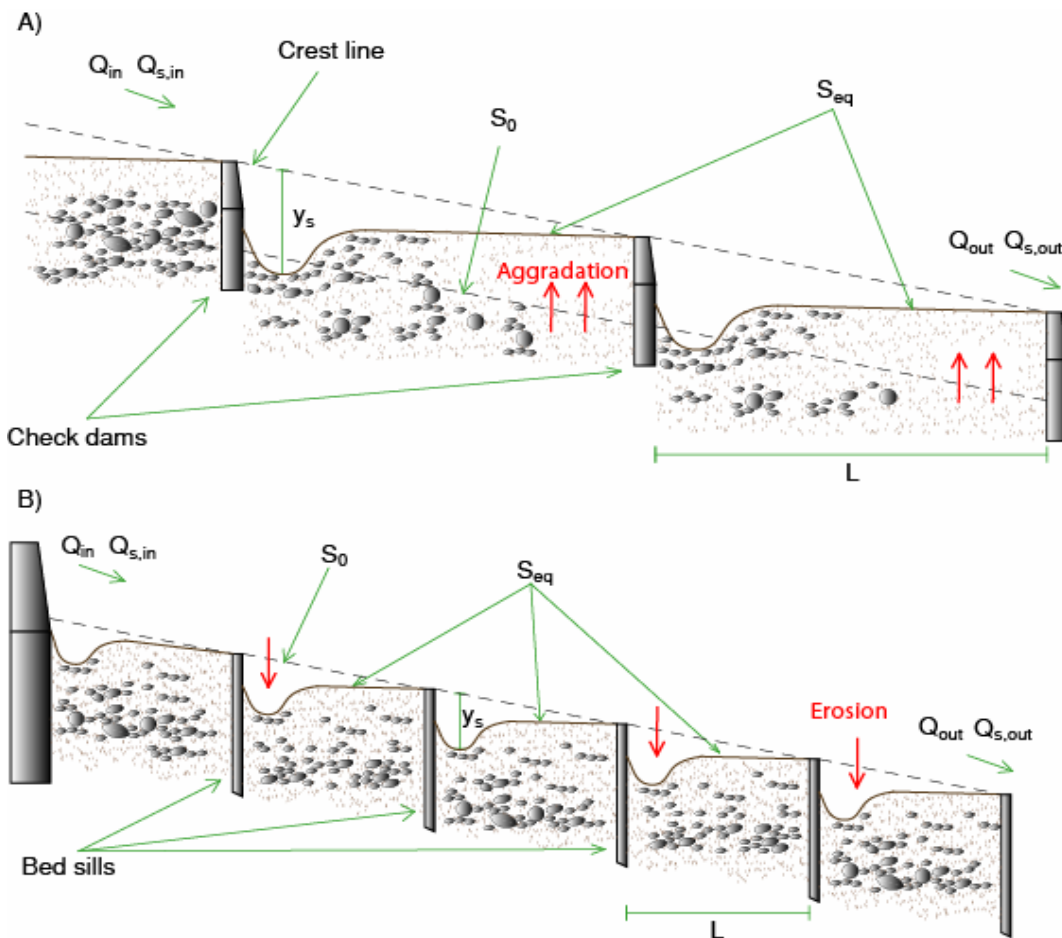


**Figure 2.1 - Hydraulic and morphological functioning of A) check dams; B) bed sills.**

jets issued from work crests diffuse their energy in turbulent rollers inside the pools below. Further downstream, uniform flow can be established if the river bed presents an equilibrium slope for a significant length. This condition is satisfied when the distance between the works is sufficiently large. If subcritical conditions hold in the upstream river reach ( $F_R < 1$ ), flow over work crests features critical conditions at the equilibrium stage ( $F_R = 1$ ). At the edge of the sill, flow becomes supercritical, being accelerated by gravity as an overfall jet. This is usually assumed for natural rivers where bed gradients achieve maximum values in the range of 1-2%. Nevertheless, as shown by laboratory tests (see CHAPTER 3), slightly supercritical conditions may hold for steeper bed slopes ( $F_R \approx 1.1 \div 1.4$ ). In this case supercritical flows achieve the crest of the works before featuring jet characteristics. A sequence of bed sills in a river reach also changes the local characteristics of the flow. Falling jets, free or partially submerged depending on the drop characteristics, cause a local-scouring phenomenon which can be so deep as

to undermine the foundations of the works, leading to failure of the structure. The scour takes place immediately downstream of bed sills and occurs as a consequence of the concentration of energy losses at this location. A reliable prediction of the maximum scour depth is therefore needed to design safe control works for flood events having return periods,  $T_R$ , of about 50 to 100 years.

## 2.3 MAXIMUM SCOUR DEPTH DOWNSTREAM OF BED SILLS

### 2.3.1 Physical definition of scouring

According to *Gaudio et al.* [2000], for a wide channel of constant width the dependence of the equilibrium maximum depth of the scour hole,  $y_s$ , due to flows impinging over uniform sediment beds can be expressed as follows:

$$y_s = f_{y,l} (g, \nu, \rho_w, \rho_s', q, q_{s,in}, h_{u,eq}, D, S_0, S_{eq}, L) \quad (2.1)$$

where  $g$ ,  $\nu$ ,  $\rho_w$ ,  $q$  and  $D$  follow the notation defined in CHAPTER 1;  $\rho_s' = (\rho_s - \rho_w)$  is the submerged density of sediments, being  $\rho_s$  the density of sediments;  $q_{s,in}$  is the volumetric sediment discharge per unit width supplied by the upstream slopes;  $h_{u,eq}$  is the normal water depth at the equilibrium stage;  $S_0$  and  $S_{eq}$  are the initial and equilibrium bed slopes; and  $L$  is the horizontal spacing between sills. This is a general definition of the maximum scour depth, accounting for hydraulic, geometric and sediment properties (see Figure 2.2). For certain conditions, the number of independent variables may be reduced by applying relationships that hold among some of them. When the spacing between sills is large enough, then there should be uniform flow conditions upstream of each sill at the equilibrium stage. For large values of sill spacing  $L$ , a uniform flow depth resistance formula (e.g. Gauckler-Strickler/Manning) can be reasonably used to link the unit discharge,  $q$ , to the normal depth,  $h_{u,eq}$ , and the equilibrium slope,  $S_{eq}$ , as follows:

$$q = \frac{1}{n} h_{u,eq}^{5/3} \cdot S_{eq}^{1/2} \quad (2.2a)$$

$$\frac{1}{n} \sim \frac{1}{D^{1/6}} \quad (2.2b)$$

where  $n$  is the Manning's roughness coefficient. It is noticed that such parameter does not represent a new variable to be introduced in the list of Eq. (2.1), as it is essentially a function of the grain size,  $D$ . This hypothesis holds if the boundary shear stress is mainly linked to single grain properties, as it is usually assumed for gravel beds. In case of developed bed forms,  $n$  can be expressed as a function of empirical relationships that can be found in literature. However, it should be observed that grain-scale dynamics and sediment-flow interactions may affect the morphological properties of the sediment bed, by resulting in increase of boundary roughness and friction coefficients. That is, formulae that are based on simply grain-size relationships, such as Eq. (2.2b) proposed by Strickler, have to be used carefully. In case of experimentations to be carried out based on such relationships, preliminary observations on bed friction are then recommended.

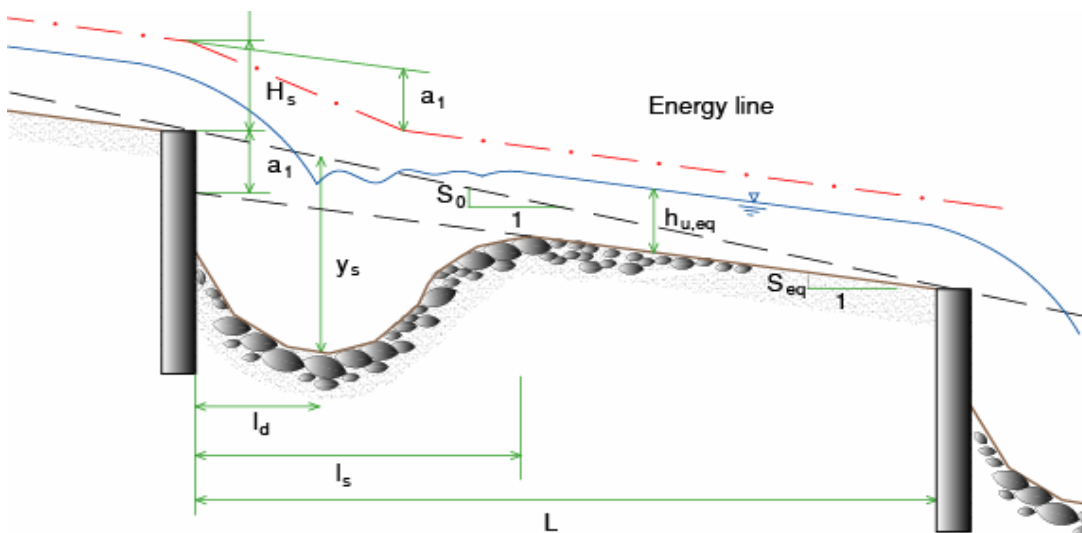


**Figure 2.2 - Schematic of scour hole geometry downstream of bed sills.**

In the initial phase (i.e. when the mean bed slope is  $S_0$ ) the erosive process takes place if the net sediment transport capacity  $q_s' = (q_s - q_{s,in})$  is positive, otherwise aggradation may occur. The sediment transport capacity of the flow,  $q_s$ , can be estimated by applying a sediment transport formula for uniform flow conditions (e.g. the Meyer-Peter-Müller relation). Equilibrium conditions are achieved once  $q_s' = 0$ . The



upstream sediment supply,  $q_{s,in}$ , can then be linked to the hydrodynamics of the flow and the size of the sediments, as follows:

$$q_s = q_{s,in} = f_\theta (S_{eq}, h_{u,eq}, g, \Delta, D) \cong d (\theta - \theta_c)^e \quad (2.3)$$

where  $\theta$  is the dimensionless shear stress or Shields' mobility parameter;  $\theta_c$  is the critical Shields' mobility parameter as defined in section 1.4.1;  $d$  and  $e$  are parameters depending on the sediment transport formula adopted. In cases of no upstream sediment feed ( $q_{s,in} = 0$ ), Eq. (2.3) reduces to the threshold of particle motion for fully developed turbulence flows (e.g. Shields' criterion, 1936), which can be expressed as:

$$\theta = \theta_c = \frac{h_{u,eq} \cdot S_{eq}}{\Delta D} \quad (2.4)$$

*Gaudio et al.* [2000] carried out experiments applying clear-water conditions and analytical derivations neglected the effect due to sediment transport. Sediment supply effect on local scouring will be described in detail in the next CHAPTER 3. Accounting for Eqs. (2.2a) and (2.4), the equilibrium slope and normal depth can be expressed as functions of the flow rate,  $q$ , and the size of sediments,  $D$ :

$$S_{eq} = \frac{\theta_c \Delta D}{h_{u,eq}} \quad (2.5a)$$

$$h_{u,eq} = \frac{(q \cdot n)^{6/7}}{(\theta_c \Delta D)^{3/7}} \quad (2.5b)$$

An important step forward was the introduction of the concept of the morphological jump. This defines a geometrical correspondence between the initial and equilibrium bed slopes and the spacing between sills:

$$a_1 = (S_0 - S_{eq})L \quad (2.6)$$

This relationship permits the removal of both the initial bed slope,  $S_0$ , and the spacing between sills,  $L$ . It may be argued that, by considering the geometry of the system (see Figure 2.2), the influence of these two variables on the scour hole resides essentially in the development of the morphological jump. It is observed that  $a_1$  represents both the head drop from upstream to downstream water levels,  $a_H$ , and the difference in height between the crest of the work and the bottom of the downstream undisturbed bed level,  $a_D$ . In turn, if identical flow conditions are expected upstream and downstream of the scour hole, then the tailwater depth,  $h_0$ , is accounted for by the normal depth,  $h_{u,eq}$ , and approximately all the potential energy at the drop,  $a_1$ , is dissipated by turbulent rollers due to jet impingement within the scour hole. Eq. (2.1) thus reduces to the following:

$$y_s = f_y(g, \nu, \rho_w, \rho_s, q, D, a_1) \quad (2.7)$$

The above general relation holds for clear-water and steady-flow conditions. It is further required that sediments are well sorted, i.e. a single grain size can be assumed as the characteristic size of the whole sediment bulk, and the distance between the sills must be large enough for uniform flow conditions to be established downstream of the scour hole.

### 2.3.2 Dimensional approach

Allowing for the dimensional structure of Eq. (2.7), the application of the Buckingham's  $\pi$ -theorem leads to the identification of the following system of algebraic equations (see section 1.4.3):

$$\begin{aligned} [L]: \quad & \lambda_g + 2\lambda_\nu + 2\lambda_q + \lambda_{a_1} + \lambda_D + \lambda_y = 0 \\ [T]: \quad & -2\lambda_g - \lambda_\nu - \lambda_q = 0 \\ [M]: \quad & \lambda_{\rho_w} + \lambda_{\rho_s} = 0 \end{aligned} \quad (2.8)$$

which represents the matrix equation  $A\lambda = 0$ , where  $\lambda = (\lambda_g, \lambda_\nu, \lambda_{\rho_w}, \lambda_{\rho_s}, \lambda_q, \lambda_D, \lambda_{a_1}, \lambda_y)^T$  is the vector of the exponents of a generic dimensionless combination of the variables listed in Eq. (2.7). Assuming  $g$ ,  $q$  and  $\rho_w$  as repeating variables, that is  $\lambda_w = (0, \lambda_\nu, \dots,$

$0)^T$ ,  $\lambda_{\rho s} = (0, \dots, \lambda_{\rho s}, \dots, 0)^T$ ,  $\lambda_D = (0, \dots, \lambda_D, \dots, 0)^T$ ,  $\lambda_{a1} = (0, \dots, \lambda_{a1}, \dots, 0)^T$  and  $\lambda_y = (0, \dots, \lambda_y)^T$  are chosen as basis for the nullity of the dimension matrix  $N(A)$ , leads to:

$$\begin{aligned} [L]: \quad \lambda_g &= -1/3 \cdot (\lambda_{a1} + \lambda_D + \lambda_y) \\ [T]: \quad \lambda_q &= -2/3 \cdot (\lambda_{a1} + \lambda_D + \lambda_y) - \lambda_v \\ [M]: \quad \lambda_{\rho w} &= -\lambda_{\rho s} \end{aligned} \tag{2.9}$$

According to the results above, if  $|\lambda_v| = |\lambda_{\rho s}| = |\lambda_D| = |\lambda_{a1}| = |\lambda_y| = 1$  (where the notation  $|\lambda|$  stands for modulus of the vector), the following groups can be identified:

$$\pi_v = \frac{q}{v} \tag{2.10a}$$

$$\pi_\rho = \frac{\rho_s'}{\rho_w} \tag{2.10b}$$

$$\pi_D = \frac{\sqrt[3]{q^2 / g}}{D} \tag{2.10c}$$

$$\pi_{a1} = \frac{a_1}{\sqrt[3]{q^2 / g}} \tag{2.10d}$$

$$\pi_y = \frac{y_s}{\sqrt[3]{q^2 / g}} \tag{2.10e}$$

The dimensionless parameters in Eqs. (2.10c) to (2.10e) can be rewritten by introducing the critical specific energy  $H_s = 1.5(q^2/g)^{1/3}$ , which replaces  $g$  in the original list of variables. In this new form,  $\pi_{a1} \equiv a_1/H_s$  is the ratio between the energy dissipated by jet diffusion within the scour hole, which is equal to the morphological jump, and the critical specific energy of the flow;  $\pi_D \equiv H_s/D$  represents the relative roughness; and  $\pi_y \equiv y_s/H_s$  is the dimensionless scour depth. The parameters  $\pi_v = q/v$  and  $\pi_\rho = \rho_s'/\rho_w$  are the Reynolds number of the mean flow,  $R_E$ , and the relative submerged density of sediments,  $\Delta$ , respectively. The original dimensional relationship given in Eq. (2.7) is then rewritten in the following equivalent dimensionless form:

$$\frac{y_s}{H_s} = \Phi_{y,1} \left( \frac{q}{v}, \Delta, \frac{a_1}{H_s}, \frac{H_s}{D} \right) \quad (2.11)$$

Assuming a weak dependence of the scour depth on the Reynolds number in conditions of fully developed turbulent flow, and the relative submerged grain density being constant and equal to approximately 1.63, led the equation below, which is valid for clear-water conditions and uniform sediments:

$$\frac{y_s}{H_s} = \Phi_y \left( \frac{a_1}{H_s}, \frac{H_s}{\Delta D} \right) \quad (2.12a)$$

It is noticed that removing  $R_E$  can be verified a posteriori by data inspection to satisfy the requirements of a complete self-similarity (see section 1.4.4). Carrying out similar derivations leads to an analogous expression for the prediction of the length of the scour hole,  $l_s$ :

$$\frac{l_s}{a_1} = \Phi_x \left( \frac{a_1}{H_s}, \frac{a_1}{\Delta D} \right) \quad (2.12b)$$

which can be obtained by choosing  $a_1$  as repeating variable instead of  $g$ . Such choice will become clearer in next CHAPTER 3.

In their original paper, *Gaudio et al.* [2000] obtained a reduced form of Eq. (2.12a) where the dimensionless scour depth was linearly dependent only on the parameter  $a_1/(\Delta D)$ , which is found by rearranging the original dimensionless groups. This result was validated by experimental evidence from streams with a relatively low gradient ( $S_0 \leq 1.6\%$ ) and relatively large spacing,  $L$ . Later studies by *Lenzi et al.* [2002] on steeper streams ( $S_0$  ranging from 7.8 to 14.8%) proposed a predictive formula accounting for both  $a_1/H_s$  and  $a_1/(\Delta D)$ . However, the order of magnitude of the calibration coefficients, which were obtained by multiple regression analysis of the experimental data, clearly indicate that the influence of  $a_1/(\Delta D)$  could be neglected without significant effect on the results. The main experimental data collected in these studies are reported in Table 2.1 and Table 2.2. Attempts to predict the length of the

scour hole by applying dimensionless relationships in a form different from that given in Eq. (2.12b) generally did not lead to good results.

**Table 2.1 - Data from Gaudio et al. [2004]. Mild-slope tests**

Test #	Q (m <sup>3</sup> /s)	S <sub>0</sub>	S <sub>eq</sub>	a <sub>1</sub> (m)	L (m)	y <sub>s</sub> (m)	H <sub>s</sub> (m)
T04	0.048	1.60%	0.63%	0.029	2.0	0.070	0.123
T05	0.058	1.60%	0.49%	0.032	2.0	0.100	0.140
T06	0.059	1.60%	0.59%	0.042	2.0	0.112	0.142
T08	0.060	1.60%	0.55%	0.021	2.0	0.100	0.143
T09	0.062	1.65%	0.41%	0.057	2.0	0.171	0.146
T11	0.045	1.30%	0.68%	0.037	2.0	0.090	0.118
T12	0.081	1.30%	0.51%	0.027	2.0	0.101	0.175
T13	0.080	1.30%	0.61%	0.053	2.0	0.164	0.173
T14	0.080	1.30%	0.60%	0.044	2.0	0.139	0.173
T15	0.080	1.30%	0.58%	0.035	2.0	0.130	0.173
T16	0.080	1.30%	0.58%	0.018	2.0	0.110	0.173
T22	0.060	0.85%	0.37%	0.039	6.0	0.204	0.143
T23	0.060	0.85%	0.37%	0.032	5.0	0.140	0.143
T24	0.060	0.85%	0.37%	0.019	3.0	0.120	0.143
T25	0.060	0.85%	0.37%	0.035	5.5	0.160	0.143
T26	0.060	0.85%	0.39%	0.042	6.5	0.205	0.143
T27	0.060	1.00%	0.30%	0.051	6.5	0.258	0.143
T28	0.045	1.20%	0.23%	0.061	6.5	0.236	0.118
T29	0.045	1.20%	0.23%	0.061	6.5	0.238	0.118

**Table 2.2 - Data from Lenzi et al. [2002]. Steep-slope tests**

Test #	Q (m <sup>3</sup> /s)	S <sub>0</sub>	S <sub>eq</sub>	a <sub>1</sub> (m)	L (m)	y <sub>s</sub> (m)	H <sub>s</sub> (m)
H1	0.011	7.85%	6.80%	0.011	1.050	0.050	0.049
H2	0.013	7.85%	6.50%	0.014	1.050	0.066	0.053
H3	0.014	7.85%	5.30%	0.027	1.050	0.082	0.058
H4	0.017	7.85%	4.60%	0.034	1.050	0.095	0.064
H5	0.018	7.85%	4.40%	0.036	1.050	0.106	0.066
H6	0.004	11.45%	9.60%	0.019	1.050	0.035	0.026
H7	0.008	11.45%	8.80%	0.028	1.050	0.064	0.038
H8	0.010	11.45%	7.60%	0.040	1.050	0.075	0.045
H9	0.013	11.45%	6.20%	0.055	1.050	0.106	0.053
H10	0.014	11.45%	5.30%	0.065	1.050	0.122	0.058
H11	0.004	14.80%	10.40%	0.046	1.050	0.071	0.025
H12	0.006	14.80%	9.00%	0.061	1.050	0.095	0.033
H13	0.009	14.80%	7.30%	0.079	1.050	0.133	0.043

### 2.3.3 Froude number and jet inclination

For model testing to be used as an acceptable way of estimating prototype scour development, clearly some scaling relationship has to be assumed between the two. This is usually based on the Froude number,  $F_R$ . *Mason and Arumugam* [1985] reported that scaling errors occurred in the formulae accounted for in their comparative study. The Froude scale errors were then compared with the prototype/model errors obtained from

data analysis. The results indicated a clear relationship between the two, confirming the validity of adopting the Froude law as the basis for scaling dimensions linked to local scour phenomena. In the analysis carried out in section 2.3.2, the Froude number,  $F_R$ , did not appear. This is because, at the equilibrium stage, the Froude number can be expressed as a function of the flow rate,  $q$ , and the size of sediments,  $D$ , as follows:

$$F_R = \frac{q}{\sqrt{g h_{u,eq}^3}} = \frac{1}{\sqrt{g q^{2/7}}} \cdot \left( \frac{\theta_c \Delta D}{n^2} \right)^{9/14} \quad (2.13a)$$

Moreover, being  $h_{u,eq}/H_s \sim (F_R)^{-2/3}$ , accounting for Eqs. (2.5b) and (2.13a) leads to the following scaling law:

$$F_R^{-2/3} \sim \left( \frac{H_s}{D} \right)^{2/7} \Rightarrow F_R \sim \left( \frac{D}{H_s} \right)^{3/7} \quad (2.13b)$$

Therefore  $F_R$  is a dependent variable of those listed in Eq. (2.7) and there is no need to include it in the list itself. Also, relationships in the form of Eq. (2.12a) do satisfy a Froude similarity, according to the power-type law given in Eq. (2.13b).

It was mentioned previously that some authors consider that scour depth is affected by the impact angle of the jet, a steep impact angle producing a greater scour depth. Neither the jet inclination is included in the original list of independent variables. Accounting for the dimensional relation of Eq. (1.12) proposed by *Bormann and Julien* [1991] for the jet deflection angle,  $\varphi_{jet}$ , of partially submerged jets, where  $a_1 = a_D$ , and assuming the jet having similar characteristics to the approaching flow, i.e.  $h_{jet} \approx h_{u,eq}$ , lead to:

$$\tan \varphi_{jet} = f \left( \frac{a_1}{H_s}, F_R \right) \quad (2.14a)$$

where

$$h_{jet} \cong h_{u,eq} = \sqrt[3]{\frac{4}{9} H_s} \cdot F_R^{-(2/3)} \quad (2.14b)$$

in which the downstream face angle of the sill is neglected, being  $\varphi_{struct} = \pi/2$ , as well as the ratio of the jet thickness to the tailwater depth, which is considered to assume values very close to the unity. In turn, if Eq. (2.14a) holds, jet inclination is also accounted for in the original analysis, being  $a_1/H_s$  explicitly listed in Eq. (2.11), and  $F_R$  being retrieved as a function of  $H_s/D$ . It is further observed that, if subcritical conditions hold in the in the upstream reach, then critical flow occurs at the sill, by resulting in jet geometries that do not depend upon the Froude number. This point will be widely discussed in CHAPTER 3, where data on scouring due to both subcritical and supercritical flows are examined.

## 2.4 EFFECT OF SILL SPACING AND SEDIMENT SIZE GRADING

### 2.4.1 Geometrical interference

Dimensional analysis proposed in section 2.3 leads to Eqs. (2.12a) and (2.12b) where  $L$  has been suppressed from the list of independent variables. It was stated that this assumption holds if sills spacing is large enough, since at the equilibrium stage  $L$  and  $S_0$  are meaningful only combined together into the morphological jump,  $a_1$ . In this conditions, scour achieves its potential size, being no constrain given at the boundaries. *Lenzi et al.* [2003b] first introduced evidence regarding the disturbance of scour development due to closely spaced sills. If the downstream boundary condition, i.e. the non-erodible point at the subsequent sill position, is closer than a certain critical distance to the scour hole, the size and shape of the scour hole significantly differ compared to those which may form in an unrestricted geometry. This effect, termed geometrical interference, invalidates existing formulae for the special case of closely spaced sills. Such interference mainly affects scouring by reducing the maximum depth and length of the scour hole at the equilibrium stage of the scour process. For this reason, a formal distinction is introduced between the potential maximum scour depth,  $y_s$ , achieved for largely spaced sills and the actual maximum depth of the scour hole,  $y_{s,i}$ , where the  $i$  subscript stands for “interfering” bed sills.

Prediction of the depth of scour requires the development of an appropriate formula that takes into account the possible interference of subsequent sills, as the

spacing  $L$  is insufficient to permit potential scour formation. To allow for the effect of structure spacing, the length  $L$  should be added to the list in Eq. (2.7) as an independent variable, leading to the introduction of a new dimensionless group. The following general relation can be derived by applying dimensional analysis [Marion *et al.*, 2004]:

$$\frac{y_{s,i}}{H_s} = \Phi_{y,2} \left( \frac{a_1}{H_s}, \frac{H_s}{\Delta D}, \frac{L}{H_s} \right) \quad (2.15)$$

Eq. (2.15) should satisfy few constraints in order to be physically meaningful. In particular, for large sill spacing the maximum scour depth will approach its potential value, that is  $y_{s,i} \rightarrow y_s$  for  $L \rightarrow \infty$ ; for small values of the inter-sill distance,  $L$ , scouring almost does not take place and  $y_{s,i} \rightarrow 0$ . In turn, it follows:

$$\frac{y_{s,i}}{H_s} = \begin{cases} y_s / H_s & \text{for } L / H_s \rightarrow \infty \\ 0 & \text{for } L / H_s \rightarrow 0 \end{cases} \quad (2.16)$$

Regarding Eq. (2.12a) as a self-similar transformation of the idealized non-interfering scour process, the first limit of Eq. (2.16) satisfies the requirements of a complete self-similarity or similarity of the first kind in  $L/H_s$ , i.e.  $y_{s,i}/H_s$  is independent of  $L/H_s$  for  $L/H_s \gg 1$ . This condition does not hold for the lower limit, however the hypothesis of an incomplete self-similarity may be formulated for  $L/H_s \rightarrow 0$ . Assuming a smooth behavior of the function  $y_{s,i}/H_s$ , then Eq. (2.15) can be rewritten as the product of two functions:

$$\frac{y_{s,i}}{H_s} = \Phi_y \left( \frac{a_1}{H_s}, \frac{H_s}{\Delta D} \right) \cdot \begin{cases} (L/H_s)^\beta & \text{for } L/H_s < 10^{-1} \\ \Phi_L & \text{for } 10^{-1} < L/H_s < 10^1 \div 10^2 \\ 1 & \text{for } L/H_s > 10^1 \div 10^2 \end{cases} \quad (2.17)$$

where  $\Phi_L$  is assumed to be an exponentially damped function which approaches asymptotically the unity, and  $\Phi_L \leq 1$  for  $0 < L/H_s < \infty$ . However, for real cases geometrical interference is expected to be meaningful for  $L/H_s > 1$ , therefore  $(L/H_s)^\beta$  can be replaced by  $\Phi_L$ . At the limits of the domain the function must be defined as follows:



$$\Phi_L \left( \frac{L}{H_s} \right) = \begin{cases} 1 & \text{for } L/H_s \rightarrow \infty \\ 0 & \text{for } L/H_s \rightarrow 0 \end{cases} \quad (2.18)$$

*Marion et al.* [2004] proposed the following expression for  $\Phi_L$ , which was calibrated on the basis of experimental data from the work by *Lenzi et al.* [2002, 2003b] and new data presented in that work (see data reported from Table 2.3 to Table 2.5):

$$\Phi_L = 1 - \exp \left( -\beta_y \frac{L}{H_s} \right) \quad (2.19)$$

where  $\beta_y$  is a calibration exponent. It is noticed that  $\beta_y$  may depend on both  $a_1/H_s$  and  $H_s/D$ . However, the data obtained on tests on scour hole interference led to a constant value  $\beta_y = 0.14$ . The effect of the geometrical interference is shown in Figure 2.3, where non-interfering data from *Gaudio et al.* [2000] are also displayed. The vertical y-axes expresses the reduction of the ratio of actual to potential scour depth. The latter was evaluated by *Marion et al.* [2004] using predictive formulae for non-interfering scours. The vertical dashed line delimits the range  $L/H_s < 15$  where interference is clearly present. The horizontal dashed line marks the ideal non-interference condition (i.e., ratio of actual to potential scour depth = 1).

**Table 2.3 - Data from Lenzi et al. [2003b]. Interfering tests**

Test #	Q (m <sup>3</sup> /s)	S <sub>0</sub>	S <sub>eq</sub>	a <sub>l</sub> (m)	L (m)	y <sub>s</sub> (m)	H <sub>s</sub> (m)
T14	0.011	7.85%	6.80%	0.011	1.050	0.050	0.049
T15	0.013	7.85%	6.50%	0.014	1.050	0.066	0.053
T16	0.014	7.85%	5.30%	0.027	1.050	0.082	0.058
T17	0.017	7.85%	4.60%	0.034	1.050	0.095	0.064
T18	0.018	7.85%	4.40%	0.036	1.050	0.106	0.066
T19	0.004	11.45%	9.60%	0.019	1.050	0.035	0.026
T20	0.008	11.45%	8.80%	0.028	1.050	0.064	0.038
T21	0.010	11.45%	7.60%	0.040	1.050	0.075	0.045
T22	0.013	11.45%	6.20%	0.055	1.050	0.106	0.053
T23	0.014	11.45%	5.30%	0.065	1.050	0.122	0.058
T24	0.004	14.80%	10.40%	0.046	1.050	0.071	0.025
T25	0.006	14.80%	9.00%	0.061	1.050	0.095	0.033
T26	0.009	14.80%	7.30%	0.079	1.050	0.133	0.043

The ratio  $L/H_s$  was obtained from dimensional derivations and defined as the new dimensionless group allowing for geometrical interference, with no regard to its actual

effect on scouring. From a physical point of view, this parameter seems to represent properly the disturbance due to the closeness of sills. For a given flow rate,  $q$ , the critical specific energy,  $H_s$ , is constant. Then, the interference of sills will reduce as  $L$  increases, and the scour hole will achieve its potential size as  $L$  becomes greater than a critical threshold. On the other hand, for a given constant value of  $L$ , decreasing flow rates lead to smaller values of both  $a_1 = (S_0 - S_{eq})L$ , being  $S_{eq} \approx q^{-6/7}$  according to Eq. (2.5a), and  $H_s = 1.5(q^2/g)^{1/3}$ . Allowing for Eqs. (2.12a) and (2.12b), it is then expected that scour size will reduce, approaching the non-scouring critical condition for  $S_{eq} \rightarrow S_0$ , by resulting in non-interfering geometries of the sequence of bed sills. In turn, geometrical interference is not merely dependent on the sill distance,  $L$ , but it is a function of the interaction between geometry and flow characteristics, which is well represented by the ratio  $L/H_s$ .

**Table 2.4 - Data from Marion et al. [2004]. Non interfering tests**

Test #	Q (m <sup>3</sup> /s)	S <sub>0</sub>	S <sub>eq</sub>	a <sub>1</sub> (m)	L (m)	y <sub>s</sub> (m)	H <sub>s</sub> (m)
7-S1	0.030	6.20%	1.85%	0.076	1.75	0.298	0.108
8-S1	0.025	6.20%	2.40%	0.067	1.75	0.235	0.095
9-S1	0.015	6.20%	4.46%	0.030	1.75	0.159	0.068
10-S1	0.012	6.20%	5.24%	0.017	1.75	0.096	0.058
11-S1	0.020	6.20%	3.87%	0.041	1.75	0.181	0.083
12-S1	0.020	8.00%	2.52%	0.096	1.75	0.232	0.082
13-S1	0.015	8.00%	3.77%	0.074	1.75	0.191	0.068
14-S1	0.025	8.00%	2.05%	0.104	1.75	0.256	0.095
15-S1	0.030	8.00%	1.61%	0.112	1.75	0.275	0.108
16-S1	0.018	8.00%	2.87%	0.090	1.75	0.209	0.075
17-S1	0.009	8.00%	5.60%	0.042	1.75	0.108	0.047
18-S1	0.017	4.50%	3.60%	0.016	1.75	0.078	0.073
19-S1	0.024	4.50%	3.15%	0.024	1.75	0.126	0.092
20-S1	0.027	4.50%	2.22%	0.040	1.75	0.163	0.100
21-S1	0.020	4.50%	3.39%	0.019	1.75	0.126	0.082
22-S1	0.030	4.50%	1.80%	0.047	1.75	0.167	0.108
23-M3	0.028	6.20%	2.65%	0.053	1.50	0.240	0.103
23-M4	0.028	6.20%	1.85%	0.065	1.50	0.237	0.103
24-M3	0.018	6.20%	3.97%	0.033	1.50	0.169	0.076
24-M4	0.018	6.20%	2.93%	0.049	1.50	0.170	0.076
25-M3	0.023	6.20%	2.37%	0.057	1.50	0.207	0.089
25-M4	0.023	6.20%	1.49%	0.071	1.50	0.201	0.089
26-M3	0.023	8.00%	2.23%	0.087	1.50	0.243	0.089
26-M4	0.023	8.00%	1.83%	0.093	1.50	0.250	0.089
27-M3	0.018	8.00%	2.00%	0.090	1.50	0.207	0.075
27-M4	0.018	8.00%	3.01%	0.075	1.50	0.202	0.075
28-M3	0.028	8.00%	0.40%	0.115	1.50	0.276	0.101
28-M4	0.028	8.00%	0.96%	0.106	1.50	0.263	0.101

**Table 2.5 - Data from Marion et al. [2004]. Interfering tests**

Test #	Q (m <sup>3</sup> /s)	S <sub>0</sub>	S <sub>eq</sub>	a <sub>1</sub> (m)	L (m)	y <sub>s</sub> (m)	H <sub>s</sub> (m)
7-S2	0.030	6.20%	0.00%	0.047	0.75	0.172	0.108
8-S2	0.025	6.20%	0.00%	0.047	0.75	0.138	0.095
9-S2	0.015	6.20%	3.87%	0.017	0.75	0.063	0.068
10-S2	0.012	6.20%	0.00%	0.047	0.75	0.097	0.058
11-S2	0.020	6.20%	0.00%	0.047	0.75	0.121	0.083
12-S2	0.020	8.00%	0.00%	0.060	0.75	0.156	0.082
13-S2	0.015	8.00%	0.00%	0.060	0.75	0.147	0.068
14-S2	0.025	8.00%	0.00%	0.060	0.75	0.165	0.095
15-S2	0.030	8.00%	0.00%	0.060	0.75	0.173	0.108
16-S2	0.018	8.00%	0.00%	0.060	0.75	0.139	0.075
17-S2	0.009	8.00%	5.60%	0.018	0.75	0.061	0.047
18-S2	0.017	4.50%	3.60%	0.007	0.75	0.047	0.073
19-S2	0.024	4.50%	3.15%	0.010	0.75	0.061	0.092
20-S2	0.027	4.50%	0.99%	0.026	0.75	0.063	0.100
21-S2	0.020	4.50%	2.73%	0.013	0.75	0.051	0.082
22-S2	0.031	4.50%	0.00%	0.034	0.75	0.077	0.109
7-S3	0.030	6.20%	0.00%	0.047	0.75	0.160	0.108
8-S3	0.025	6.20%	0.00%	0.047	0.75	0.126	0.095
9-S3	0.015	6.20%	3.63%	0.019	0.75	0.064	0.068
10-S3	0.012	6.20%	5.00%	0.009	0.75	0.047	0.058
11-S3	0.020	6.20%	0.00%	0.047	0.75	0.115	0.083
12-S3	0.020	8.00%	0.00%	0.060	0.75	0.152	0.082
13-S3	0.015	8.00%	0.00%	0.060	0.75	0.117	0.068
14-S3	0.025	8.00%	0.00%	0.060	0.75	0.165	0.095
15-S3	0.030	8.00%	0.00%	0.060	0.75	0.202	0.108
16-S3	0.018	8.00%	0.00%	0.060	0.75	0.123	0.075
17-S3	0.009	8.00%	5.60%	0.018	0.75	0.059	0.047
18-S3	0.017	4.50%	3.60%	0.007	0.75	0.045	0.073
19-S3	0.024	4.50%	3.15%	0.010	0.75	0.051	0.092
20-S3	0.027	4.50%	0.99%	0.026	0.75	0.057	0.100
21-S3	0.020	4.50%	2.44%	0.015	0.75	0.049	0.082
22-S3	0.031	4.50%	0.00%	0.034	0.75	0.067	0.109
7-S4	0.030	6.20%	0.00%	0.031	0.50	0.070	0.108
8-S4	0.025	6.20%	0.00%	0.031	0.50	0.072	0.095
9-S4	0.015	6.20%	3.73%	0.012	0.50	0.046	0.068
10-S4	0.012	6.20%	2.11%	0.020	0.50	0.041	0.058
11-S4	0.020	6.21%	0.00%	0.031	0.50	0.055	0.083
12-S4	0.020	8.00%	0.00%	0.040	0.50	0.114	0.082
13-S4	0.015	8.00%	0.00%	0.040	0.50	0.102	0.068
14-S4	0.025	8.00%	0.00%	0.040	0.50	0.113	0.095
15-S4	0.030	8.00%	0.00%	0.040	0.50	0.107	0.108
16-S4	0.018	8.00%	0.00%	0.040	0.50	0.096	0.075
17-S4	0.009	8.00%	5.60%	0.012	0.50	0.050	0.047
18-S4	0.017	4.50%	0.00%	0.023	0.50	0.046	0.073
19-S4	0.024	4.50%	0.00%	0.023	0.50	0.024	0.092
20-S4	0.027	4.50%	0.00%	0.023	0.50	0.046	0.100
21-S4	0.020	4.50%	0.00%	0.023	0.50	0.051	0.082
22-S4	0.031	4.50%	0.00%	0.023	0.50	0.053	0.109
23-M1	0.028	6.20%	0.00%	0.031	0.50	0.079	0.103
23-M2	0.028	6.20%	0.00%	0.031	0.50	0.080	0.103
24-M1	0.018	6.20%	0.00%	0.031	0.50	0.105	0.076
24-M2	0.018	6.20%	0.00%	0.031	0.50	0.053	0.076
25-M1	0.023	6.20%	0.00%	0.031	0.50	0.082	0.089
25-M2	0.023	6.20%	0.00%	0.031	0.50	0.069	0.089

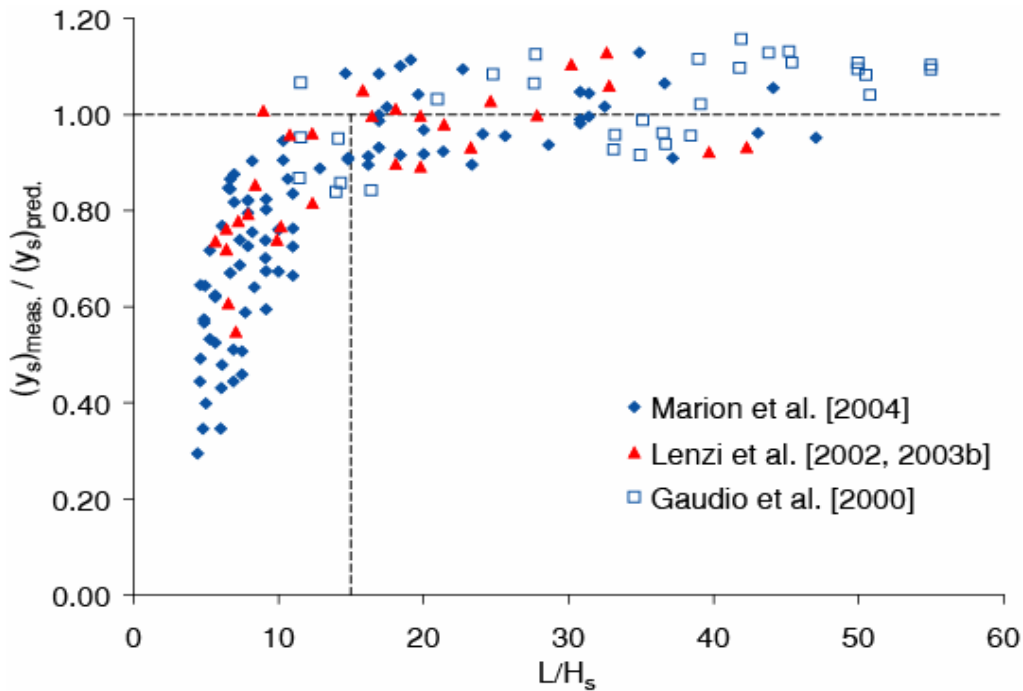


Figure 2.3 - Effect of geometrical interference on local scouring. Modified after Marion et al. [2004].

From an energetic point of view, assuming at the equilibrium a steady and quasi-uniform flow along the staircase-like sequence of bed sills, the product:

$$E_H = S_0 L = a_1 + S_{eq} l_s + S_{eq} (L - l_s) \quad (2.20)$$

represents the stream potential energy which must be dissipated along the distance  $L$  between two sills. The height  $a_1$  is roughly the drop energy associated with the free jet impinging into the pool tailwater. Approximately, the drop energy  $a_1$  is locally dissipated in the scour hole whereas the remaining  $E_H - a_1$  potential energy is more widely dissipated downstream as the water flows past the sloping bed (see energy line in Figure 2.2). If this regular bed span is long enough, the water-level slope attains the value  $S_{eq}$ , indicating that steady, uniform flow is then established. The passage between the complex hydrodynamics within the scour hole and the uniform flow is rather smooth and a transition zone is observed where flow convergence occurs and the bed gradually reaches the downstream final slope. A complete dissipation of the drop energy  $a_1$  requires the scour to achieve its potential size, i.e.:

$$a_1 \Leftrightarrow (y_s, l_s) \quad (2.21)$$

Geometrical interference induces an altered flow pattern, and consequently reduced scour size. The drop energy associated with the free jet impinging into the pool tailwater is only partially dissipated into the scour hole. This residual potential energy may cause undesired excessive erosion along the downstream reach. Therefore, for practical purposes bed sills should be designed accounting for this constraint, and the threshold shown in Figure 2.3 is to be considered as the lower limit for sill spacing.

#### 2.4.2 Non-uniform sediments

Comparing experimental results obtained for well-graded sediments [Lenzi *et al.*, 2002] and the data relevant to a well-sorted mixture [Marion *et al.*, 2004] indicates a significant effect of the mixture composition on the final size of the scour downstream of bed sills. The effect is to be attributed not only to the potential to develop armoring (i.e. coarsening) of the bed surface in the scour hole, which is a typical phenomenon in degrading beds [Ashida and Michiue, 1971], but also to the adjusted particle mobility determined by the different exposure of particles to the flow [e.g., Andrews and Parker, 1987].

Laboratory tests are usually carried out within idealized conditions, that is uniform sediments are used with relative small values of the mean diameter of the grains,  $D$ , compared with the tailwater depth,  $h_0$ , and then micro-roughness conditions hold. This may affect the prediction of empirical relationships obtained in such a controlled environments, when applied to natural high-gradient streams, where sediment size may varies a few orders of magnitude, ranging from fine sand to coarse gravel, cobbles and boulders. It is expected that macro-roughness conditions hold for almost all flow regimes. Equilibrium bed slope,  $S_{eq}$ , is usually computed on the basis of Shields' criterion. Corrective coefficients should be introduced in case of non-uniform sediments, both for incipient motion conditions and fully developed transport [Proffitt and Sutherland, 1983; Wilcock and Crowe, 2003]. It is well known that tendency to grain mobility is reduced when the ratio  $h_0/D$  decreases [e.g. Shvidchenko and Pender, 2000]. This effect can be accounted for, for example, by adopting the following relationship [Armanini, 2005]:

$$\theta_{c,nu} = \theta_c \cdot \left(1 + 0.67\sqrt{D/h_0}\right) \quad (2.22)$$

in which the “*nu*” subscript stands for “non-uniform” sediments.

In terms of particle stability, assuming that sediments have a single grain size involves the identification of the same length scale,  $D$ , for both driving and resisting forces. For non-uniform sediments the length scale affecting the hydraulic behavior of rough boundaries is different from the actual size of the sediments. Such hydraulic behavior can be represented by that of a uniform sediment bed characterized by an equivalent grain size,  $D_s$ . It is expected that coarser grains most affect wall roughness. Many studies on this topic suggested values of the equivalent diameter greater than  $D_{50}$ . *Einstein* [1950] proposed  $D_{65}$ , which is mostly accepted as reference value, while *Meyer-Peter and Müller* [1948] adopted  $D_{90}$ . Neglecting the effects due to grain shape, it is drawn that for  $D = D_s$  grains experience hydrodynamic conditions similar to those for uniform sediment beds. For  $D > D_s$  grains rise above the mean bed surface, being more exposed to flow entrainment. These particles will be mobilized for values of the Shields’ mobility parameter,  $\theta_{c,nu}$ , smaller than the critical value,  $\theta_c$ . By contrast, for  $D < D_s$  grains are subjected to weaker driving forces when compared to uniform sediment conditions, as they are mostly displaced within the viscous boundary layer. Such a behavior is known as “hiding and exposure” effect, being the former referred to fine sediments and the latter to the coarser ones. *Egiazaroff* [1965] theoretically derived a relationship accounting for the physical phenomena shortly described above. Assuming the mean grain size,  $D_m$ , as the equivalent roughness length, the hiding and exposure effect can be accounted for as follows:

$$\theta_{c,nu} = \xi_c \cdot \theta_c = \xi_c \cdot \frac{\tau_c}{(\gamma_s - \gamma)D} \quad (2.23a)$$

where

$$\xi_c = \xi_c \cdot \left[ \frac{\ln 19}{\ln(19D/D_m)} \right]^2 \quad (2.23b)$$

Although the hiding and exposure effect tends to mitigate the different mobility of fine and coarse sediments, still smaller particles are more inclined to be entrained by the flow, and sediment bed becomes coarser. Such well known phenomenon, which is termed armoring, is typical of natural water-worked sediment beds, especially if the lack of upstream sediment supply induces degradation of the longitudinal river-bed profile. If this process lasts for long time, all small particles are entrained from the bed surface, and coarse particles form an armor layer that protects from entrainment the finer sediment in the sub-layer. As a consequence, surface roughness increases affecting the flow characteristics. Equilibrium bed slope can be roughly approximated by using  $D_{90}$  in Eqs. (2.5a) and (2.5b). Similar processes may be expected within the scour hole, where severe scouring occurs, and armoring may develop even more intensely than for bed degradation. A deep discussion upon these phenomena goes beyond the purposes of the present analysis. According to *Marion et al.* [2004] the effect of non-uniform sediments is considered to be physically explained by using the momentum of the first and second order of the grain size distribution, i.e. the geometric mean size,  $D_{50}$ , and standard deviation,  $\sigma_g$ . The latter was substituted by the sorting index,  $SI$ , which is equal to the geometric standard deviation,  $\sigma_g$ , only for log-normal distributions (that usually approach grain-size distributions), and it is defined as:

$$SI = \frac{1}{2} \left( \frac{D_{84}}{D_{50}} + \frac{D_{50}}{D_{16}} \right) \quad (2.24)$$

In order to account for the effect of non-uniform sediments, the parameter  $SI$  is added to the list in Eq. (2.7) as an independent dimensionless group, leading to:

$$\frac{y_{s,nu}}{H_s} = \Phi_{y,3} \left( \frac{a_1}{H_s}, \frac{H_s}{\Delta D}, SI \right) \quad (2.25)$$

Allowing for the physical meaning of Eq. (2.25), it is expected that for  $SI = 1$  the relation for uniform sediments must be retrieved, which means  $y_{s,nu} = y_s$ . For the largest values of the sorting index small depths will develop, almost approaching non-scouring conditions, that is  $y_{s,nu} \rightarrow 0$  for  $SI \rightarrow \infty$ . In turn, it follows:

$$\frac{y_{s,nu}}{H_s} = \begin{cases} y_s / H_s & \text{for } SI = 1 \\ 0 & \text{for } SI \rightarrow \infty \end{cases} \quad (2.26)$$

Following arguments similar to those presented in the previous section, the limit in Eq. (2.26) does not satisfy the requirements of a complete self-similarity for  $SI \rightarrow \infty$ . A similarity of the second kind or incomplete self-similarity in  $SI$  is hypothesized in this case for  $SI \gg 1$ , while a complete self-similarity clearly holds for  $SI \sim 1$ . Since a power-type representation satisfies also the constraint for  $SI = 1$ , such law is assumed to hold all over the range of  $SI$ , being strictly valid only for  $SI \gg 1$ . Then Eq. (2.25) can be rewritten as follows:

$$\frac{y_{s,nu}}{H_s} = \Phi_y \left( \frac{a_1}{H_s}, \frac{H_s}{\Delta D} \right) \cdot \Phi_{SI} \quad (2.27a)$$

where

$$\Phi_{SI} = SI^{-\alpha_y} \quad (2.27b)$$

and

$$\alpha_y = \alpha_y \left( \frac{a_1}{H_s}, \frac{H_s}{\Delta D} \right) \quad (2.27c)$$

The value of  $\alpha_y$  was assumed constant and calibrated by *Marion et al.* [2004] on the basis of experimental data for both uniform and non-uniform sediments. They found that  $\alpha_y = 0.19$  led to a satisfying prediction of the data.

It is interesting to note that scouring is more affected by sorting than by the actual size of sediment in its own. In fact, as anticipated in the previous section and will be discussed later on, the group  $H_s/D$  is much less significant in determining the maximum scour depth than  $a_1/H_s$  is. From a physical point of view, this can be explained by considering that the effect of sediment size is also accounted for by the parameter  $a_1/H_s$ , being the equilibrium bed slope,  $S_{eq}$ , dependent on the grain diameter,  $D$ . If corrective coefficients as given in Eqs. (2.22) and (2.23a) are applied and  $D_{90}$  is used as the characteristic grain size, then particular phenomena due to relative submergence (which is linked to  $H_s/D$ ), hiding and exposure effect, and coarsening of sediment bed can be



taken into account in terms of equilibrium bed slope. However, as stated above, sediment sorting may cause armoring to develop even more intensely within the scour hole than along the longitudinal bed profile. This may explain the reason why sorting affects scouring more than the characteristic size does.

Although Eqs. (2.27a) and (2.27b) were originally derived on the basis of experimental evidence, the physical nature of  $SI$  and its effect on scouring and the hypothesis of an incomplete self-similarity in  $SI$ , which have been discussed here, established that such equations represent a proper formulation to explain how sediment sorting affect local scouring. Eq. (2.27c) shows a dependency of  $\alpha_y$  on the original parameters, which are used to predict non-interfering scours in uniform sediment beds. Despite experimental evidence, such relation may not be neglected and further inspection of data or new data set on non-uniform sediments may lead to a non-constant behavior of  $\alpha_y$ . In fact, assuming that sediment sorting mainly affects scouring in terms of armoring, such process depends not only on  $SI$ , but also on how deep and how intense is scouring, i.e. on the value of  $y_s$ , and thereafter on  $a_1/H_s$  (and  $H_s/D$ ). Thus it is expected that scour hole size is reduced, when compared to uniform sediment conditions, because of the effect of armoring, which is directly caused by  $SI$ , and more weakly by an increase of  $\alpha_y$  with  $a_1/H_s$ .

### 2.4.3 Analogy between bed sills and step-and-pools

High-gradient streams often naturally exhibit a similar step-and-pool architecture, which likely represents self adjustment of the stream towards a condition of higher bed stability [Wohl *et al.*, 1997; Chin, 1999; Lenzi, 2002]. These natural structures are usually associated with an altered flow pattern, termed tumbling flow, forming sequences of free impinging jets and submerged hydraulic jumps. Some authors [Whittaker and Jaeggi, 1982; Whittaker, 1987] stated that step-and-pools behave as stable structures for return periods,  $T_R$ , of about 30 to 40 years. In case of extreme events, failure may occur due to boulder undermining, by resulting in headcut downstream migration. Toe scouring at pools has been observed to be a primary factor in the destruction of steps, both in the field [Lenzi, 2001] and in the laboratory [Lenzi and Comiti, 2003], where about 76 per cent of all step break-ups were due to pool scouring. More rarely failure can be due to lateral bank erosion or entrainment of the boulders that form the structure. After extreme events, stable natural morphological

structures reform that are in equilibrium with hydrodynamic conditions relevant to ordinary floods. Accordingly, mimicking natural step-and-pool systems by using sequences of artificial check dams or bed sills might grant channel beds with better stability and resistance against erosion. Further understanding of the natural shapes of step-and-pool systems is expected to provide enhanced design guidance for artificial control structures, the better to reproduce a stream profile that should be as close as possible to a natural configuration.

From Figure 2.3 it appears that interference onsets when the ratio  $L/H_s$  is smaller than about 15, independent of sediment size and grading. Typically, natural step-and-pool sequences have step spacing in accordance within the above range during high flows, when the parameter  $L/H_s$  in such a natural tumbling flow pattern becomes very small, as long as the steps are not destroyed. *Comiti* [2003] carried out field measurements on natural channels of the Italian Alps (with mean gradients ranging from 7 to 16%) and found an average value of  $L/H_s = 6.5$ , when assuming bankfull conditions for the estimation of the formative flow rate. Eqs. (2.17) and (2.19) might in part explain the great stability of these step-and-pool sequences. In fact, the dimensional and geometrical analogies between scour pools below grade-control structures (i.e. bed sills and check dams) and pools below natural steps were found to be statistically significant by *Comiti* [2003]. However, interference phenomena might be less important in natural step-and-pool systems where typically the coarse particles forming the bottom of pools are very large compared to pool dimensions, which is different from the experimental flume situations where  $L/D_{90} \gg L/H_s$ . Moreover, as discussed in section 2.4.1, despite the increase in bed stability exhibited by this particular morphological pattern, some issues arise concerning the amount of energy dissipated within a step-and-pool sequence. In turn, the likely “release” of residual energy in the downstream reaches, where river morphology resembles more common patterns, should induce the designer to carefully evaluate whether an interfering-type sequence of structures is to be used (better resistance of the stabilized reach) or avoided (likely flow energy excess in the downstream reaches).

## 2.5 SIMILARITY OF SCOURING IN TIME

It was already discussed that different stages occur during local scouring development, and there are real cases in which the time factor is important, although often only the maximum scour depth in the equilibrium phase is relevant. *Gaudio and Marion* [2003] carried out experimental tests on scour development downstream of bed sills with steady-flow and clear-water conditions on uniform sediment beds. They defined a time scale for the specific phenomenon, named the morphological time,  $t_\xi = T_s$ , and proposed the following relationship:

$$\frac{y_s(t)}{y_s} = \Phi_T \left( \frac{t}{T_s} \right) \quad (2.28a)$$

where

$$\Phi_T = 1 - \exp \left( -\gamma_y \frac{t}{T_s} \right) \quad (2.28b)$$

in which the calibration coefficient  $\gamma_y$  was assumed constant and was found equal to 0.41. The physical definition of morphological time will be given and discussed in CHAPTER 5, where the more general case of scour development under unsteady flows is dealt with. At this stage we are more interested on the nature of Eqs. (2.28a) and (2.28b) and we have only to say that the definition of  $T_s$  is not based, a priori, on any particular length scale. From the general relationship expressed by Eq. (1.1), given in Chapter 1 for the time development local of scouring, it follows:

$$\gamma_y = -\ln \left[ 1 - \frac{y_s(T_s)}{y_s} \right] \quad (2.29)$$

i.e., accounting for the experimental value of  $\gamma_y$ , it results  $y_\xi = y_s(T_s) \approx y_s/3$ , which does not match but it is not that far from the value of  $a_1$ , as can be drawn by direct comparison of experimental data. Allowing for the definition of morphological jump, the physical meaning of this outcome is that the time development of local scouring downstream of bed sills is somehow related to the time needed for the general

aggradation to achieve an equilibrium bed slope,  $S_{eq}$ . Indeed, scouring downstream of bed sills is the result of plunging jet diffusion within the scour hole and the general erosion occurring between two subsequent sills. By comparing Eq. (1.1) and Eq. (2.28b) it can be seen that the exponent  $\xi$  of the dimensionless temporal parameter,  $t/t_\xi = t/T_s$ , is equal to 1 in this case, contrasting the results obtained for other type of scour processes which report  $\xi = 0.3-0.5$ . Again, this reflects the dual nature of scouring at sills, for which the initial phase, namely  $t < T_s$ , turns out to be relatively slower compared with different kind of scouring, since general aggradation has to occur before local scouring can fully develop. This is somehow “compensate” by a subsequent relatively faster development phase, when general erosion has already achieved an equilibrium stage, and scouring progresses with typical mechanisms due to jet impingement.

It is now stressed that relationships in the form of Eq. (2.28a) show (or assume) a self-similar behavior of scouring in time, that is the temporal trends of different scours collapse along a single dimensionless curve. In general the function representing  $y_s(t)/H_s$  depends upon the same parameters obtained from dimensional analysis for the maximum scour depth at the equilibrium stage and the new dimensionless group  $t/T_s$ . Assuming a solution of the form of Eq. (2.28a) involves a strong statement on the similarity of the process. Indeed, as independently obtained by *Breusers* [1967] and showed in Eq. (1.2), following similar arguments to those discussed in the previous sections leads to formulate an hypothesis of incomplete self-similarity in  $t/T_s$  for  $t \ll T_s$ , expressed as:

$$\frac{y_s(t)}{H_s} = (1 - e^{-\gamma_y}) \cdot \left(\frac{t}{T_s}\right)^\xi \cdot \Phi_y \left( \frac{a_1}{H_s}, \frac{H_s}{\Delta D} \right)$$

where the coefficient  $1 - \exp(-\gamma_y) = \gamma_y^\xi / y_s$  rises from having chosen  $y_s$  and  $T_s$  as spatial and temporal scales, respectively, being  $\gamma_y = y_s(T_s)$ . The experimental findings by *Gaudio and Marion* [2003], according to which  $\xi = 1$  for scouring at bed sills, can be reasonably verified to hold observing the trend in Figure 2.4 for the smallest values of  $t/T_s$ .

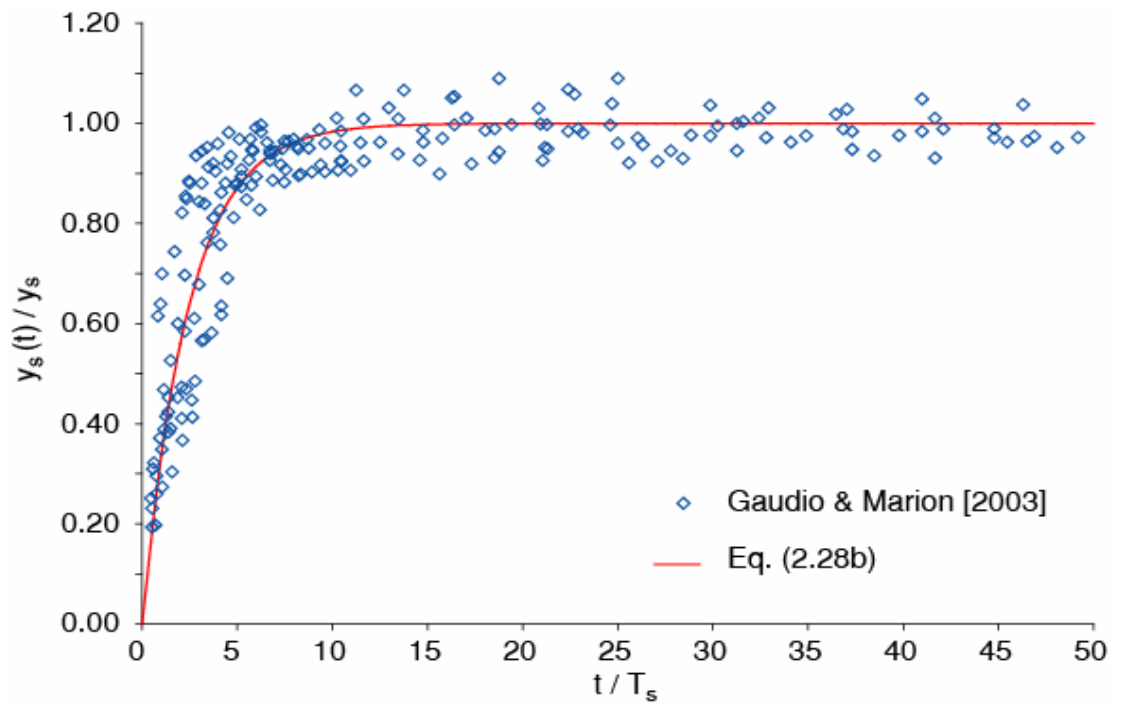


Figure 2.4 - Local scour time development. Modified after Gaudio and Marion et al. [2003].



## **CHAPTER 3 SEDIMENT SUPPLY EFFECT ON LOCAL SCOURS**

### **3.1 SUMMARY**

CHAPTER 3 presents the results of experimental tests carried out by the author in 2003 about the pattern of local scouring generated at the toe of bed sills. The aim of this study is to evaluate the effect of upstream sediment supply on the scour depth and shape. The experiments simulated conditions of a steady upstream sediment supply which had the same grain size composition as the sediment deposit placed on the bed of the flume. The geometric characteristics of three scour holes developed under conditions of steady-flow discharge and steady upstream sediment supply were measured during 48 different tests. This provided a data set containing measurements of 144 scour holes. Three different sediment-feed rates were used, tests were also performed with clear-water conditions. Geometrical interference between sills was not observed. A natural river gravel with a limited grain size was used. Section 3.3 describes details of the experimental settings. The collected data were analyzed using dimensionless groups developed in previous clear-water studies. In section 3.4 it is shown that the imposed sediment transport does not require the introduction of new dimensionless parameters into existing scour depth and length prediction formula. The effects of sediment feed are shown to be incorporated in the existing dimensionless parameters. The new data set is used to re-calibrate existing scour depth formula. In section 3.5 the influence of jet erosion on scour geometry is also discussed. Inspection of the data indicates a possible two-stage behavior, with the threshold between behaviors related to the ratio of the value of the morphological jump created at a scour

hole and the flow specific energy at the bed sill. In the next section the implications are discussed of considering either clear-water or sediment-supply conditions for the prediction of the maximum scour downstream of bed sills.

## 3.2 CLEAR-WATER AND SEDIMENT-SUPPLY CONDITIONS

### 3.2.1 Prediction of clear-water scour depth

The processes which transport sand, gravel and cobbles in high-gradient mountain streams play a fundamental role in defining their morphologic characteristics. Channel cross-sections are potentially mobile, and the current morphology of a reach reflects historic patterns of erosion or deposition that have occurred along its length. In particular, during storm events, the input boundary conditions of such river reaches are characterized by a flow discharge,  $Q$ , and also a sediment discharge,  $Q_{s,in}$ . In such a dynamic environment the stabilization of channel morphology is often achieved by reducing the slope. As discussed in the previous chapter, this can be accomplished by dividing the longitudinal profile of a river reach into a number of lower-slope intermediate steps through the construction of a sequence of bed sills or check dams. The vertical steps formed by such structures cause the water to plunge over the sill, and, unless the toe of the structure is protected, the plunging jet erodes the bed locally generating a deep scour hole. Designers must take this local scour into account in order to avoid structural failure. Quantitative predictive formulae of the scour dimensions are therefore required. Prediction formulae for scour depth that are available for different scouring phenomena have all been developed from experimental tests on scale models, but without an upstream sediment supply [Rajaratnam, 1981; Mason and Arumugam, 1985; Mason, 1989; Whittaker, 1987; Chatterjee et al., 1994; D'Agostino, 1994; Habib et al., 1994; Stein and Julien, 1994; Hoffmans and Pilarczyk, 1995; Hoffmans, 1998; Marion et al., 1998; Gaudio et al., 2000; Gaudio and Marion, 2003; Lenzi et al., 2002; Lenzi et al., 2003b; Marion et al., 2004]. All these studies have ignored the influence of the upstream sediment input which is likely to occur in these mountain streams during high flows.

Dimensional Analysis was first used by Gaudio et al. [2000] to identify appropriate dimensionless groups for scouring at bed sills, as described in CHAPTER 2.



They found that the morphological jump was the most important quantity in determining the size of the scour hole using data collected in experimental tests conducted at low bed slopes. This work was subsequently extended to steeper channels with graded sediments by *Lenzi et al.* [2002] and these data provided the following relationship:

$$\frac{y_s}{H_s} = 0.44 + 1.45 \left( \frac{a_1}{H_s} \right)^{0.86} + 0.06 \left( \frac{a_1}{\Delta D_{95}} \right)^{1.49} \quad (3.1)$$

Eq. (3.1) was calibrated using experimental data in the ranges  $0.16 \leq a_1/(\Delta D_{95}) \leq 1.15$  and  $0.22 \leq a_1/H_s \leq 1.87$ , with a coefficient of determination  $R^2 = 0.95$ . It was validated with field measurements from scour holes measured below 73 grade-control structures (check dams and bed sills) in six mountain rivers located in the Eastern Italian Alps [*Lenzi et al.*, 2003a]. For the data collected in the experimental tests,  $a_1/H_s$  and  $a_1/(\Delta D_{95})$  are in the same order of magnitude. The values of the calibration coefficients seem to indicate that the relative weight of  $a_1/(\Delta D)$  on the determination of the maximum scour depth is in the order of few per cent, compared with the influence of  $a_1/H_s$ . Therefore, the former parameter could be neglected without significant effect on the results. This also reflect the evidence that, although the use of the  $D_{95}$  produced the best correlation, nevertheless experimental results turned out to be almost insensitive to the choice of the representative grain size.

Other parameters, such as graded sediment composition and geometrical interference were subsequently examined. In CHAPTER 2, geometrical interference was defined as the reduction of scouring caused by the proximity of the sills, such that scouring is limited by the presence of the downstream structure. Non-interference occurs when a constant equilibrium bed slope and uniform flow is established upstream of a sill and the scour hole attains its shape that is not affected by the distance between the sills [*Comiti et al.*, 2001; *Lenzi et al.*, 2003b; *Marion et al.*, 2004]. The selection of a representative diameter to account for local scouring in graded sediment mixtures has not yet been completely solved. Most authors recommend the use of  $D_{90}$  as the appropriate diameter [*Whittaker*, 1987; *Bormann and Julien*, 1991; *D'Agostino*, 1994]

whilst others recommend  $D_{85}$  [Mason and Arumugam, 1985] or  $D_{95}$  [Aderibigbe and Rajaratnam, 1998].

Marion *et al.* [2004] demonstrated that, in high-gradient mountain rivers defined as channels with bed slope greater than 3-4%, the drop height at each structure, i.e. the morphological jump,  $a_1$ , and the specific energy available at the sill,  $H_s$ , are the most significant physical quantities that control local scouring. Using experimental data the dimensionless parameter  $a_1/H_s$  was shown to be the only term needed to predict the depth of non-interfering equilibrium scour holes for uniformly sized sediments. To take into account the effect of structure spacing, a new dimensionless group,  $L/H_s$ , was added. The effect of sediment composition was accounted for using a grading parameter called the sorting index  $SI$  (equal to the standard deviation,  $\sigma_g$ , for log-normal distributions). According to Marion *et al.* [2004], the relationship, which is appropriate for estimating scour at interfering sills and for both graded and uniform sediment beds, is:

$$\frac{y_s}{H_s} = 2.7 \left( \frac{a_1}{H_s} \right)^{0.43} SI^{-0.19} \left( 1 - e^{-0.14 \frac{L}{H_s}} \right) \quad (3.2)$$

which was calibrated for the range  $0.22 < a_1/H_s < 1.87$ , with a coefficient of determination  $R^2 = 0.87$ . All the data used in the calibration of these relationships, Eqs. (3.1) and (3.2), were obtained from laboratory tests that were characterized by long-term equilibrium configurations and clear-water conditions.

### 3.2.2 Influence of sediment supply

No local-scouring observations were made in conditions of upstream sediment feed which is common in real mountain rivers. It was thought that upstream sediment supply would significantly reduce potential scour depth during extreme events. Recent experimental observations [Marion, personal communication] have indicated that the flood peak discharge may not be the most effective measure of scour depth development, as it normally coincides with large sediment supply into the river. Effects of sediment supply on scour length have also to be evaluated as, along with scour depth, this quantity controls scour hole shape. In their studies on scouring processes, without

an upstream sediment supply, several authors [Rajaratnam, 1981; Whittaker, 1987; Bormann and Julien, 1991; Chatterjee et al., 1994; D'Agostino, 1994; Habib et al., 1994; Gaudio et al., 2000; Lenzi et al., 2002] found that the scour hole profiles are affine. This finding needs to be compared with scour hole configurations formed in the presence of upstream sediment feeding in order to test its generality. Both the above aspects of scour hole development suggest that it is important to carry out experiments designed to study the influence of upstream sediment transport in order to complete the observation of local-scouring mechanisms under all probable conditions.

The fundamental form of Eqs. (3.1) and (3.2), which were then calibrated with the available data, was presented in CHAPTER 2. As already observed, dimensional analysis was derived based on the assumption of a constant geometry for the plunging jet. This assumption can be reasonably questioned as the inclination of the plunging jet is affected by the bed slope. Furthermore, while the jet pattern may be assumed independent of upstream flow conditions for subcritical flows, jet inclinations might depend upon Froude number if supercritical conditions hold (see section 0). For this reason a more general notation is introduced here for  $H_s$ , which indicates thereafter the specific energy available at each sill. According to such definition, for subcritical and critical flow conditions ( $F_R \leq 1$ )  $H_s = 1.5(q^2/g)^{1/3}$ , which is the parameter originally obtained from dimensional analysis; for supercritical flow conditions ( $F_R > 1$ )  $H_s = (h_{u,eq} + v^2/2g)$ , where  $v = q/h_{u,eq}$  is the mean flow velocity. The implications of this assumption will be examined later.

The presence of upstream sediment feed requires the addition of another dimensionless parameter into Eq. (2.12a). It is possible to make the equilibrium bed slope,  $S_{eq}$ , i.e. the slope that forms when sediment discharge matches the upstream sediment feed, explicitly dependent on both the flow and sediment discharges per unit width,  $q$  and  $q_{s,in}$ :

$$S_{eq} = f(q, q_{s,in}, n, \Delta, D, \theta_c) \quad (3.3)$$

where the Manning's roughness coefficient  $n$ ,  $\Delta$ ,  $D$  and the critical value of the Shields' parameter,  $\theta_c$ , are determined using accepted relationships. Using established hydraulic resistance and excess shear stress bed load sediment transport formulae, it is observed

that the equilibrium bed slope decreases with flow discharge, whilst it increases with sediment discharge. It seems reasonable to expect that the incoming sediment transport affects the final conditions only by changing the equilibrium bed slope. Consequently it involves reducing scour depth only by increasing the bed slope given the definition of morphological jump,  $a_1 = (S_0 - S_{eq})L$ . The hypothesis that this study proposes to verify is that changes in the incoming sediment transport does not influence local scouring in any other way, for example by adding an ‘impact’ effect between moving sediment particles and the sediment particles on the bed. This would imply that any sediment transport effect is linked essentially to the equilibrium bed slope and therefore to the morphological jump, which is present in Eq. (2.12a). As a result, from a dimensional point of view, there should be no difference between Eq. (2.12a), which is valid for clear-water conditions, and any new formula applicable in the more common situation of incoming sediment transport. The first goal of this study is to verify this and thus extend the validity of Eqs. (3.1) and (3.2) to conditions of upstream sediment supply. If the validation is successful, then new data collected under conditions of sediment feed can be combined with existing no-feed data in order to investigate if the existing calibrated Eqs. (3.1) and (3.2) need to be revised.

### 3.3 EXPERIMENTAL SET-UP AND PROCEDURE

A series of laboratory experiments to collect data to quantify the impact of upstream sediment supply on scour hole development was carried out at Hydraulic Laboratory of the University of Padua in 2003. An illustration of the experimental flume is shown in Figure 3.1. A glass-sided tilting flume 10 m-long, 0.5 m wide, 0.5 m-deep was used. The sediment used was graded river gravel, with the following characteristics:  $D_{10} = 5.5$  mm,  $D_{30} = 7.2$  mm,  $D_{50} = 8.7$  mm,  $D_{60} = 9.5$  mm,  $D_{90} = 13.9$  mm, and with sorting index  $SI = 1.48$ . As the grain size distribution used approximates a log-normal distribution,  $SI$  corresponds closely to the standard deviation  $\sigma_g$ . Although this value is slightly above the threshold proposed by *Breusers and Raudkivi* [1991] for the definition of uniformly sized natural sediment ( $\sigma_g = 1.35$ ), the sediment used in these tests was considered to be uniform as its uniformity coefficient  $C_u = D_{60}/D_{10}$  is equal to 1.75. *Lambe and Whitman* [1969] consider sediment uniform if this value was

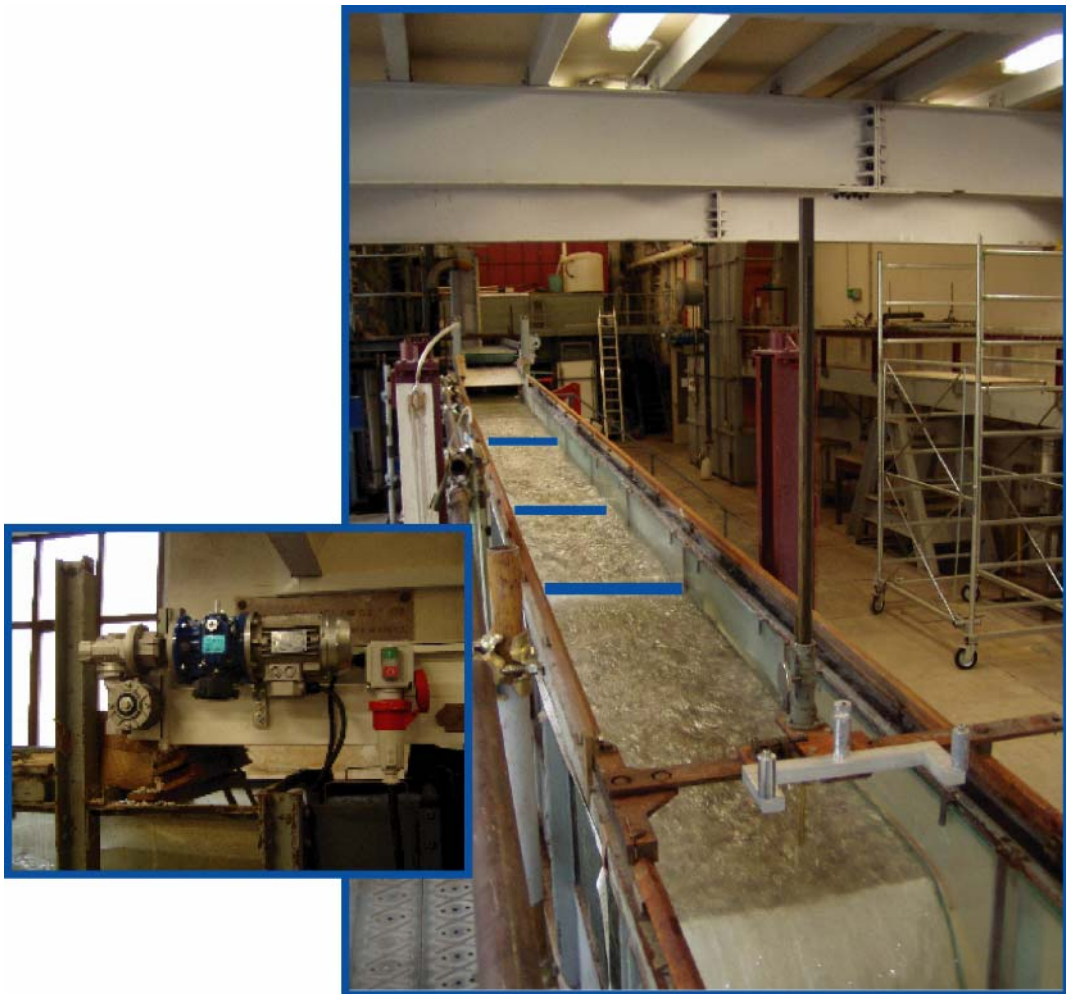


**Figure 3.1 - Experimental set-up: bed sills inserted in a sediment bed along the flume; upstream sediment feeder.**

less than 2. At the start of each test, the sediment was well mixed and a 330 mm thick sediment deposit was placed and scrapped flat so that the sediment deposit had the same slope as the flume. Rectangular wooden plates, 330 mm-deep, 500 mm-wide and 10 mm-thick were used to simulate transverse control structures, such as bed sills. They were inserted vertically into the gravel deposit. In all the experiments four plates were used: the first sill was inserted 2.25 m from the flume inlet, the spacing between the first and the second sill ( $L_1$ ) and between the third and the fourth sill ( $L_3$ ) was 2 m, whilst the spacing between the second and the third sill ( $L_2$ ) was 1.5 m. Samples of the river gravel were weighed and placed onto a conveyor belt at the upstream end of the flume. This allowed known sediment-feed rates to be fed into the flume at its inlet. At the downstream end of the flume the water flowed over a tail gate into a tank, which collected the sediments exiting the flume. The sediments were removed in the tank and

the then water passed over a weir into a sump. A pump raised the water from the sump to the inlet tank of the flume, which had a “honeycomb” flow straightener inside it to reduce secondary currents and to create uniform fully turbulent flow conditions quickly within the flume. The flow discharge was measured using an electromagnetic flow meter, positioned in the inlet pipe to the flume. Measurements of the water level and bed level profiles were made with a point gauge mounted on a gantry which was manually moved along rails on top of the walls of the flume and set parallel to its base. The slope of the flume could be manually adjusted. Tests were performed with bed slopes ranging between 4.2 and 7.4%, with steady-flow discharges between 18 and 26 l/s and with steady input sediment rates between 0.0 and 71.1 g/sm.

At the start of each test the sediments were carefully mixed over the whole deposit depth, to avoid preferential sorting and compaction which may biased the development of scouring depths and the wooden plates inserted. Water was then pumped into the flume at a low discharge (4-5 l/s) so that the flow depth increased slowly to avoid sediment movement before the desired flow discharge value was attained. Once the whole sediment deposit was saturated, the discharge was raised to the desired value, and the conveyor belt, previously prepared with an adequate charge of river gravel, was turned on. Tests lasted five to six hours. This duration was found to be long enough to reach equilibrium conditions; scour development was observed to take place within the first two hours. Tests 18, 26 and 27 had a longer duration of fifteen hours. Comparing scour depth and bed slope measured after the first six hours and after the end of the tests did not show any significant difference. This confirmed that a test duration of six hours was adequate to attain scour hole equilibrium, due to the high values of both  $S_0$  and  $Q$  with respect to the previous cited studies.

During the last two hours in every test, the three scour holes were measured every ten minutes, recording the maximum scour depth with the respect to the slope line between the top of the sills. Bed elevations were measured adjacent to flume walls at the left and right sides of the flume by observing the bed surface position through the glass flume walls. It was necessary to make repeated measurements because observations during preliminary feasibility tests showed that there was a temporal oscillation of scour depth around an mean value, after equilibrium had been attained. This variation was

**Table 3.1 - Experimental data collected in this study [Padova, 2003]**

Test #	S <sub>0</sub>	Q (l/s)	Q <sub>s</sub> (g/s)	Y <sub>s,1</sub> (cm)	Y <sub>s,2</sub> (cm)	Y <sub>s,3</sub> (cm)	l <sub>s,1</sub> (cm)	l <sub>s,2</sub> (cm)	l <sub>s,3</sub> (cm)
1	4.2%	18.0	0.0	9.0	6.0	9.5	48.0	38.0	51.0
2	4.2%	18.0	10.7	5.6	5.0	5.9	43.0	38.0	41.0
3	4.2%	18.0	21.3	5.5	4.9	5.7	33.0	43.0	41.0
4	4.2%	18.0	35.5	4.7	4.1	5.4	33.0	33.0	31.0
5	4.2%	22.0	0.0	14.5	11.0	14.8	63.0	68.0	65.0
6	4.2%	22.0	10.7	7.7	7.5	12.1	58.0	38.0	56.0
7	4.2%	22.0	21.3	6.8	6.1	7.7	38.0	43.0	61.0
8	4.2%	22.0	35.5	5.7	5.8	6.9	41.0	35.0	36.0
9	4.2%	26.0	0.0	17.3	14.3	16.3	73.0	61.0	71.0
10	4.2%	26.0	10.7	13.2	8.9	12.5	63.0	63.0	56.0
11	4.2%	26.0	21.3	9.4	7.3	8.8	65.0	48.0	56.0
12	4.2%	26.0	35.5	8.1	7.1	10.0	48.0	43.0	46.0
13	5.0%	18.0	0.0	17.3	14.5	18.0	60.0	58.0	59.0
14	5.0%	18.0	10.7	9.6	9.2	10.7	43.0	38.0	46.0
15	5.0%	18.0	21.3	8.4	7.0	9.7	50.0	38.0	39.0
16	5.0%	18.0	35.5	6.9	5.8	7.3	41.0	33.0	46.0
17	5.0%	22.0	0.0	21.0	17.5	20.8	68.0	65.0	71.0
18	5.0%	22.0	10.7	14.4	12.2	14.4	53.0	53.0	56.0
19	5.0%	22.0	21.3	12.2	10.6	13.5	58.0	53.0	51.0
20	5.0%	22.0	35.5	9.7	8.7	10.1	45.0	43.0	51.0
21	5.0%	26.0	0.0	24.3	22.8	23.5	78.0	88.0	81.0
22	5.0%	26.0	10.7	17.6	13.6	18.4	68.0	68.0	61.0
23	5.0%	26.0	21.3	17.2	13.0	16.5	68.0	63.0	70.0
24	5.0%	26.0	35.5	13.0	10.7	14.1	63.0	50.0	63.0
25	6.2%	18.0	0.0	21.5	17.5	20.0	56.0	58.0	56.0
26	6.2%	18.0	10.7	17.4	15.8	16.5	53.0	50.0	50.0
27	6.2%	18.0	21.3	15.5	13.3	16.0	55.0	48.0	51.0
28	6.2%	18.0	35.5	14.2	12.1	13.9	46.0	48.0	46.0
29	6.2%	22.0	0.0	23.8	21.0	23.8	63.0	63.0	61.0
30	6.2%	22.0	10.7	20.9	19.4	21.1	58.0	58.0	56.0
31	6.2%	22.0	21.3	19.4	17.6	19.2	58.0	58.0	56.0
32	6.2%	22.0	35.5	19.5	17.2	18.8	55.0	56.0	53.0
33	6.2%	26.0	0.0	26.7	25.0	26.3	63.0	65.0	61.0
34	6.2%	26.0	10.7	23.2	21.3	25.1	68.0	73.0	65.0
35	6.2%	26.0	21.3	23.2	19.6	23.5	63.0	63.0	61.0
36	6.2%	26.0	35.5	20.8	16.6	19.6	63.0	63.0	61.0
37	7.4%	18.0	0.0	24.0	21.3	24.0	53.0	48.0	54.0
38	7.4%	18.0	10.7	19.0	16.2	20.8	48.0	48.0	46.0
39	7.4%	18.0	17.8	20.3	18.4	21.2	45.0	45.0	43.0
40	7.4%	18.0	35.5	17.7	15.2	18.1	45.0	48.0	46.0
41	7.4%	22.0	0.0	27.0	24.0	27.0	55.0	53.0	53.0
42	7.4%	22.0	17.8	23.8	21.0	24.4	56.0	56.0	53.0
43	7.4%	22.0	21.3	22.8	19.7	22.3	60.0	60.0	54.0
44	7.4%	22.0	35.5	21.9	19.0	21.6	55.0	54.0	51.0
45	7.4%	26.0	0.0	28.8	24.8	28.3	68.0	68.0	66.0
46	7.4%	26.0	10.7	25.5	24.1	27.4	63.0	68.0	62.0
47	7.4%	26.0	21.3	25.1	21.7	24.7	63.0	66.0	63.0
48	7.4%	26.0	35.5	25.0	21.5	25.4	61.0	68.0	63.0

present only during tests with constant sediment transport, whilst it was absent during clear-water tests. In addition, sediment feeding sometimes caused a lack of two-dimensionality of the scour shape. In these cases, the scour depth was estimated as the average between the two lateral measurements across the bed. These data were used to ensure that a state of long-term equilibrium had been achieved in all tests. In the last half an hour of a test, measurements of the water profiles were made at 5-cm intervals along the flume centerline. After the pump was turned off and the flume carefully drained, measurements of the bed elevation were also made at 5-cm intervals along the flume centerline. The data measured during these tests are presented in Table 3.1.

### 3.4 ANALYSIS OF EXPERIMENTAL RESULTS

#### 3.4.1 Maximum scour depth

The variability of the equilibrium bed slopes measured in each of the three reaches between the sills was very small (see Table 3.2); the mean relative error  $\varepsilon_{Seq}$  is equal respectively to 5.6%, 6.3% and 6.7%. This confirms that an equilibrium bed slope and uniform flow was established before reaching the subsequent downstream sill. Examination of the variation in the equilibrium bed slope demonstrated that there was no geometrical interference between the sills. Froude numbers,  $F_R = v/(gh_{u,eq})^{0.5}$ , and grain Reynolds numbers,  $R_E^* = u^* D_{90}/\nu$  where  $u^* = (gh_{u,eq} S_{eq})^{0.5}$  is the shear velocity, are also reported in Table 3.2. These values show that the flows were fully turbulent ( $R_E^* > 70 \div 400$ , as reported by different authors) and supercritical ( $F_R > 1$ ) or near-critical ( $F_R \cong 1$ ). The experimental data were now examined using the dimensionless groups proposed by *Marion et al.* [2004]. The maximum scour depth normalized by the specific flow energy,  $y_s/H_s$  was plotted against the drop ratio,  $a_1/H_s$ . The morphological jump was computed using the mean equilibrium bed slope; the values of  $a_1$  are reported in Table 3.2. These results were obtained for three different sediment-feed rates and for a limited number of clear-water tests. Figure 3.2 indicates that the experimental data, when plotted in a dimensionless form, collapses reasonably. The range of validity of this pattern is  $0.07 < a_1/H_s < 1.19$ . This is the first important result of this study as it shows that the impact of the upstream sediment feed can be accounted for in a similar



**Table 3.2 - Experimental parameters measured and calculated in this study [Padova, 2003]**

Test #	$S_{eq}$	$S_{eq,1}$	$S_{eq,2}$	$S_{eq,3}$	$a_1=a_3$ (cm)	$a_2$ (cm)	$H_s$ (cm)	$F_R$	$R_E^*$
1	2.80%	2.50%	2.70%	3.20%	2.8	2.1	7.8	1.19	1408
2	3.40%	2.90%	3.40%	3.40%	2.0	1.5	7.9	1.30	1519
3	3.60%	3.10%	3.80%	3.10%	1.7	1.3	8.0	1.34	1546
4	4.00%	3.60%	4.00%	4.20%	0.5	0.4	8.1	1.42	1589
5	2.40%	2.30%	2.30%	2.70%	3.5	2.7	8.8	1.17	1416
6	2.90%	2.90%	3.20%	2.80%	2.4	1.8	8.9	1.25	1519
7	3.20%	3.40%	3.40%	3.30%	1.6	1.2	9.0	1.31	1564
8	3.50%	3.30%	3.70%	3.70%	1.2	0.9	9.1	1.35	1628
9	2.30%	2.50%	1.60%	2.90%	3.8	2.8	9.8	1.09	1474
10	2.60%	2.70%	2.50%	2.40%	3.3	2.5	9.9	1.19	1534
11	2.90%	2.90%	2.80%	2.90%	2.6	2.0	10.0	1.23	1605
12	3.10%	2.90%	3.30%	3.40%	2.0	1.5	10.0	1.26	1657
13	2.80%	2.70%	2.80%	3.00%	4.3	3.2	7.8	1.23	1401
14	3.60%	3.60%	3.60%	4.00%	2.6	1.9	8.0	1.37	1525
15	3.90%	3.50%	3.80%	4.10%	2.4	1.8	8.1	1.42	1564
16	4.10%	3.70%	4.20%	4.40%	1.8	1.4	8.1	1.44	1603
17	2.60%	2.40%	2.70%	2.70%	4.8	3.6	8.8	1.15	1461
18	3.10%	3.30%	2.90%	3.20%	3.7	2.8	9.0	1.28	1547
19	3.20%	3.10%	3.30%	3.30%	3.5	2.6	9.0	1.31	1574
20	3.50%	3.30%	3.50%	3.80%	2.9	2.2	9.1	1.33	1635
21	2.10%	1.80%	2.30%	2.30%	5.8	4.3	9.8	1.06	1423
22	2.90%	2.90%	2.50%	3.30%	4.2	3.1	10.0	1.26	1579
23	3.00%	2.90%	3.40%	2.90%	3.9	2.9	10.0	1.25	1620
24	3.50%	3.40%	3.50%	3.50%	3.0	2.3	10.0	1.27	1735
25	2.90%	3.00%	2.70%	3.20%	6.5	4.8	7.8	1.21	1429
26	3.60%	3.80%	3.20%	4.00%	5.1	3.8	8.0	1.34	1547
27	3.90%	3.10%	3.80%	4.00%	5.1	3.9	8.1	1.40	1570
28	3.90%	3.90%	4.00%	3.80%	4.6	3.5	8.1	1.44	1565
29	2.50%	2.40%	2.20%	2.80%	7.5	5.6	8.8	1.15	1431
30	3.00%	2.90%	3.10%	3.40%	6.1	4.6	9.0	1.29	1531
31	3.40%	3.40%	3.40%	3.40%	5.6	4.2	9.1	1.33	1599
32	3.70%	3.50%	4.20%	3.40%	5.0	3.7	9.2	1.41	1647
33	2.10%	2.00%	2.30%	1.90%	8.2	6.1	9.8	1.10	1402
34	2.60%	2.40%	2.90%	2.70%	7.0	5.3	9.9	1.22	1539
35	2.90%	2.90%	2.80%	2.90%	6.6	5.0	10.0	1.23	1605
36	3.10%	3.10%	3.10%	3.60%	5.9	4.4	10.1	1.30	1642
37	2.60%	2.50%	2.40%	3.20%	9.3	7.0	7.8	1.19	1359
38	3.50%	3.70%	4.00%	3.80%	7.1	5.3	7.9	1.33	1525
39	3.60%	3.30%	4.10%	3.60%	7.5	5.6	8.0	1.37	1536
40	4.10%	4.20%	4.10%	4.20%	6.5	4.9	8.1	1.42	1616
41	2.20%	2.40%	2.10%	2.70%	10.0	7.5	8.8	1.09	1375
42	3.20%	3.30%	3.20%	3.20%	8.3	6.3	9.0	1.31	1552
43	3.20%	3.30%	3.30%	3.10%	8.3	6.3	9.0	1.28	1574
44	3.70%	3.60%	4.50%	3.60%	7.0	5.2	9.2	1.41	1633
45	2.20%	1.90%	2.10%	2.80%	10.3	7.7	9.8	1.06	1459
46	2.70%	2.80%	2.80%	2.70%	9.3	7.0	9.9	1.20	1549
47	2.80%	3.00%	2.60%	3.00%	9.1	6.8	9.9	1.21	1597
48	3.00%	3.30%	2.40%	3.20%	8.8	6.6	9.9	1.17	1656

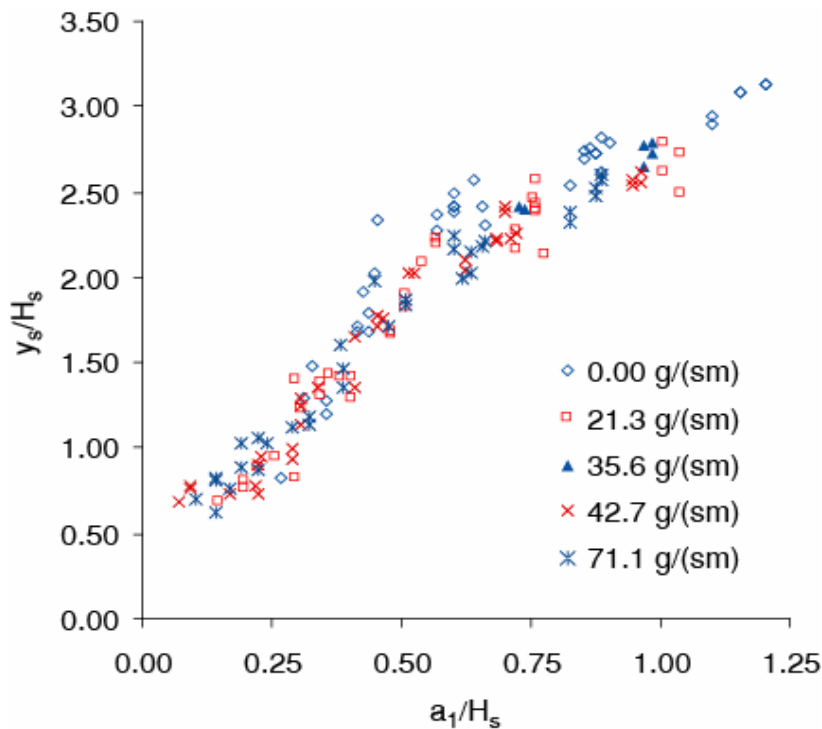


Figure 3.2 - Experimental data [Padova, 2003] divided into series according to upstream sediment-feed rate.

manner to that previously used in clear-water conditions. Comparing tests with similar hydraulic conditions, the only effect of the sediment transport is to increase the equilibrium bed slope and as a consequence reduce the value of  $a_1$ . This confirms that the effect of incoming sediment transport is mainly accounted for in the value of the morphological jump parameter,  $a_1$ . These data justify the approach proposed, which is to recalibrate the existing scour depth formula in the form of Eq. (3.2), but using the new and existing scour depth data obtained in both clear-water and upstream sediment-feed conditions. Figure 3.3 shows the prediction of the existing scour depth formulae of *Marion et al.* [2004] and *Lenzi et al.* [2002], compared with the new experimental measurements. In general Eq. (3.2) for high-gradient streams seems to provide a reasonable prediction, although it overestimates normalized scour depth for low values of ratio  $y_s/H_s$ . Validity range of Eq. (3.2) is slightly shifted with respect to the range of the experimental data. Eq. (3.1), obtained by *Lenzi et al.* [2002] using data from both high and low bed slopes, slightly underestimates the measured maximum scour depth over the data interval. It seems plausible that the term  $a_1/(\Delta D_{95})$  could be completely neglected in Eq. (3.1). By doing this a better correlation for low values of ratio  $y_s/H_s$  is

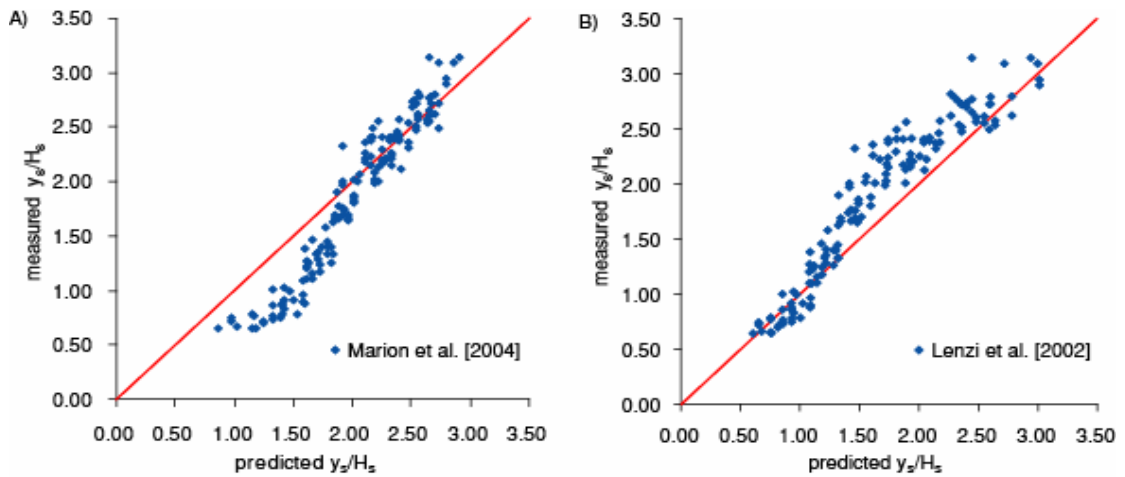


Figure 3.3 - Comparison of predicted and measured maximum scour depths from this study [Padova, 2003]. A) Eq. (3.2), B) Eq. (3.1).

obtained. Closer examination seems to show that it may be inappropriate to approximate all data with a unique curve. Eq. (3.2) is very effective for  $y_s/H_s > 2.0$  (corresponding to  $a_1/H_s > 0.6$ ) where the dimensionless maximum scour depth increases approximately with the square root of the normalized morphological jump, but in the interval  $0.8 < y_s/H_s < 2.0$  ( $0.2 < a_1/H_s < 0.6$ ) the trend seems to follow an almost linear trend with an exponent close to that in Eq. (3.1) of *Lenzi et al.* [2002]. The possibility to identify different formulae for distinct ranges of  $a_1/H_s$  will be explored further in the following sections. It is noted for  $y_s/H_s < 0.8$  ( $a_1/H_s < 0.2$ ), the dimensionless ratio between maximum scour depth and specific flow energy appears to be attaining a stable value of approximately 0.6 to 0.7 rather than declining steadily to zero. Despite this evidence it is reasonable to use an expression like Eq. (3.2) for predicting the scour depth taking into account the geometrical interference produced by neighboring bed sills and the non-uniform grain size. Figure 3.4 contains all data observed during the current tests and those obtained from previous experiments, considering both high and low bed slopes, uniform and mixed grain sizes, and clear-water and sediment-feed conditions. A regression of these data, described in Table 3.3, adjusts the calibration coefficients of Eq. (3.2) to the following:

$$\frac{y_s}{H_s} = 3.0 \left( \frac{a_1}{H_s} \right)^{0.60} SI^{-0.19} \left( 1 - e^{-0.25 \frac{L}{H_s}} \right) \quad (3.4)$$

This calibration is valid for  $0.07 \leq a_1/H_s \leq 1.87$  with a coefficient of determination  $R^2 = 0.86$ , which was similar in value to the original calibration of *Marion et al.* [2004].

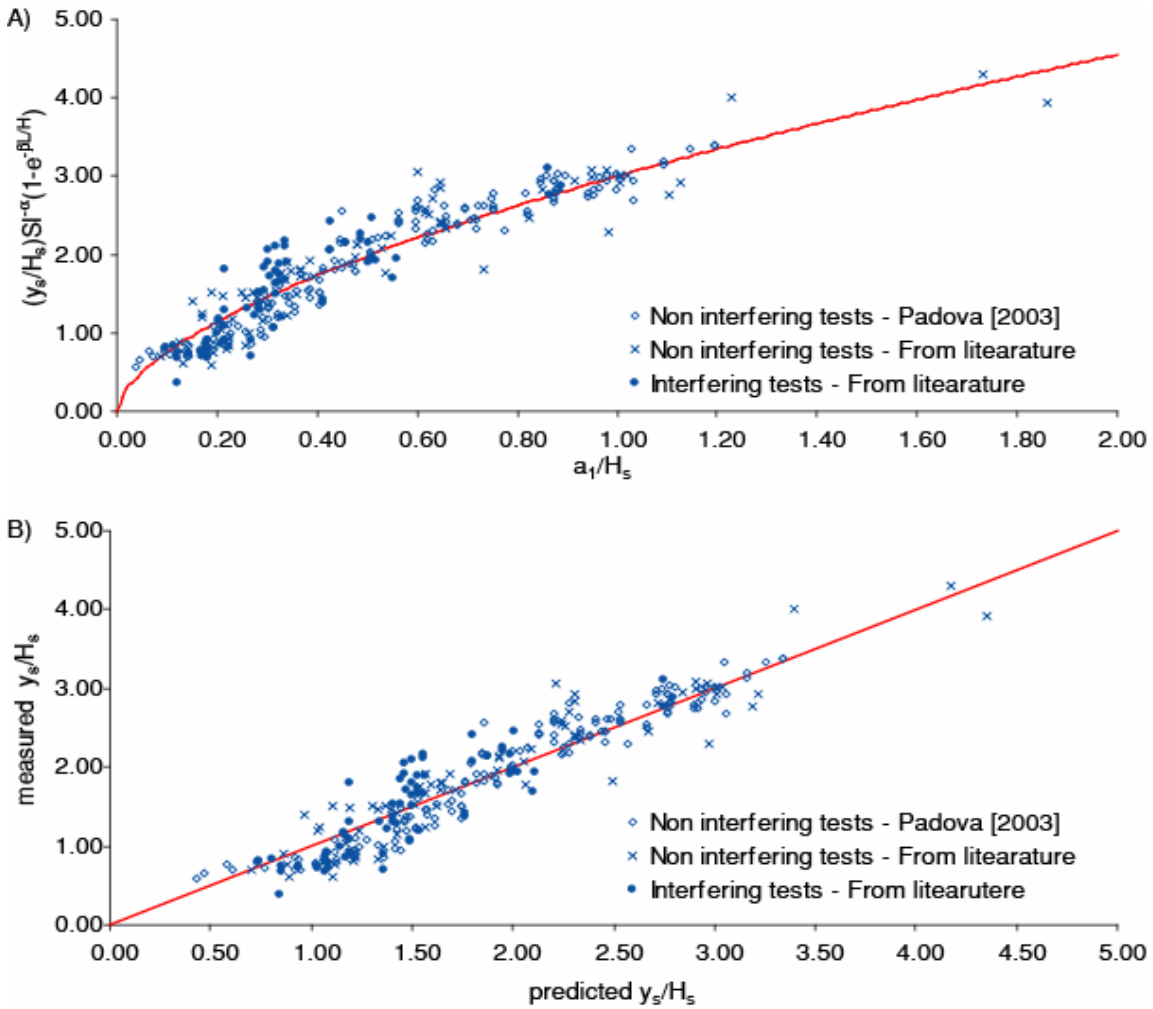


Figure 3.4 - A) Regression of all available experimental data from literature and this study [Padova, 2003], see Table 3.3 B) Prediction of normalized maximum scour depth calculated with Eq. (3.4).

**Table 3.3 - Summary of all experimental studies**

	Gaudio et al. [2000]	Gaudio and Marion [2003]	Lenzi et al. [2002]	Lenzi et al. [2003b]	Marion et al. [2004]	Marion et al. [2004]	This study Padova [2003]
Number of measured scour holes	19	12	13	13	27	60	144
Sills Spacing L (m)	2.0 - 6.0	2.5	1.05	0.525	1.50	0.50 - 0.75	1.5 - 2.0
Geometrical interference	no	no	no	yes	no	yes	no
Initial Bed Slope $S_0$ (%)	0.9 - 1.7	0.6 - 1.1	7.85 - 14.8	7.85 - 14.8	4.5 - 8.0	4.5 - 8.0	4.2 - 7.4
Equilibrium Bed Slope $S_{eq}$ (%)	0.3 - 0.7	0.2 - 0.3	4.4 - 10.4	--- (*)	1.9 - 5.4	--- (*)	2.07 - 4.27
Flow Discharge Q (l/s)	45.0 - 80.0	12.0 - 19.0	4.0 - 17.5	7.0 - 29.0	9.0 - 30	8.7 - 30.6	18.0 - 26.0
Sediment Discharge $q_s$ (g/(sm))	0.0	0.0	0.0	0.0	0.0	0.0	0.0 - 71.1
Sediments $D_{50}$ (mm)	4.1 - 8.5	1.8	8.6	8.6	8.7	8.7	8.7
Sediments SI (-)	1.32 - 1.35	1.21	5.93	5.93	1.48	1.48	1.48

(\*) Equilibrium bed slopes were not reached in experiments with geometrical interference

### 3.4.2 Scour hole length

Scour hole length,  $l_s$ , has also been normalized with the specific flow energy at a sill and plotted against the drop ratio,  $a_1/H_s$ . As anticipated in CHAPTER 2 (see section 2.3.2) this normalization displays only a very weak correlation ( $R^2 = 0.20$ ) of scour length to drop height. The correlation decreases with the increasing size of the morphological jump normalized by the specific flow energy,  $a_1/H_s$ . For values of  $a_1/H_s > 0.6$ , the ratio  $l_s/H_s$  tends towards an approximately stable value ranging between 6.0 and 7.0. This suggests that the specific flow energy is the most important quantity in

determining scour length. In particular this experimental evidence highlights the connection between the scour length and the length of the hydraulic jump, which was experimentally observed to be equal to nearly six times the downstream normal water depth. This two-zone behavior could be explained by examining the different jet inclinations of the flow over the sills. When the initial bed slope increases (and  $a_1$  grows) the plunging jet becomes more vertical and thus the horizontal development of the scour hole loses its link with the geometry of the plunging jet (and thus with  $a_1$ ). The scour length then attains a value approximately equal to the hydraulic jump length. A better defined trend is obtained if the parameters  $l_s/a_1$  and  $H_s/a_1$  are compared, as suggested by some other studies [e.g. *Lenzi et al.*, 2003a]. In Figure 3.5 it is observed clearly that the experimental data follow a trend. Previous authors have suggested a linear relation, but the new data suggest better correspondence is achieved with a power law, though with an exponent close to unity. The following relationship is proposed:

$$\frac{l_s}{a_1} = 7 \left( \frac{H_s}{a_1} \right)^{0.86} \quad (3.5)$$

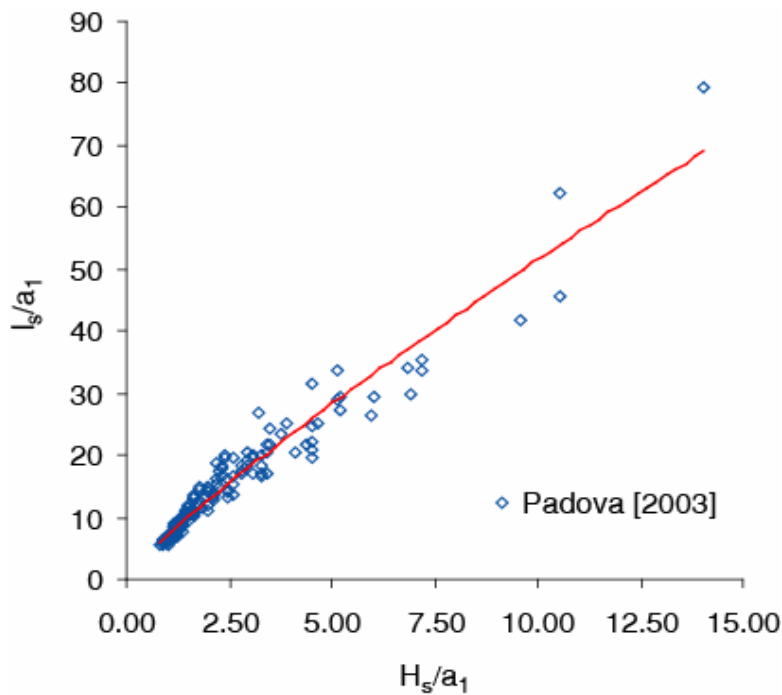


**Figure 3.5 - Regression of experimental data from this study [Padova, 2003]; normalized scour length against the inverse of the drop-ratio.**

Eq. (3.5) describes the best fit for  $l_s/a_1$  against  $H_s/a_1$  and takes the form of a power law. The most significant result is that this new relationship, Eq. (3.5), can better describe the variation in scour length for both the clear-water and upstream sediment-supply tests and is valid for  $0.84 < H_s/a_1 < 14.1$ , with a coefficient of determination  $R^2 = 0.94$ .

### 3.5 DISCUSSION

#### 3.5.1 Effect of jet inclination

Analysis by *Lenzi et al.* [2003a] suggested that the geometry of a scour hole is linked directly to the specific energy of the flow over the sill. They demonstrated this by normalizing the maximum scour depth against the total specific flow energy available at each sill,  $a_1 + H_s$ . They plotted this dimensionless parameter against the drop ratio,  $a_1/H_s$ , for the observed field data, suggesting the following range:

$$0.6 \leq \frac{y_s}{a_1 + H_s} \leq 1.4 \quad (3.6)$$

Figure 3.6 contains data from this study as well as data from all the studies listed in Table 3.3. Examination confirms the range of values of  $y_s/(a_1 + H_s)$  noted by *Lenzi et al.* [2003a]. It demonstrates two distinct pattern of behavior not noted in previous studies. This suggests that at values of  $a_1/H_s > 0.6$  different physical processes could be dominant. A plausible explanation for this behavior is the angle of impact of the jet. *Bormann and Julien* [1991] found that the jet impact angle plays a major part in determining the scour depth as well as its geometry. Considering the angle of the plunging jet with the horizontal plane, the more tilted the jet, the higher the erosion intensity and the steeper the downstream side of the scour hole. Therefore, with the growth of the morphological jump, the maximum scour depth rises not only because of a bigger availability of potential energy (that is  $a_1$ ), but also because of a more inclined jet with respect to the horizontal plane. This hypothesis can be examined by establishing the angle of jet impact based on geometrical considerations and predicted flow conditions. Assuming a drop  $a_1$  and knowing the flow conditions at the sill, the tangent

of the angle of jet impact to the horizontal plane,  $a_1$  below the sill crest, can be expressed as a ratio of the vertical and horizontal jet velocity components  $v_y$  and  $v_x$ :

$$\tan \varphi_{jet} = \frac{v_y}{v_x} \cong \begin{cases} \frac{\sqrt{2ga_1}}{\sqrt{\frac{2}{3}gH_s}} = \sqrt{3} \sqrt{\frac{a_1}{H_s}} & \text{for } F_R \leq 1 \\ \frac{\sqrt{2ga_1}}{\sqrt{\frac{2F_R^2}{2+F_R^2}gH_s}} = \sqrt{\frac{2+F_R^2}{F_R^2}} \sqrt{\frac{a_1}{H_s}} & \text{for } F_R > 1 \end{cases} \quad (3.7)$$

Eq. (3.7) shows that the jet angle depends mainly on  $a_1/H_s$  and weakly on Froude number. This result is a direct consequence of having defined  $H_s$  as the energy available at the crest edge in section 3.2.2, which partially allow for the effect of  $F_R$  on jet inclination. If  $H_s$  is considered as the critical specific energy instead, such definition would involve a stronger dependency of  $\varphi_{jet}$  on Froude number in Eq. (3.7) for  $F_R > 1$ . This therefore implies that jet angle is implicitly accounted for in the previous dimensional analysis. Using Eq. (3.7) and examining Figure 3.6 closely indicates that, for angles of impact lower than approximately  $50^\circ$ , the maximum scour depth depends on both  $a_1$  and  $H_s$ . As the jet angle increases above  $50^\circ$  the ratio of the maximum scour depth to the total specific energy at the sill becomes constant.

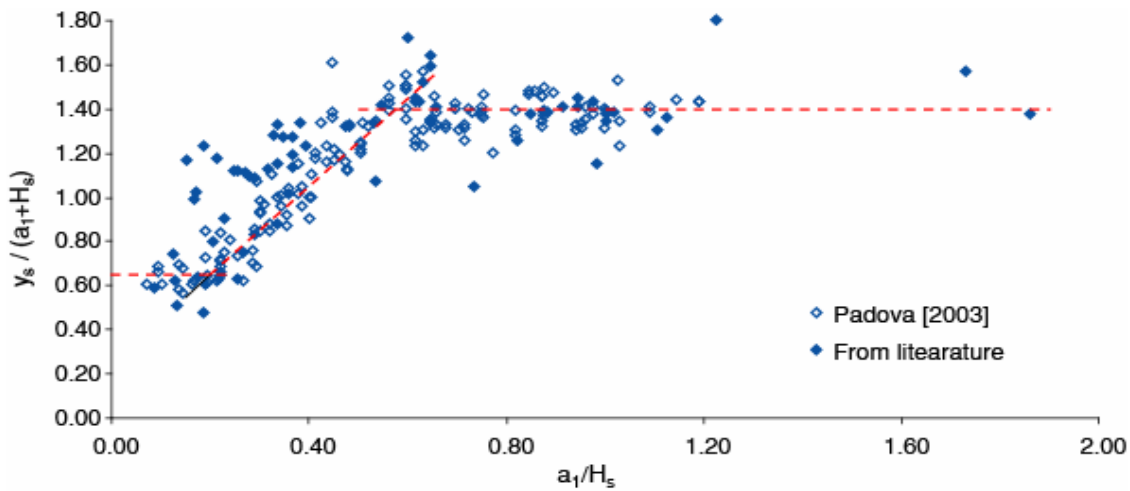


Figure 3.6 - Scour depth normalized to total specific flow energy against normalized drop height, using data from this study [Padova, 2003] and data from previous studies, see Table 3.3.



### 3.5.2 Scour hole shape

The analysis above explains the trend of maximum scour depth normalized to the total specific flow energy with the varying of the dimensionless ratio  $a_1/H_s$ . By applying this analysis to the experimental data collected in this study, a comparable pattern of results was found. Figure 3.6 shows the trend of increasing drop ratio,  $a_1/H_s$ , on the total energy normalized by maximum scour depth,  $y_s/(a_1 + H_s)$ . For  $a_1/H_s \cong 0$ , which represents a very low morphological jump with the respect to the specific flow energy,  $y_s/(a_1 + H_s)$  attains a stable low value around 0.6 to 0.7; as the drop ratio rises, the tendency appears to be linear until the value  $a_1/H_s = 0.6$  is reached, then the linear trend ends. After this, the ratio  $y_s/(a_1 + H_s)$  appears to have reached a constant asymptotic value of around 1.4. The two equations below can be used to describe this pattern of behavior:

$$\begin{aligned} \frac{y_s}{(a_1 + H_s)} &= 0.25 + 2.0 \frac{a_1}{H_s} && \text{for } 0.2 < \frac{a_1}{H_s} < 0.6 \\ y_s &= 1.4(a_1 + H_s) && \text{for } \frac{a_1}{H_s} > 0.6 \end{aligned} \quad (3.8)$$

The measured scour lengths have also been normalized with the total specific energy at the sill, according to the previous approach, but the trend associated with the data is not particularly strong. It shows a very slow decreasing trend: the parameter  $l_s/(a_1 + H_s)$  attains an almost constant value of around 4.5 for small drop ratios, thereafter the trend drops, reducing to values of around 3.0 for larger drop ratios. In general a weak link was observed, which underlines that the scour length is essentially linked to the specific flow energy, and is only slightly influenced by the size of the morphological jump.

The shape of the scour hole can be described by the ratio between the longitudinal distance from the sill to the location of the deepest scouring,  $l_d$ , and the maximum scour depth,  $y_s$ . Figure 3.7 shows this length-to-depth ratio plotted against the normalized drop height. The ratio  $l_d/y_s$  initially attains high values that reflects the generation of long, shallow scour holes due to the dominant action of the flow energy with the respect to the erosion drop-pattern. As long as the drop ratio is lower than about 0.6, corresponding to jet angle less than approximately  $50^\circ$  a strong negative correlation

holds, with  $l_d/y_s$  reducing from 4.0-4.5 to roughly 1.1-1.2. This is the range in which the plunging jet is mainly in the vertical direction and the scour hole becomes deeper and less elongated. At  $a_1/H_s$  around 0.6, a change in the trend is indicated, the ratio  $l_d/y_s$  no longer declines and stabilizes at a value of around 1.15. After that threshold,  $a_1/H_s = 0.6$ , the action of the jet becomes less efficient, and the scour length and depth seem to increase according to a constant ratio. This confirms that similar scour hole patterns are observed in both clear-water conditions and those with upstream sediment feed.

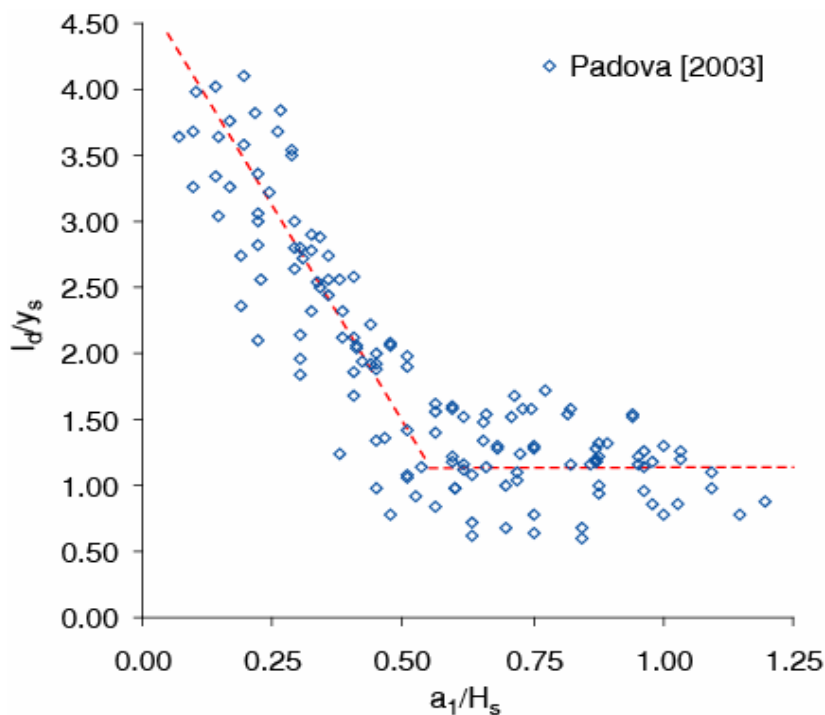


Figure 3.7 - Length to depth ratio against normalized drop height from this study [Padova, 2003].

### 3.6 CONCLUSIONS

In this chapter new experimental data were presented on the geometry of scour holes downstream of bed sills placed in steep gravel bed streams when an imposed upstream sediment feed is present. Initial examination of the data indicated that the local scour depth decreased as the sediment discharge increased, when all other factors remained fixed. The percentage reduction in maximum scour depth ( $y_s$ ) in case of sediment feed compared with the value of  $y_s$  in clear-water tests is considerable (see Table 3.1). This agreed with previous theoretical approaches used for scour holes with

no sediment supply. Existing dimensionless relationships to predict scour depth and length which had originally been calibrated with data from experimental tests in clear-water conditions were compared with the new data. A reasonable correspondence was observed. This correspondence indicated that the impact of the upstream sediment transport rate can be accounted for in the variable which describes the morphological jump and that another variable is not required to describe the impact of sediment transport on the development of the local-scouring phenomenon. For drop ratios,  $a_1/H_s$ , greater than 0.6, Eq. (3.2) from *Marion et al.* [2004], obtained with uniformly sized sediment, predicts the new data reasonably well. When  $a_1/H_s$  is less than 0.6 this relation overestimates normalized scour depth. For lower values of the ratio  $a_1/H_s$ , Eq. (3.1), obtained by *Lenzi et al.* [2002] on both high and low gradient river data, seems to provide better prediction than the formula of *Marion et al.* [2004]. In general it can be said that both formulae provide reasonable predictions, if applied for appropriate ranges of drop ratio. It has been shown that a slight correction of the coefficients in Eq. (3.2) leads to an expression that is still valid over a large range for both high and low gradient bed slopes. Geometrical interference and non-uniform grain size are also accounted for. The drop ratio value  $a_1/H_s = 0.6$  describes a threshold at which the physical mechanisms of erosion that cause the scour depths appear to change and this is reflected in the performance of the two formulae. This suggests that there may be two types of physical mechanisms responsible for scour hole formation that were not apparent from the initial dimensionless analysis of the data. These appear to depend on the jet inclination and the balance between efficiency of the jet to remove sediment and armoring processes to resist local erosion. The two modes of scour hole formation were also indicated by examining the scour depth normalized by the total specific energy and the geometric length of the scour hole. Both factors indicated that at a drop ratio of approximately 0.6 the dominant mechanism of scour hole formation changed. The data suggested that this change was linked to the jet inclination over the sill and the consequences on its efficiency to transport sediment.



## **CHAPTER 4 AFFINITY AND SIMILARITY OF SCOUR HOLES**

### **4.1 SUMMARY**

It is stated throughout this work that excessive erosion of gravel bed rivers represents a hazard, which is often controlled by the construction of bed sills. Most research efforts have focused on predicting scour depth, which may affect the structure at the free overfall, as opposed to volumetric scour dimensions and sediment yield contribution due to local scour, which may affect downstream morphology and water quality as well as the structure but are much more difficult to measure in an actively eroding plunge pool. In CHAPTER 4, shape and volume of equilibrium local scour holes at bed sills in high-gradient streams are investigated by analyzing steady-flow scour profiles at the equilibrium stage. Geometric properties of the scour profile are analytically discussed and verified on the basis of new data from experimental tests described in CHAPTER 3 (see section 3.3) and data from literature. A model is presented in section 4.3 to organize data analysis into a conceptual frame, which is based on the formal relationships for scour depth and length ensued from dimensional analysis, and on the assumption that scours exhibit definite geometric properties. In section 4.4 scour profiles are normalized by scaling the depths and the longitudinal distance from the upstream sill with the maximum dimensions of the scour hole. Results show evidence of a universal geometric affinity of the scour. Geometric similarity is also found to occur, but only in a limited range of physical conditions. An appropriate definition of such geometric properties is given in the text. Prediction formulae are proposed which link the eroded volume to the geometric, hydraulic and sediment

properties. Evidence on the scaling nature of the scour hole shapes have important implications on the prediction of the eroded volume, which are widely discussed in section 4.5. In turn, a correct evaluation of the eroded volume is necessary for the optimization of the design of the inter-sill distance. Next section provides a synthetic outline that illustrates the implications in river hydraulics of handling sediment volumes that are entrained due to local scouring.

## 4.2 SCOUR SHAPE AND VOLUME

Bed sills are a common solution to stabilize degrading bed rivers. Often such structures are used to control erosion in the proximity of bridge piers and abutments or in channels downstream of dams. Predictive formulae calibrated on experimental and field data for both scour depth and length are available to designers to take into account likely structural failure and for protecting river embankments to avoid excessive bank erosion. [*Gaudio et al.*, 2000; *Lenzi et al.*, 2003a; *Marion et al.*, 2004; *Meftah and Mossa*, 2006; *Martin Vide and Andreatta*, 2006]. To date relationships are not given for scouring at bed sills, which link the scour volume to the hydraulic characteristics of the flow and the sediment properties. Prediction of river bed evolution over time may be achieved by applying numerical integrations for the solution of the Saint Venant and Exner equations. Recently, mathematical models were proposed for the prediction of the scouring processes by turbulent plunging and horizontal jets [*Hogg et al.*, 1997; *Jia et al.*, 2001; *Adduce and Sciortino*, 2006]. Calibration with experimental data or empirical laws were used as a result of the extreme complexity of the flow field generated within the scour hole. As for bed sills, the estimation of the eroded volumes due to local scouring can be easily performed by investigating bed profiles and applying dimensional analysis developed for predicting the scour hole size.

In their studies on scouring processes, several authors [*Rajaratnam*, 1981; *Whittaker*, 1987; *Bormann and Julien*, 1991; *Chatterjee et al.*, 1994; *D'Agostino*, 1994; *Habib et al.*, 1994] found that the scour hole profiles are affine, i.e. can be reduced to a unique profile with appropriate scaling of the horizontal and vertical coordinates. *Gaudio et al.* [2000] verified the geometric affinity of local scour holes at bed sills in mild slope flumes, while *Lenzi et al.* [2002] verified it for steep gradients. Geometric similarity, which requires both longitudinal and vertical scour dimensions to be scaled

with the same factor, was never observed in the case of local scouring at bed sills. In CHAPTER 1 (see section 1.3.2) it was reported that *Farhoudi and Smith* [1985] demonstrated that this property holds at any time of the scour process for scour profiles downstream of hydraulic jump, if constant tailwater conditions are applied. Experimental tests [*Comiti et al.*, 2001; *Lenzi et al.*, 2003b; *Marion et al.*, 2004] were performed to evaluate the interference of scour development due to closely spaced sills. As described in CHAPTER 2, if the downstream boundary condition, i.e. the non-erodible point at the subsequent sill position, is closer than a certain critical distance to the scour hole is, the size and shape of the scour hole are significantly different from those which may form in unconstrained geometric conditions. For this reason, experimental tests where geometrical interference between sills was observed are not addressed to in this study.

In some cases, the eroded volume due to local scour must be evaluated to compute sediment mass balance. Reservoirs constructed in the last century for hydropower generation, storage or flood attenuation produce substantial changes to water flows and sediment loading along the stream channels, with significant impacts on river morphology [*Surian*, 1999]. As a more evident alteration, dams cause the trapping of solids conveyed by the river with consequent reduction of bed and suspended load in the reach downstream. Sediment transport capacity exceeds the supply due to slope erosion, and grains are entrained from the bed. Long-term general erosion, the timescale of which is normally of the order of several years or longer, occurs starting from the toe of a dam and, as a result, the downstream channel reach may have to be stabilized with bed sills. From the dam management standpoint, sediment deposition is the principal issue affecting the useful life of reservoirs. Among the techniques to mitigate silting of reservoirs, a structural measure is to reduce sediment yield using traps for bed material such as storage basins or check-dams. Although designed for other purposes, upstream reservoirs may have the same function. *Morris and Fan* [1998] stated that trapping by upstream dams is the most important factor controlling deposition in many reservoirs. Smaller structures can also have a significant impact on the delivery of gravels and sands when constructed widely across the watershed, but the lower cost of check-dams is offset by the large number of structures that is typically required. In addition, because the cost per unit of storage volume tends to decrease as a function of dam height, to trap

a given volume of sediment, a few larger structures will be more cost-effective than many smaller structures. The benefit of storage may be compromised if sequences of bed sills are not designed to prevent the opposite effect of downstream erosion and control the volume of solids that are entrained.

Further insights on the shape of the scour holes at bed sills are also required to deal with scour development over time. Many scour phenomena are time dependent [Hoffmans and Verheij, 1997], usually reaching the equilibrium or final depth of local scour rapidly in live-bed conditions, but rather more slowly in clear-water conditions [Mohamed and McCorquodale, 1992; Coleman *et al.*, 2003]. Clear-water data from Melville and Chiew [1999] on local scour at bridge piers indicate that 50% of the equilibrium scour depth is attained in a period varying from 0.1 to 10% of time to equilibrium, depending on the flow intensity, while, 80% of the maximum scour depth is developed in a period varying from only 5 to almost 40% of the time to equilibrium. Similarly, studies of temporal evolution of local scouring downstream of bed sills in steady flow conditions showed that the scour depth reaches values close to those at equilibrium in a short-term erosive phase, while it continues increasing during the successive long-term phase [Gaudio and Marion, 2003]. As formulae for predicting the development of scour depth with time are available, results from the present study can be used for the evaluation of local scour volumes eroded before reaching steady conditions.

### 4.3 THEORETICAL FRAMEWORK

#### 4.3.1 Similarity and affinity of scour hole profiles with uniform sediments

Assuming constant relative density of sediment and neglecting viscous effects, in the previous chapter it was showed that, for a wide channel of constant width with uniform sediments, the equilibrium maximum dimensions of the scour hole at non-interfering bed sills can be expressed as:

$$\frac{y_s}{H_s} = \Phi_y \left( \frac{a_1}{H_s} \right) = 3.0 \left( \frac{a_1}{H_s} \right)^{0.60} \quad (4.1a)$$

and



$$\frac{l_s}{a_1} = \Phi_x \left( \frac{a_1}{H_s} \right) = 7.0 \left( \frac{a_1}{H_s} \right)^{-0.85} \quad (4.1b)$$

Eqs. (1.1) and (1.2) were obtained from laboratory tests performed in both clear-water and sediment feeding conditions: they show that the ratio  $a_1/H_s$  is the most significant parameter controlling not only the maximum depth, but also the length of the scour hole at equilibrium. This represent a simplification of the original relationships derived from dimensional analysis, which neglects a direct effect of sediment size on scouring, i.e. neither  $H_s/D$  or  $a_1/D$  are taken into account. Such assumption, which comes from both experimental evidence and from considering that grain size is accounted for in the definition of the morphological jump,  $a_1$ , will be used throughout the following analysis. According to the findings of CHAPTER 3,  $H_s$  is defined as the specific energy of the flow available at the sill, in order to account for the effect of  $F_R$  on jet inclination in case of supercritical flows.

An affine transformation is a transformation that preserves collinearity (i.e., all points initially lying on a straight line still lie on a straight line after the transformation) and ratios of parallel segments. A particular case is the anisotropic variation of scale, which is defined by the following matrix equation:

$$\begin{bmatrix} X' \\ Y' \end{bmatrix} = \begin{bmatrix} \tilde{X} & 0 \\ 0 & \tilde{Y} \end{bmatrix} \begin{bmatrix} X \\ Y \end{bmatrix} \quad (4.2)$$

where the coordinates of the point  $P'(X', Y')$  lying on the plane  $\pi'$  correspond to the coordinates of the point  $P(X, Y)$  lying on the plane  $\pi$ ,  $\tilde{X}$  and  $\tilde{Y}$  being dimensionless positive real values. A property of affine transformations is that, if  $F$  and  $F'$  are the original and transformed figures respectively, the relevant areas,  $A_F$  and  $A_{F'}$ , are linked by the following relation:

$$A_{F'} = \det \begin{bmatrix} \tilde{X} & 0 \\ 0 & \tilde{Y} \end{bmatrix} \cdot A_F = \tilde{X}\tilde{Y} \cdot A_F \quad (4.3)$$

Eq. (4.3) describes the affine transformation of a scour hole profile into another. The scour hole can be described with the function  $y = f(x)$ , where  $y$  is the scour depth, with respect to the initial bed level, at the longitudinal abscissa  $x$ , measured starting from the upstream bed sill. If scour hole profiles are normalized, i.e. the coordinates are scaled with suitable dimensional factors,  $\tilde{x}$  and  $\tilde{y}$  respectively along the  $x$  and  $y$  axes, dimensionless curves are obtained:

$$y^* = f_1(x^*) \quad (4.4a)$$

where

$$y^* = \frac{y}{\tilde{y}}; \quad x^* = \frac{x}{\tilde{x}} \quad (4.4b)$$

Scour hole profiles are then affine if the dimensionless curves can be superimposed. It follows that the local scour area,  $A_s$  (local scour volume,  $V_s$ , for unit flume width,  $B$ , limited to the scour length,  $l_s$ ) can be computed as follows:

$$A_s = \frac{V_s}{B} = \int_0^{l_s} y(x) dx = \int_0^{l_s^*} \tilde{y} y^*(x^*) \tilde{x} dx^* = \tilde{y} \tilde{x} \cdot \int_0^{l_s^*} f_1(x^*) dx^* \quad (4.5)$$

with  $l_s^* = l_s/\tilde{x}$ ; the last integral is constant for all the scour holes, depending on the shape of the normalized curves. If the equilibrium maximum scour depth,  $y_s$ , and length,  $l_s$ , are used to scale the coordinates of the scour hole profiles ( $\tilde{x} = l_s$  and  $\tilde{y} = y_s$ ), then Eqs. (1.1) and (1.2) can be taken into account and Eq. (4.5) becomes:

$$A_s = \frac{V_s}{B} = a_1 \Phi_x \left( \frac{a_1}{H_s} \right) \cdot H_s \Phi_y \left( \frac{a_1}{H_s} \right) \cdot K_1 \quad (4.6a)$$

i.e.

$$\frac{A_s}{a_1 H_s} = K_1 \cdot \Phi_1 \left( \frac{a_1}{H_s} \right) \quad (4.6b)$$

where

$$K_1 = \int_0^1 f_1(x^*) dx^* \quad (4.6c)$$

and  $\Phi_1 = \Phi_x \Phi_y$ . While  $l_s$  is suitable for scaling the  $x$ -coordinate [Gaudio *et al.*, 2000; Lenzi *et al.*, 2002], some issues arise about the scale factor  $\tilde{y}$ . In fact, considering the scour depth, with respect to the initial bed, at the end of the local scour hole,  $y(x = l_s)$ , it results:

$$\frac{y(l_s)}{y_s} = \frac{a_1 - (S_0 - S_{eq}) \cdot l_s}{y_s} = \frac{a_1}{y_s} - \frac{(S_0 - S_{eq})L}{y_s} \cdot \frac{l_s}{L} = \frac{a_1}{y_s} \cdot \left(1 - \frac{l_s}{L}\right) \quad (4.7)$$

Taking into account Eqs. (1.1) and (1.2), Eq. (4.7) can be rewritten in terms of  $a_1/H_s$  and  $a_1/L$ , as follows:

$$\frac{y(l_s)}{y_s} = \frac{\frac{a_1}{H_s}}{\Phi_y \left(\frac{a_1}{H_s}\right)} \cdot \left[1 - \Phi_x \left(\frac{a_1}{H_s}\right) \cdot \frac{a_1}{L}\right] \quad (4.8)$$

Once all the hydraulic and sediment characteristics are fixed,  $a_1/H_s$  increases linearly with  $L$ , while  $a_1/L = S_0 - S_{eq}$  is constant, and the functions  $\Phi_y$  and  $\Phi_x$  follow a positive and negative trend, respectively. Since  $\Phi_y$  grows less than linearly, as stated by Eq. (4.1a), Eq. (4.8) shows that  $y(l_s)/y_s$  depends on  $L$  and affinity cannot occur. Similar conclusions may be drawn for the general term  $y(x)/y_s$ . The analysis performed in previous works by different authors about affinity of local scour holes did not account for this limitation, due to the weak dependence of  $y(x)/y_s$  on  $L$ .

A more productive approach to the problem is to divide the scour area into two parts:  $A_g = a_1 L/2$ , due to general erosion, and  $A_s'$ , due to local scouring only (Figure 4.1, dashed area). The net local scour depths,  $y'(x)$ , measured starting from the plane having slope  $S_{eq}$  is the best choice to show affinity. If the maximum net scour depth,  $y_s' \approx y_s - a_1$ , is the new scaling factor, the ratio  $y'(l_s)/y_s' = 0$  does not depend on  $L$  and affinity is theoretically possible. It follows that:

$$(y')^* = f_2(x^*) \quad (4.9a)$$

where

$$(y')^* = \frac{y'}{y'_s}; \quad x^* = \frac{x}{l_s} \quad (4.9b)$$

Let now  $V'_s$  and  $A'_s$  denote the net scour volume and the net scour area respectively. Eq. (4.6a) is easily rewritten in terms of net quantities:

$$A'_s = \frac{V'_s}{B} = \tilde{x}\tilde{y} \int_0^{l'_s} f_2(x^*) dx^* = l_s y'_s \int_0^1 f_2(x^*) dx^* \quad (4.10a)$$

i.e.

$$\frac{A'_s}{a_1 H_s} = K_2 \cdot \Phi_2 \left( \frac{a_1}{H_s} \right) \quad \text{for affinity} \quad (4.10b)$$

where

$$K_2 = \int_0^1 f_2(x^*) dx^* \quad (4.10c)$$

and  $\Phi_2 = \Phi_x(\Phi_y - a_1/H_s)$  is a function of  $a_1/H_s$ .

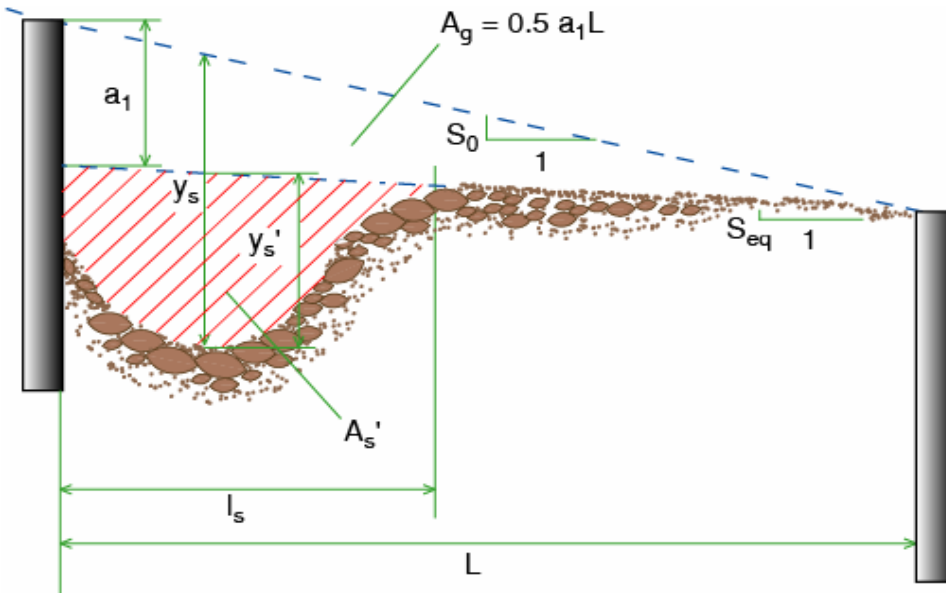


Figure 4.1 - Schematic of the local scour hole between two bed sills at equilibrium.  $A_g$  is the general erosion area (volume per unit width);  $A'_s$  is the net local scour area.

Under the assumption the scour is affine, according to the transformation defined in Eq. (4.2), geometric similarity follows only if the ratio  $\tilde{x}/\tilde{y} = l_s/y_s'$  is constant for all scour holes. This is not always verified, but it can be observed that:

$$\frac{l_s}{y_s'} = \frac{\Phi_x\left(\frac{a_1}{H_s}\right)}{\Phi_y\left(\frac{a_1}{H_s}\right) - \frac{a_1}{H_s}} \cdot \frac{a_1}{H_s} \equiv \Phi_{xy}\left(\frac{a_1}{H_s}\right) \quad (4.11)$$

i.e. scour hole profiles are similar whenever the value of the parameter  $a_1/H_s$  is fixed. Taking into account Eq. (4.11), it is possible to rewrite Eq. (4.10a) to yield:

$$A'_s = \frac{V'_s}{B} = l_s y_s' \int_0^1 f_2(x^*) dx^* = \Phi_{xy}\left(\frac{a_1}{H_s}\right) (y_s')^2 \int_0^1 f_2(x^*) dx^* \quad (4.12a)$$

i.e.

$$\frac{A'_s}{H_s^2} = K_3 \cdot \Phi_3\left(\frac{a_1}{H_s}\right) \quad \text{for similarity} \quad (4.12b)$$

where

$$K_3 = \Phi_{xy}\left(\frac{a_1}{H_s}\right) \cdot \int_0^1 f_2(x^*) dx^* \quad (4.12c)$$

and  $\Phi_3 = (\Phi_y - a_1/H_s)^2$  is a function of  $a_1/H_s$ . It must be stressed that  $K_3$  is not a constant as  $K_1$  and  $K_2$ , but it is introduced here for convenience, as will become apparent in the following sections.

### 4.3.2 Similarity and affinity of scour hole profiles with non-uniform sediments

For non-uniform sediments, Eqs. (1.1) and (1.2) can be corrected using a grading parameter, e.g. the sorting index,  $SI$  (equal to the geometric standard deviation,  $\sigma_g$ , for log-normal grain-size distributions), as follows (the subscript “*nu*” refers to non-uniform sediments):

$$\left(\frac{y_s}{H_s}\right)_{nu} = \left(\frac{y_s}{H_s}\right) \cdot SI^{-\alpha_y} \quad (4.13a)$$

$$\left(\frac{l_s}{a_1}\right)_{nu} = \left(\frac{l_s}{a_1}\right) \cdot SI^{-\alpha_x} \quad (4.13b)$$

where  $\alpha_y$  e  $\alpha_x$  are calibration exponents for the net maximum depth and length of the scour hole respectively. As discussed in CHAPTER 2, Eq. (4.13a) was obtained by *Marion et al.* [2004], who found  $\alpha_y = 0.19$  using data from tests with different grain size distributions [*Lenzi et al.*, 2002; *Lunardi*, 2002]. Eq. (4.13b) is proposed here by analogy with Eq. (4.13a). To date no experimental data were used to estimate the dependence of the scour hole length on sorting index, i.e. to evaluate  $\alpha_x$ . The effect of sediment sorting on  $l_s$  is expected to be much smaller [*Aderibigbe and Rajaratnam*, 1998] than the reduction effect on the maximum scour depth. It is anticipated here that data used in this study satisfy Eq. (4.13b) for  $\alpha_x = 0.03$ . This value is so small that the effect of sediment sorting on scour length could be neglected without significant change of the results, i.e. assuming  $\alpha_x = 0$ .

According to the analysis which led to Eqs. (4.12a) and (4.12b), the following dimensionless formulation of the local scour volume for sediment mixtures holds (see Appendix to CHAPTER 4):

$$\left(\frac{A'_s}{a_1 H_s}\right)_{nu} = \frac{A'_s}{a_1 H_s} \cdot \left[1 - \left(1 - SI^{-\alpha_y}\right) \left(\frac{\Phi_y}{\Phi_y - a_1/H_s}\right)\right] \quad \text{for affinity} \quad (4.14a)$$

$$\left(\frac{A'_s}{H_s^2}\right)_{nu} = \frac{A'_s}{H_s^2} \cdot \left[1 - \left(1 - SI^{-\alpha_y}\right) \left(\frac{\Phi_y}{\Phi_y - a_1/H_s}\right)\right] \quad \text{for similarity} \quad (4.14b)$$

In the next paragraphs laboratory data from literature and data from the same experiments described in CHAPTER 3 will be analyzed in order to: 1) confirm that affinity of the net scour hole profiles is apparent over a wide range of hydraulic, sediment transport and geometric conditions, 2) verify the dependence of similarity of the scour hole profiles on the drop ratio,  $a_1/H_s$ ; and 3) demonstrate that Eqs. (4.10b) and (4.12b) are appropriate functional relations for the dimensionless net scour area,  $A'_s$ .

## 4.4 EXPERIMENTS AND RESULTS

### 4.4.1 Laboratory data

The present data on scour hole profiles were collected from three series of high-gradient laboratory experiments, performed under long-term steady flows and both clear-water and sediment supply conditions. They were carried out over the last few years using rectangular cross-sectional tilting flumes at the Hydraulic Laboratory of the University of Padua (Italy) and at HR Wallingford Ltd (UK).

Twenty-seven clear-water tests were performed in a 10 m long, 0.5 m wide, 0.5 m deep glass-sided flume, as described in *Marion et al.* [2004]. The sediment used was uniform gravel ( $SI = 1.48$ ), with  $D_{50} = 8.7$  mm. Bed slopes ranged from 3.0 to 8.0%, with flow discharges ranging between 9.0 and 30.3 l/s. Forty-eight sediment-supply and clear-water tests were subsequently conducted using the same gravel as the first series of experiments. The sediment supply had the same grain size composition as the sediment deposit placed on the bed of the flume. The following parameters were used: initial bed slopes from 4.2 to 7.4%, water discharges from 18 to 26 l/s, and constant sediment rates up to 35.5 g/s. Full description of the sediment supply equipment and the experimental system is presented in CHAPTER 3. According to the previous notation such data series are identified as “Padova [2003]”. Thirteen clear-water tests were performed at HR Wallingford in a 5.57 m long, 0.60 m wide, 0.25 m deep flume, on slopes ranging from 7 to 14%, water discharge between 4.0 and 17.5 l/s, and non-uniform gravel with  $D_{50} = 8.5$  mm and  $SI = 5.95$  [*Lenzi et al.*, 2002]. This data series was used to take into account the effect of sediment grading on scour shape.

In order to guarantee long-term equilibrium conditions, the test duration was set on the basis of direct observations to be conservative with respect to the time needed to achieve complete scour development (i.e. when scouring no longer increased and net sediment transport became zero). At the end of each test, the equilibrium bed slope,  $S_{eq}$ , was attained downstream of the scour hole and this was evaluated from the bed profiles; the morphological jump,  $a_1$ , was then calculated by using the relationship given in the previous chapters. In no test was the scour length so long as to produce interference between the sills.

#### 4.4.2 Affinity of scour hole profiles

The coordinates  $x$  and  $y'(x)$  of the net scour hole profile were scaled with the length and the net maximum depth,  $l_s$  and  $y'_s$  respectively. The profiles turn out to be approximately affine (see Figure 4.2). According to the definition of  $x$  and  $y'$  (see section 4.3.1), the origin of the Cartesian axes is at the point where the equilibrium bed slope plane, which can be assumed as approximately horizontal, intersects the vertical plane of the upstream bed sill.

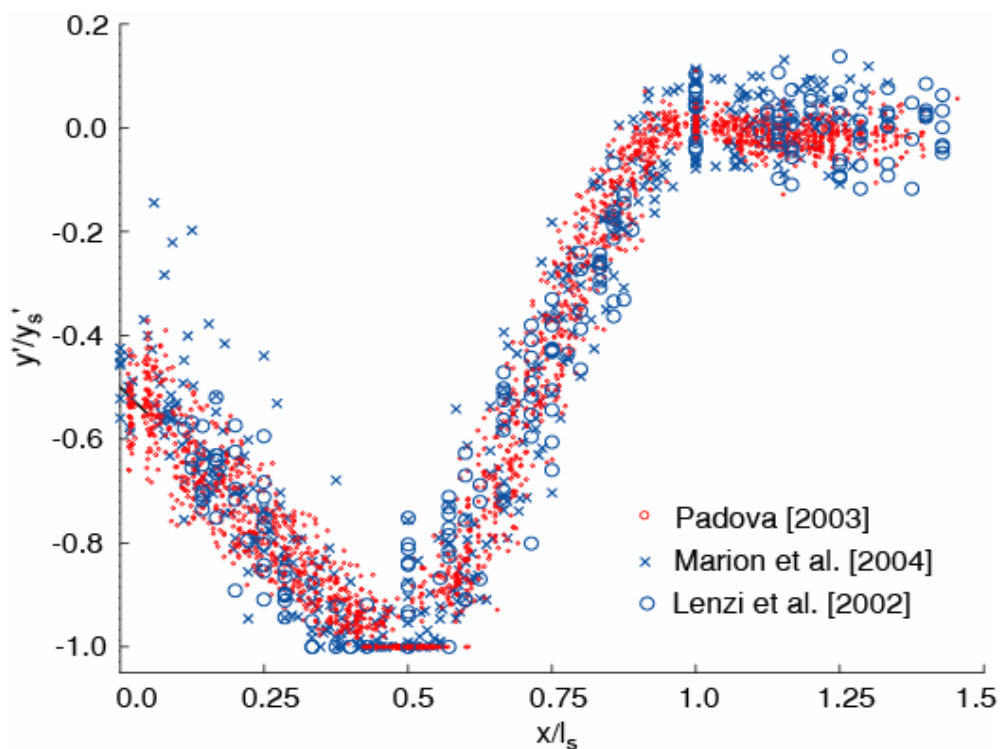


Figure 4.2 - Affine dimensionless scour hole profiles.

As stated in Eqs. (4.5) and (4.10a), geometric affinity implies that the net scour area is linearly dependent on the product of the scale factors. Figure 4.3 shows the behavior of  $A'_s$  with  $l_s y'_s$  for local scour holes in high-gradient streams, which can be expressed with the following least squares linear regression equation, according to Eq. (4.10a):

$$A'_s = K_2 \cdot y'_s l_s = 0.6 \cdot y'_s l_s \quad (4.15a)$$

$$A'_{s,nu} = K_2 \cdot y'_{s,nu} l_{s,nu} = 0.6 \cdot y'_{s,nu} l_{s,nu} \quad (4.15b)$$



with a coefficient of determination  $R^2 = 0.98$ .

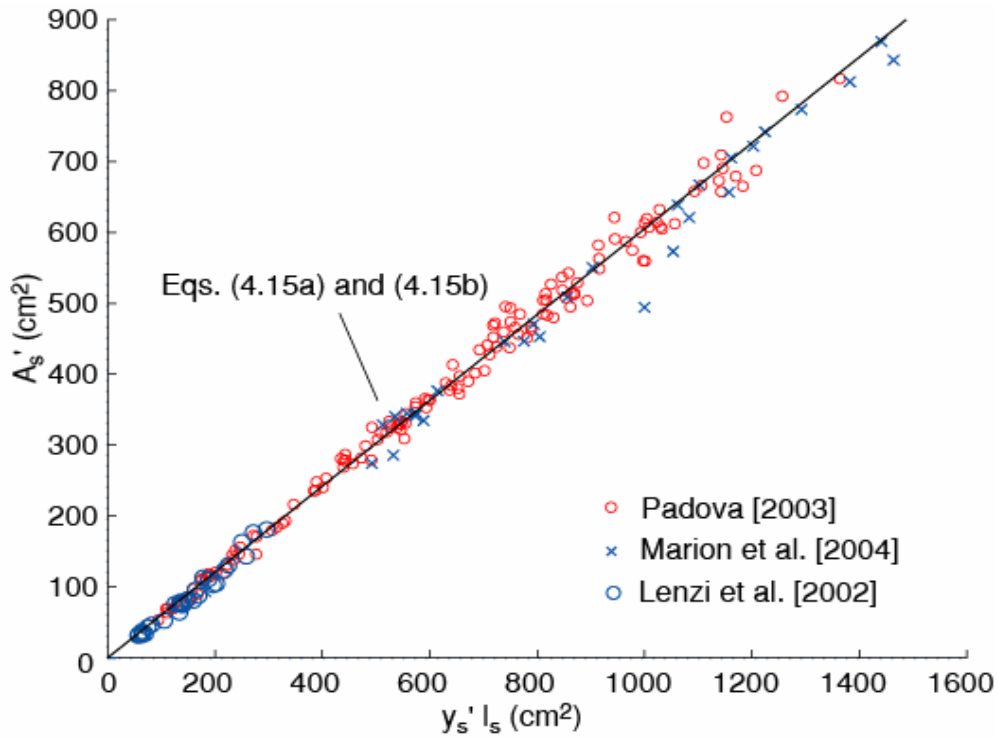


Figure 4.3 - Net local scour area versus the product maximum depth and length of the equilibrium scour hole.

#### 4.4.3 Similarity of scour hole profiles

As discussed in section 4.3.1, similarity requires the additional condition, with respect to affinity, that the ratio  $l_s/y_s'$  is constant for all tests. If this condition holds, it is easy to show that the scour hole profiles can be scaled with a unique factor, e.g.  $y_s'$ . In order to compare all data, non-uniform sediment data were normalized to take into account the effect of sorting with the following relations:

$$y_s' = \frac{y_{s,nu}}{SI^{-\alpha}} - a_1 \quad (4.16a)$$

$$l_s = \frac{l_{s,nu}}{SI^{-\alpha_x}} \cong l_{s,nu} \quad (4.16b)$$

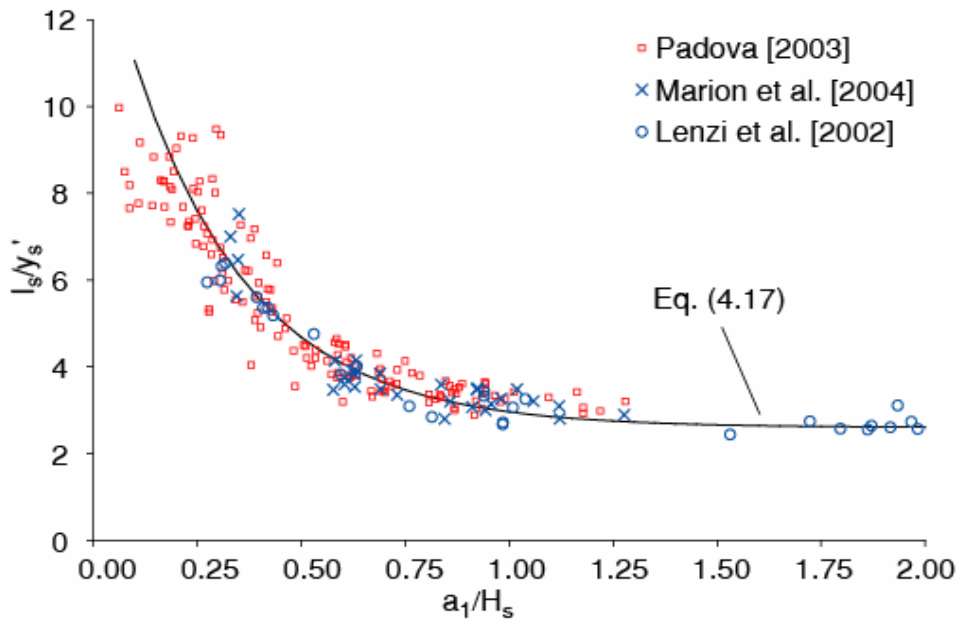


**Figure 4.4 - Net local scour length-to-depth ratio versus drop ratio.**

Figure 4.4 shows the behavior of the net scour length-to-depth ratio,  $l_s/y_s'$ , with the drop ratio,  $a_1/H_s$ . The ratio  $l_s/y_s'$  initially attained high values, which are related to the generation of long, shallow scour holes, due to the dominant action of the flow energy with respect to the plunging jet. The following least squares regression equation was obtained:

$$\frac{l_s}{y_s'} = \Phi_{xy} \left( \frac{a_1}{H_s} \right) = 2.6 + 12.0e^{-3.5 \frac{a_1}{H_s}} \quad (4.17)$$

with a coefficient of determination  $R^2 = 0.88$ . This relationship shows that scour hole profiles are similar either when  $a_1/H_s$  is constant or when it is very large, i.e. when the curve reaches the asymptotic value. This trend is explained in the next section. According to Figure 4.4, when the drop ratio is higher than about 0.7, geometric similarity is approximately verified for all scour holes. Dimensionless scour hole profiles, scaled with the net maximum scour depth, were plotted in Figure 4.5, where  $a_1/H_s$  increases from graph (a) to (f). In case of graded sediments, the different development of scour shape is taken into account by scaling the horizontal coordinate with the equivalent depth for uniform sediments,  $y_s'$ , as defined by Eq. (4.16a). Figure

4.5 confirms that similarity is applicable to scour holes falling in narrow ranges of the drop ratio and for all large drop ratios ( $a_1/H_s > 0.7$ ).

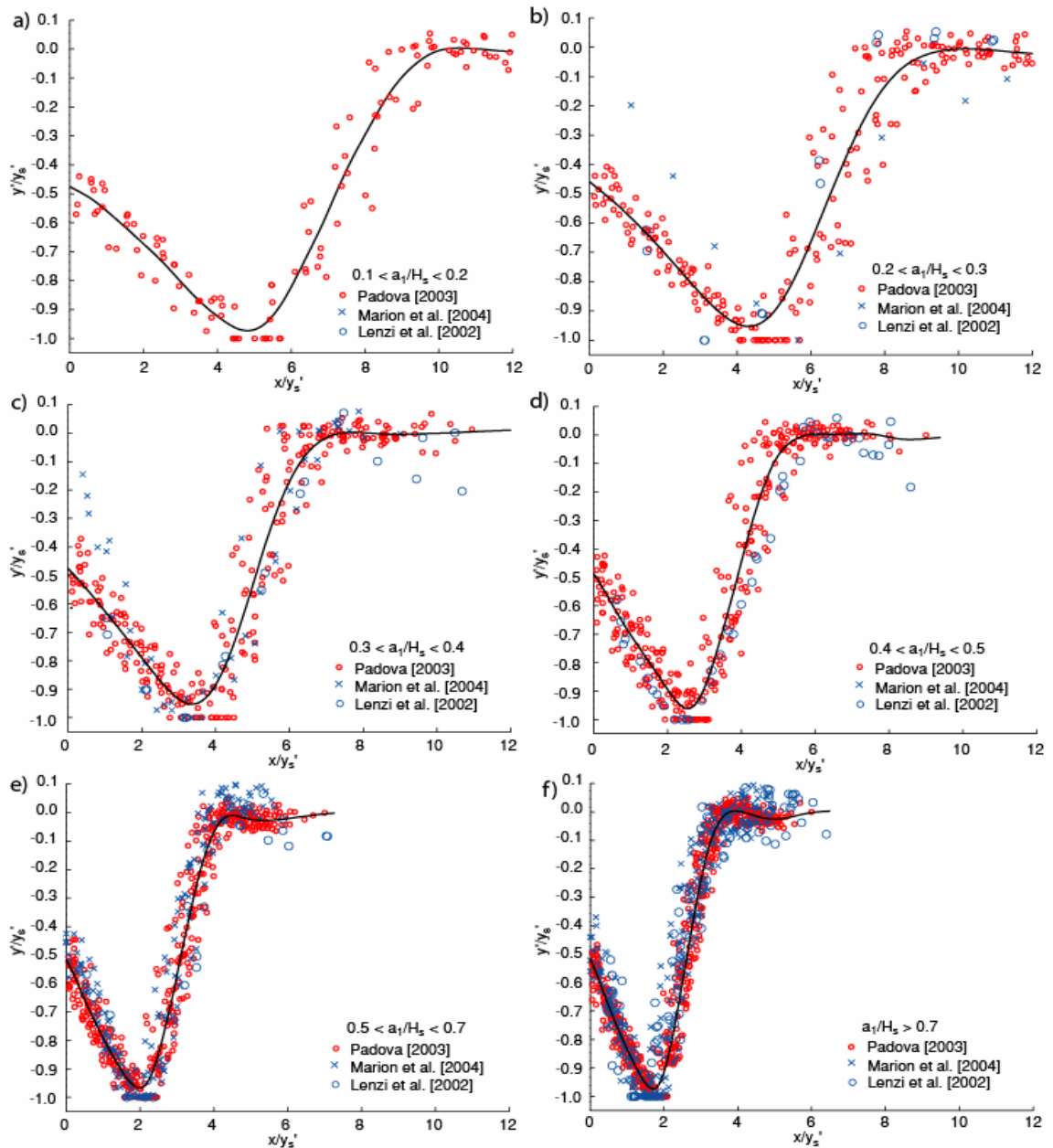
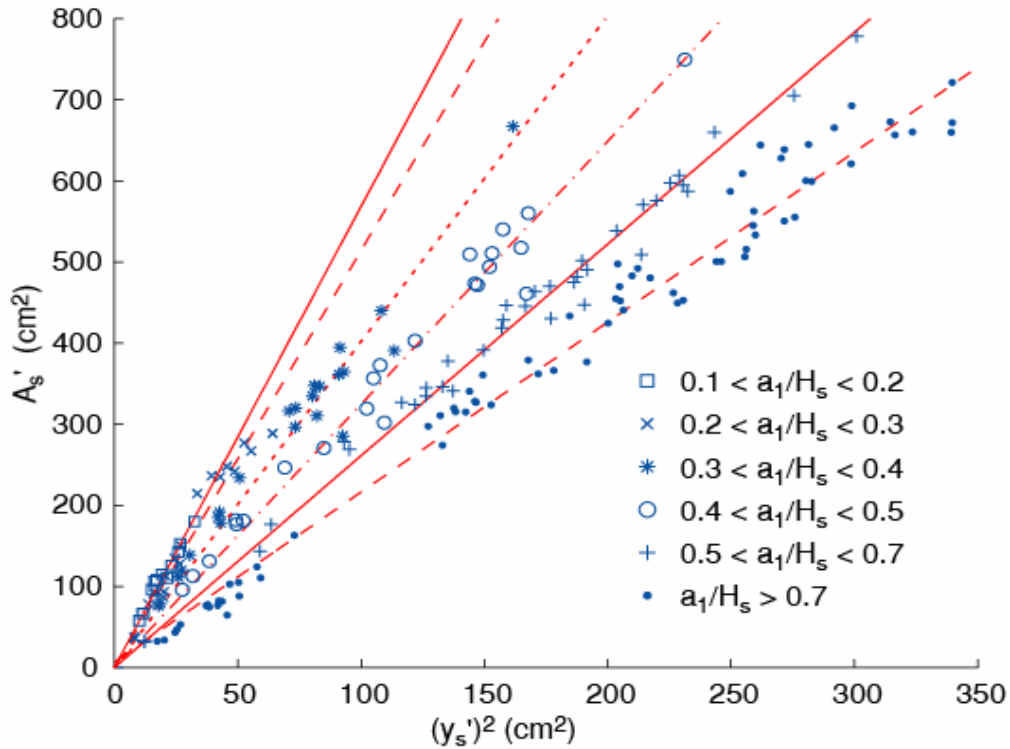


Figure 4.5 - Dimensionless scour hole profiles: similarity in dependence of the drop ratio.

Figure 4.6 shows the behavior of the net scour area,  $A_s'$ , with the square net maximum scour depth,  $(y_s')^2$ , at different drop ratios,  $a_1/H_s$ . The net scour area increases linearly once  $a_1/H_s$  is assigned, as stated by Eq. (4.12a). The function  $K_3$ , which can be calculate by taking into account Eqs. (4.15a) and (4.17), is the slope of the straight lines in Figure 4.6. Its values are reported in Table 4.1. The results demonstrate the

significance of the shape in the estimation of scour area: for scour holes with the same net maximum depth, the scour area may vary by a factor of three, depending on the drop ratio.



**Figure 4.6 - Net local scour area versus square net maximum depth: dependence on the drop ratio (data from Padova, 2003; Marion et al., 2004; Lenzi et al., 2002). The values of angular coefficients,  $K_3$ , obtained through linear regression, are reported in Table 1.**

*Farhoudi and Smith* [1985] proposed a similar approach to analyze local scouring due to horizontal jets, resulting in shallow, long scours. They found that the values of  $l_d/y_s'$  and  $l_s/y_s'$ , being  $l_d$  the longitudinal distance where the maximum scour depth occurs, ranged respectively from 3.1 to 4.8 and from 6.9 to 9.8, depending on the applied tailwater conditions. In the present study, for scour profiles with  $a_1/H_s < 0.3$ , the values of  $l_d/y_s'$  and  $l_s/y_s'$  are similar to those presented by *Farhoudi and Smith*, as showed in Figure 5. The ratio between the scour area and the square maximum depth,  $A_s'/(y_s')^2$ , which is the parameter defined as  $K_3$  in this study, was found by *Farhoudi and Smith* in the range 4.9 to 6.3. Comparing these values with the corresponding parameter in Table 4.1 shows again a reasonable agreement for  $a_1/H_s < 0.3$ .

**Table 4.1 - Relationship between drop ratio and shape coefficients**

Drop ratio $a_1/H_s$	Angular coefficient $K_3$	Downstream scour side inclination $\tan(\varphi_{scour})$	Plunging jet inclination $\tan(\varphi_{jet}) =$ $(3a_1/H_s)^{0.5}$	Downstream scour side angle $\varphi_{scour}$ ( $^\circ$ )	Plunging jet angle $\varphi_{jet}$ ( $^\circ$ )
0.1 – 0.2	5.7	0.23	0.67	13.1	33.8
0.2 – 0.3	5.1	0.30	0.87	16.7	40.9
0.3 – 0.4	4.0	0.34	1.02	18.9	45.7
0.4 – 0.5	3.2	0.40	1.16	21.8	49.3
0.5 – 0.7	2.6	0.48	1.34	25.6	53.3
> 0.7	2.1	0.59	1.69	30.5	59.4

In the case of no sediment sorting, i.e. for  $SI < 1.5$ , the dependence of the energy-normalized net scour area,  $A_s'/(H_s)^2$ , on the drop ratio is shown in Figure 4.7. Eq. (4.12b) is then approximated by the following least squares regression equations:

$$\frac{A_s'}{H_s^2} = 10.5 \frac{a_1}{H_s} \quad \text{for } \frac{a_1}{H_s} < 0.6 \quad (4.18a)$$

$$\frac{A_s'}{H_s^2} = 6 + 0.5 \frac{a_1}{H_s} \quad \text{for } \frac{a_1}{H_s} > 0.6 \quad (4.18b)$$

with coefficients of determination  $R^2 = 0.82$  and  $0.79$ , respectively. Figure 4.7 shows that the dimensionless net scour area increased with the drop ratio more rapidly for  $a_1/H_s < 0.6$  (solid line) than for  $a_1/H_s > 0.6$  (dashed line).

## 4.5 DISCUSSION

### 4.5.1 The physical process determining the scour shape

The discussion carried out in CHAPTER 3 showed two distinct types of behaviors in the development of the scour holes, which suggested the existence of different physical processes, involving different laws for the scour depth growth, changes in shape development, and, as a consequence, two different prediction formulae for evaluating the scour area. According to *Bormann and Julien* [1991], who found that the jet impact angle plays a major role in determining the scour depth as well as its

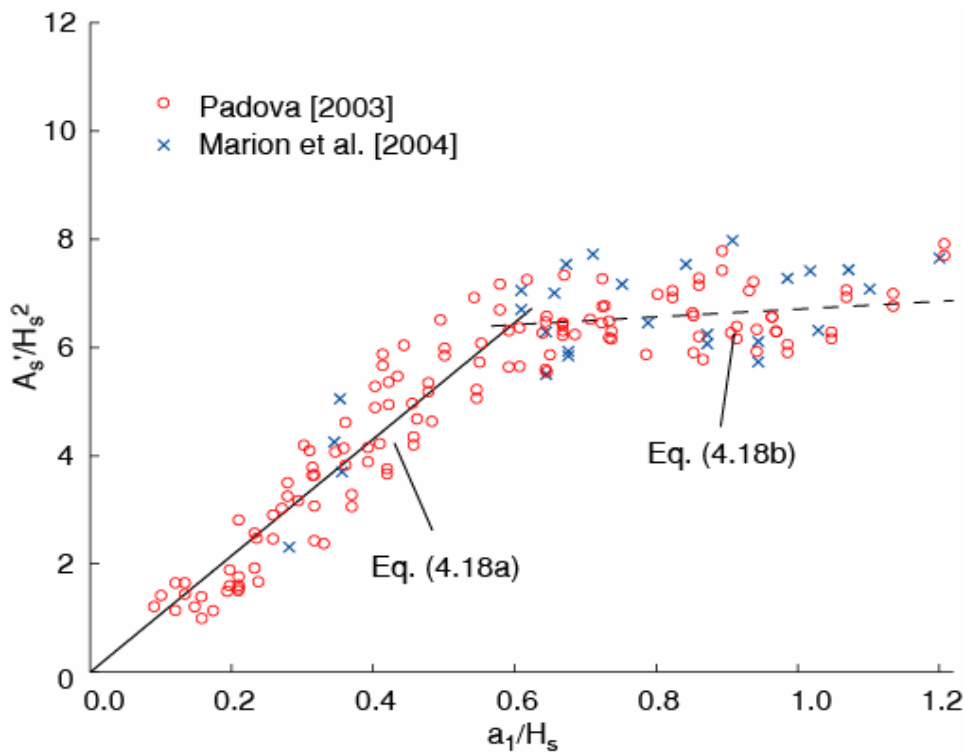


Figure 4.7 - Dimensionless net local scour area versus drop ratio.

geometry, it was stated that this two-zone behavior could be explained by examining the different jet inclinations of the flow over the sills. It was then demonstrated that the tangent of the angle of jet impact to the horizontal plane,  $\varphi_{jet}$ , at a distance  $a_1$  below the sill crest, was proportional to the square root of the drop ratio.

It is stated now that, as long as the values of  $a_1/H_s$  are smaller than about 0.7, the inclination of the plunging jet is the main parameter which controls the shape of the scour hole, because the angle formed by the downstream side of the scour hole with the horizontal plane,  $\varphi_{scour}$ , is strongly related to the jet angle. In the above range of the drop ratio, therefore, the two angular coefficients,  $\tan(\varphi_{jet})$  and  $\tan(\varphi_{scour})$ , reported in Table 4.1, scale with a constant ratio, which means also that the scour inclination increases with the square root of the drop ratio. When  $a_1/H_s$  rises above a certain threshold, scour steepness does not increase anymore, and, consequently, scour depths and lengths scale almost proportionally, approaching the asymptotic value given by Eq. (4.17), and resulting in approximately similar scour holes.

This threshold corresponds to the physical limit reached when the angle  $\varphi_{scour}$  matches the angle of repose of the sediment mass, which is approximately equal to  $30^\circ$ . Therefore, for scour holes developed in the range of the lower values of  $a_1/H_s$ , the more

tilted the plunging jet, the higher the erosion intensity and the steeper the downstream side of the scour hole. When the limit related to the sediment angle of repose is attained, scouring is constrained to develop less intensively and scour depth rises because of a bigger availability of potential energy (that is the morphological jump,  $a_1$ ), but much less (or not at all) because of a more inclined jet with respect to the horizontal plane.

It is drawn that geometric similarity of scour holes at bed sills is possible only for drop ratios,  $a_1/H_s$ , constant or sufficiently high (greater than 0.7). It means that, for given values of the discharge,  $Q$ , the median diameter,  $D_{50}$ , and the initial bed slope,  $S_0$ , similarity is possible only whether the inter-sill distance,  $L$ , is constant (trivial condition) or sufficiently high, i.e.  $L > L_{lim} = 0.7H_s/(S_0 - S_{eq})$ . Therefore, if a river reach is set with a series of sills, in case of variable  $L$  or  $L < L_{lim}$  between two successive non-interfering sills only affinity is possible, and two length scales are needed in order to get dimensionless superimposed profiles.

#### **4.5.2 The effect of armoring on scour hole reduction**

The experimental series on scouring with non-uniform sediments are limited to the data presented by *Lenzi et al.* [2002], who used only one grain-size distribution with  $SI = 5.95$ . Available data are not sufficient to completely validate Eqs. (4.14a) and (4.14b). According to these relationships, the ratio of the dimensionless net scour areas computed for non-uniform and uniform sediments, respectively, is expressed as a function of  $SI$  and  $a_1/H_s$ . The trend of this function is plotted versus  $a_1/H_s$  in Figure 4.8 for different values of  $SI$ . The dimensionless net scour area,  $A_s'/(H_s)^2$ , for data with non-uniform sediments were scaled with the expression given by Eqs. (4.18a) and (4.18b), valid for uniform sediments, and displayed in the same figure. The experimental data reasonably approach the curve corresponding to  $SI = 5.95$ , with mean relative error  $\varepsilon_{mean} = 6.8\%$  and max relative error  $\varepsilon_{max} = 14.1\%$ , showing to be consistent with the proposed formulae.

The reduction of the scour hole area in case of non-uniform sediments compared to the potential value achieved for uniform sediments is mainly due to the effect of sorting. If Eqs. (4.14a) and (4.14b) hold, the amount of eroded volume can be reduced up to 50% for highly graded sediments and high values of  $a_1/H_s$ . The weak dependence on  $a_1/H_s$  can be explained as follows: for high drops compared to the specific flow energy, the bed surface coarsening linked to hiding and exposure mechanisms is

increased with respect to low drop ratios. While scour profiles grow deeper, most of the fine and medium particles are swept up from the scour surface by the plunging jet over the bed sill and the highly turbulent rollers inside the scour hole. The armoring increases with the sediment gradation: the higher the value of  $SI$ , the higher the slope of the theoretical curves (Figure 4.8).

Bed armoring is known to reduce both general and local erosion, due to increased grain stability. This implies that controlling bed degradation using bed sills is more effective for non-uniform deposits than for uniform ones, which is the common condition in natural water courses. The effect of sorting is more important for reducing local scouring than for general bed erosion, because of the intensity of the armoring process on the scour hole surface. This must be taken into account when designing river bed protection.

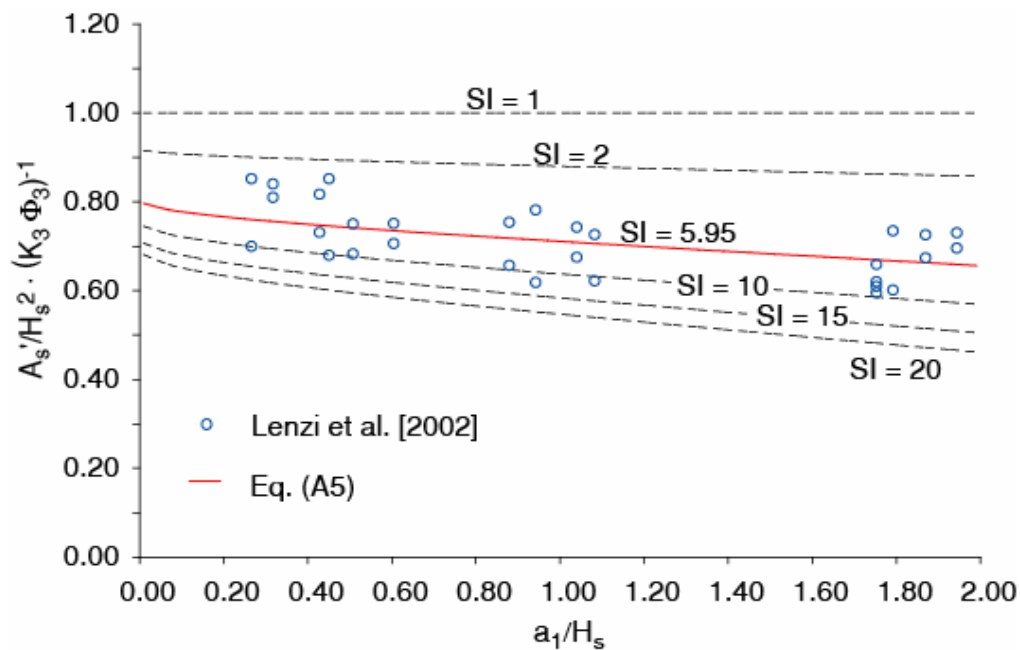


Figure 4.8 - Reduction factor of the net scour area versus  $a_1/H_s$ , for different values of  $SI$ . Comparison with data by Lenzi et al. [2002].

#### 4.5.3 Choice of the distance between structures

When a river channel is to be stabilized with respect to general bed degradation, the designer usually faces the need of limiting the overall eroded volume. Assuming a constant value of  $H_s$ , which is linked to the design discharge,  $Q$ , being  $D_{50}$  and  $S_0$



relevant to the river morphology, the sill distance,  $L$ , is the only parameter controlling the amount of eroded sediment for general erosion and local scouring. Once the value of  $L$  is set, the eroded volume per unit width (or scour area) in a reach between two structures, scaled with the square specific energy at the cross-section of the sill, is given by the following (see Figure 4.1):

$$\frac{A_{tot}}{H_s^2} = \frac{A_g}{H_s^2} + \frac{A'_s}{H_s^2} = \frac{1}{2} \frac{a_1}{H_s} \cdot \frac{L}{H_s} + K_3 \cdot \Phi_3 \left( \frac{a_1}{H_s} \right) \quad (4.19)$$

As discussed in CHAPTER 2, the ratio  $L/H_s$  is a measure of the interference degree between two successive bed sills. *Marion et al.* [2004] stated that the effect of geometrical interference on  $y_s/H_s$  is negligible for  $L/H_s > 10$  to 15. Geometrical interference induces an altered flow pattern, called “unstable tumbling flow”, as reported by *Whittaker* [1987], where the turbulent roller associated with the hydraulic jump is constrained by the closely spaced sills. Even though it leads to a reduction of the scour dimensions compared to their potential size, the drop energy associated with the free jet impinging into the pool tailwater, corresponding to  $a_1$  for non-interfering bed sills, is only partially dissipated into the scour hole. This residual potential energy, which must be dissipated along the downstream reach, may cause undesired excessive erosion. The above threshold value should be considered as the lower limit for the inter-sill distance  $L$ .

If, for a given distance  $L$ , the amount of eroded sediment is to be reduced, the river channel between two successive bed sills can be divided into  $m$  sub-reaches, by inserting a series of uniformly spaced bed sills, with distance equal to  $L' = L/m$ . In this case, taking into account Eqs. (4.18a), (4.18b) and (4.19), the total scour area,  $A_{tot}$ , can be computed as follows:

$$\frac{A_{tot}}{H_s^2} = \sum_{i=1}^m \left[ \frac{1}{2} \frac{a_1/m}{H_s} \cdot \frac{L/m}{H_s} + 10.5 \frac{a_1/m}{H_s} \right] \quad \text{for } \frac{a_1}{H_s} < 0.6 \quad (4.20a)$$

$$\frac{A_{tot}}{H_s^2} = \sum_{i=1}^m \left[ \frac{1}{2} \frac{a_1/m}{H_s} \cdot \frac{L/m}{H_s} + 10.5 \frac{a_1/m}{H_s} \right] \quad \text{for } 0.6 < \frac{a_1}{H_s} < 0.6m \quad (4.20b)$$

$$\frac{A_{tot}}{H_s^2} = \sum_{i=1}^m \left[ \frac{1}{2} \frac{a_1/m}{H_s} \cdot \frac{L/m}{H_s} + \left( 6 + 0.5 \frac{a_1/m}{H_s} \right) \right] \quad \text{for } \frac{a_1}{H_s} > 0.6m \quad (4.20c)$$

which lead to:

$$\frac{A_{tot}}{H_s^2} = \frac{1}{m} \frac{A_g}{H_s^2} + \frac{A'_s}{H_s^2} \quad \text{for } \frac{a_1}{H_s} < 0.6 \quad (4.21a)$$

$$\frac{A_{tot}}{H_s^2} = \frac{1}{m} \frac{A_g}{H_s^2} + \frac{A'_s}{H_s^2} + \left( 10 \frac{a_1}{H_s} - 6 \right) \quad \text{for } 0.6 < \frac{a_1}{H_s} < 0.6m \quad (4.21b)$$

$$\frac{A_{tot}}{H_s^2} = \frac{1}{m} \frac{A_g}{H_s^2} + \frac{A'_s}{H_s^2} + 6(m-1) \quad \text{for } \frac{a_1}{H_s} > 0.6m \quad (4.21c)$$

where  $a_1$  is the morphological jump which would occur in the case of two sills placed at the distance  $L$ . Eqs. (4.21a) - (4.21c) shows that the general erosion area,  $A_g$ , is reduced  $m$  times, while the net local scour area does not reduce for  $a_1/H_s < 0.6$ , and increases with an additional term up to the value  $6(m - 1)$  for  $a_1/H_s > 0.6$ . The local scour area is comparable with the general erosion area for  $L/H_s = 20-30$ . This fact implies that, if  $L$  is reduced in order to limit the overall eroded sediment amount, the efficiency is high if the drop ratio is decreased to values lower than 0.6; otherwise the increasing net local scour area mitigates the benefit due to the reduced general erosion.

#### 4.6 CONCLUSIONS

The study carried out in CHAPTER 4 presents data on the shape and volume of scour holes downstream of bed sills in the case of uniform and non-uniform sediments in high-gradient streams. Results confirmed the geometric affinity of the scour hole profiles, already found in previous studies by different authors. Nevertheless, different scour processes were identified at different drop ratios,  $a_1/H_s$ . Geometric similarity did not occur in general, but it was found to be a function of the drop ratio. In particular, for  $a_1/H_s > 0.7$  all the scour hole profiles can be considered approximately similar. Geometric similarity of scour hole profiles implies that the dimensionless net local scour area (which is the eroded volume per unit width),  $A'_s/H_s^2$ , can be expressed as a

function of the drop ratio. The scour volume was shown to be dependent on sediment sorting, which reduces the dimensions of the scour hole. Sorting was found to affect scour shape, being effective in mitigating the scour vertical deepening. When scour dimensions are properly normalized, the same shape relationships hold for both uniform and non-uniform sediments.

The drop ratio value  $a_1/H_s = 0.6$  was identified as a threshold at which the physical mechanisms of erosion appear to change. The scour hole shape and the amount of sediment eroded is therefore dependent on the drop ratio. For lower values of the ratio  $a_1/H_s$ , the development of the scour hole seemed to depend on the jet inclination, which is strongly correlated with the steepness of the downstream side of the scour hole. Both inclinations increased with the square root of the drop ratio, until the physical limit represented by the sediment angle of repose was reached. Above that threshold, the angle between the downstream side of the scour hole and the horizontal plane did not increase anymore and the efficiency of the jet to remove sediment was greatly reduced.

Prediction formulae of the net local scour volume were obtained for both geometric affinity and similarity, uniform and non-uniform sediments. These formulae allow the calculation of an optimized inter-sill distance, which is the only degree of freedom for the designers.

#### 4.7 APPENDIX: NON-UNIFORM SEDIMENT FORMULATION

Introducing (4.13a) and (4.13b) in Eqs. (4.10a) and (4.12a), obtained in case of affinity and similarity respectively, yields the expressions of local scour area for non-uniform sediments:

$$A'_{s,nu} = l_{s,nu} y'_{s,nu} \cdot K_2 = a_1 \Phi_x SI^{-\alpha_x} \cdot H_s \left( \Phi_y SI^{-\alpha_y} - a_1/H_s \right) \cdot K_2 \quad (\text{A.1})$$

$$A'_{s,nu} = \left( y'_s \Phi_{xy} \right) \frac{l_{s,nu}}{l_s} y'_{s,nu} \cdot K_2 = SI^{-\alpha_x} \left( \Phi_y - a_1/H_s \right) \left( \Phi_y SI^{-\alpha_y} - a_1/H_s \right) H_s^2 \cdot K_3 \quad (\text{A.2})$$

Neglecting the influence of sorting on scour length, i.e. assuming  $\beta = 0$ , the above equations can be rewritten in the appropriate dimensionless form:

$$\frac{A'_{s,nu}}{a_1 H_s} = K_2 \cdot \Phi_x (\Phi_y - a_1/H_s) \cdot \frac{\Phi_y SI^{-\alpha_y} - a_1/H_s}{\Phi_y - a_1/H_s} = \frac{A'_s}{a_1 H_s} \cdot \frac{\Phi_y SI^{-\alpha_y} - a_1/H_s}{\Phi_y - a_1/H_s} \quad (\text{A.3})$$

$$\frac{A'_{s,nu}}{H_s^2} = K_3 \cdot (\Phi_y - a_1/H_s)^2 \cdot \frac{\Phi_y SI^{-\alpha_y} - a_1/H_s}{\Phi_y - a_1/H_s} = \frac{A'_s}{H_s^2} \cdot \frac{\Phi_y SI^{-\alpha_y} - a_1/H_s}{\Phi_y - a_1/H_s} \quad (\text{A.4})$$

The last term in Eqs. (A.3) and (A.4) is the ratio between the net maximum scour depths for non-uniform and uniform sediments,  $y'_{s,nu}/y'_s$ , expressed as a function of  $SI$  and  $a_1/H_s$ . A more agreeable formulation can be achieved separating the terms linked to the drop ratio and those linked to the sorting. It follows:

$$\frac{y'_{s,nu}}{y'_s} = \frac{\Phi_y - a_1/H_s}{\Phi_y - a_1/H_s} \cdot \frac{\Phi_y \cdot (1 - SI^{-\alpha_y})}{\Phi_y \cdot \left(1 - \frac{a_1/H_s}{\Phi_y}\right)} = 1 - (1 - SI^{-\alpha_y}) \left( \frac{\Phi_y}{\Phi_y - a_1/H_s} \right) \quad (\text{A.5})$$

which is the reduction factor introduced in Eqs. (4.14a) and (4.14b).

## **CHAPTER 5**

### **SCOURING UNDER UNSTEADY FLOW: THE CASE OF FLASH FLOOD**

#### **5.1 SUMMARY**

The temporal development of clear-water local scour depth at bed sills in uniform gravel beds is considered in CHAPTER 5. A new experimental program has been carried out by the author, which started at the end of 2006 and was concluded in March 2007 at the Fluid Dynamics Laboratory of The University of Auckland (NZ). In sections 5.3 and 5.4, experiments are presented on the development of scour holes under unsteady hydraulic conditions, with the triangular-shaped hydrographs tested being of different durations and different rates of flow variation. Preliminary observations are discussed on the behavior of scour development, which is compared with the scour evolution for the steady-state case. Based on the experimental results and a theoretical framework, in section 5.5 a method is given for the definition and prediction of the scouring process under unsteady flows in terms of a dimensionless temporal parameter. In the next section a “flash flood” is defined as an event for which the scour doesn’t attain its potential magnitude, i.e. the equilibrium value for the peak hydrograph flow rate. It will be shown that this flood nature is dependent on both the characteristics of the flood event itself and the characteristics of the stream. A quantitative measure of what constitutes a flash flood is given in terms of the identified temporal parameter, which represents one of the main goal of this study. Furthermore, results show that the ratio between the final scour depth and the potential scour depth at a bed sill for a given hydrograph can be estimated as a function of the identified temporal parameter.

## 5.2 SCOURING, TIME EVOLUTION AND UNSTEADY FLOWS

It has already been discussed that the study of scour at or downstream of hydraulic structures due to horizontal and plunging jets, such as at aprons downstream of underflow gates, at grade-control structures, and at bridge piers and abutments, represents an active field of research due the frequent demand for scour size predictive formulae and schematic models in engineering. Although estimates can be made of the maximum local scour likely to occur under given flow and sediment conditions, many scour phenomena are time dependent [*Hoffmans and Verheij*, 1997]. In CHAPTER 1 it was stated that most of the scour process develops in a short-term erosive phase, subsequently increasing during a long-term phase, and finally approaching the ultimate depth asymptotically [*Mohamed and McCorquodale*, 1992; *Stein et al.*, 1993; *Hoffmans and Pilarczyk*, 1995; *Melville and Chiew*, 1999; *Dey and Barbhuiya*, 2005]. Since unfavorable flow conditions at a site may occur for limited times compared to those required for the complete scour development, it is observed that the value of the maximum equilibrium-stage scour depth relevant to the peak discharge is not the most effective parameter for designing structures. *Cardoso and Bettess* [1999] stated that with regard to scouring at bridge abutments “it is increasingly realized that the temporal evolution of local scour has some significance, particularly to predict the scour depth at a certain moment of a flood hydrograph”.

Many investigations on local scour development at different engineering works have been carried out over the last decades by applying stationary flows and defining the value of the maximum scour depth at the time  $t$  as a fraction of the maximum scour depth at the equilibrium stage, once a proper time scale was defined [*Farhoudi and Smith*, 1985; *Chatterjee et al.*, 1994; *Coleman et al.*, 2003; *Dey and Raikar*, 2007]. Some theoretical frameworks have also been proposed for the prediction of scouring processes due to steady turbulent plunging jets [*Hogg et al.*, 1997; *Jia et al.*, 2001] and horizontal jets [*Adduce and Sciortino*, 2006], resulting in numerical models simulating scour profiles at different times. The limitation of a general application of these approaches is that they only work as long as an “equivalent” steady flow rate can be identified for any unsteady hydrograph.

As for bed sills, which are commonly used in high gradient streams for preventing excessive bed degradation, predictive formulae relating local scouring downstream of

the sills to the hydraulic and sediment properties are available in literature [Gaudio *et al.*, 2000; Lenzi *et al.*, 2003; Martin Vide and Andreatta, 2006; Meftah and Mossa, 2006]. In Chapter 2, it was introduced that experimental tests on scour development at bed sills with stationary flows were carried out by Gaudio and Marion [2003] using uniform sand and mild bed slopes. According to their definition of the temporal scale of the scouring process, namely the morphological time, a more general notation is used in this study, which allows for the position of the sill along a sequence of structures. The following relationships hold for the morphological time,  $T_{s,k}$ , relevant to the  $k$ -th sill in a sequence:

$$T_{s,k} = \frac{V_{g,up} + V_{g,k}}{Q'_s} \quad (5.1a)$$

where

$$V_{g,k} = \sum_{i=1}^k V_{g,i} \quad (5.1b)$$

in which  $V_{g,i} = 0.5(S_0 - S_{eq})L_i^2 B$  is the volume of sediment entrained due to bed degradation between the  $i$ -th sill and the subsequent one (see Figure 5.1), which is obtained when equilibrium conditions for bed slope are achieved in term of Shields' parameter, or the upstream sediment supply equals the sediment transport capacity of the river reach.  $L_i$  is the inter-sill distance, and  $B$  is the cross-sectional width.  $V_{g,up}$  is the volumetric amount of sediment eroded by the flow upstream of the reach stabilized with sills, and the length of this reach is identified by an upstream control cross-section (e.g. check-dam, artificial reservoir, non-erodible rock bed). It is noted that the notation  $V_g$ , according to what discussed in CHAPTER 4, stands for eroded volume due to "general" erosion, as opposed to  $V_s$  or  $V'_s$ , which represent the total and net eroded volume due to "scouring", respectively. The effective sediment transport capacity,  $Q'_s$ , is defined as:

$$Q'_s = Q_s - Q_{s,in} \quad (5.2)$$

in which  $Q_s$ , the sediment transport capacity for a given initial bed slope,  $S_0$ , can be estimated by applying a sediment transport formula for uniform flow conditions (e.g.

the Meyer-Peter-Müller relation discussed in Section 5.6), and  $Q_{s,in}$  is the sediment rate supplied by the upstream watershed. The possibility to predict equilibrium scouring and sediment transport rate  $Q_s'$  as in Eq. (5.2) was validated by the study described in CHAPTER 3 for steady flows. In the experiments carried out by Gaudio and Marion, no upstream sediment supply was used, i.e.  $Q_{s,in} = 0$  and  $Q_s' = Q_s$ . As shown in CHAPTER 2, it was found that scour dimensions did not increase for  $t$  greater than 12 - 14 times the morphological time,  $T_{s,k}$ .

Changes in natural streams are mainly produced by flood events, which periodically occur due to intensive rainfall or seasonal snow melting. It is observed that the highest flow rates are not directly associated to the morphological characteristics of the river, due to their short duration [Surian, 1999]. This should induce researchers to face the following question: how do local phenomena, such as scouring, act in response to time-limited hydrological events of different durations and intensities? Giacometti [2000] carried out scale-model experiments on failure mechanisms for natural steps. He reported the collapse of bed sills made of cobbles due to downstream scouring taking place at very low flow rates after the occurrence of the flood peak. He argued that the peak did not last enough to lead the structures to failure, which was caused instead by the marginal low-rate increase of scour due to low flows. Following on from this observation, the experimental study presented in this chapter considers scour development downstream of bed sills due to unsteady water discharges, and how the temporal scale of the scour process relates to the duration of the flood hydrograph. As the rate of scouring varies with the flood characteristics, it is expected that the time required for the “peak-flow” equilibrium scour hole to form is longer than the period of the erosive flow action taking place. A “flash flood” is thereby defined herein as a hydrological event for which the scour depth does not attain this potential maximum that would occur at equilibrium for the peak flow rate. The goal of this study is to provide a physically-based explanation of this general definition of flash floods, and also to provide a methodology to predict the final scour depth downstream of a sill in a sequence after the occurrence of such a flood.



### 5.3 METHODS AND SETTINGS

Four series of experimental tests (Table 5.1) were carried out at the Hydraulic Laboratory of the University of Auckland (NZ). A 17 m-long, 0.45 m-wide and 0.50 m-deep tilting flume was used for all the experiments. The working length of the flume was 7 m, with three 10 mm-thick wooden plates inserted into the 0.3 m-thick sediment bed to simulate a sequence of bed sills. The sediment used was a homogeneous fine gravel of sizes  $D_{50} = 5.2$  mm and  $D_{90} = 6.7$  mm, and a geometric standard deviation of sizes of  $\sigma_g = 1.2$ . A 1 m-long fixed bed with the same roughness as the mobile bed was installed upstream of the first sill to provide similar bed-roughness and flow conditions along the flume reach. The distance between the sills was  $L_1 = L_2 = 2$  m, with the last 2 m-long reach used as storage for the grains entrained by the flow in the upstream two sediment bays (see Figure 5.1).

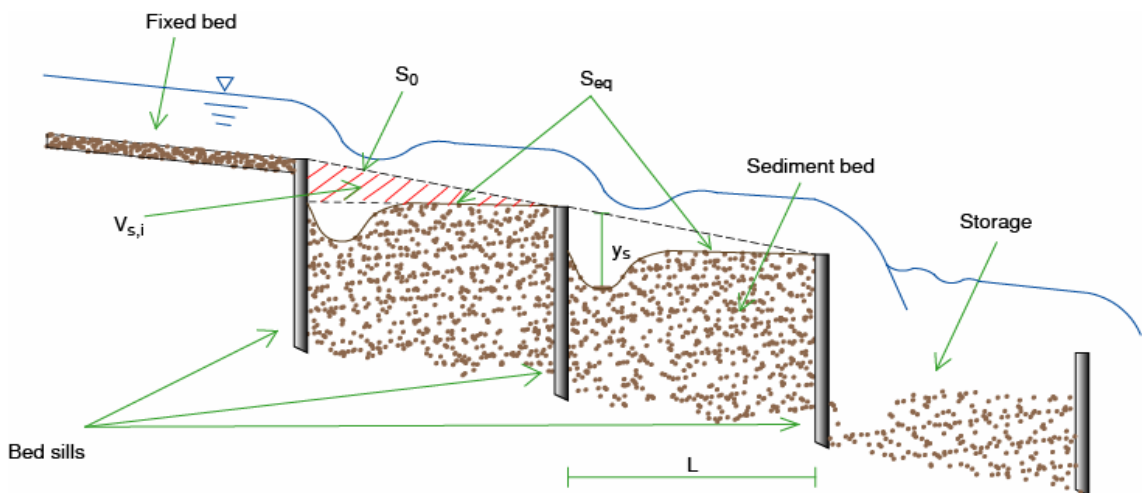


Figure 5.1 - Schematic of the experimental setup.

In these experiments, no sediment was supplied upstream and no sediment was eroded in the upstream reach, i.e.  $Q_{s,in} = 0$  and  $V_{g,up} = 0$ . For each test, a triangular-shaped flood hydrograph was simulated by gradually varying the water discharge. The flow rate, regulated by an inlet valve, was manually set by using a differential manometer. The flow increment was  $\Delta Q = 0.5$  l/s for all the experiments, and the time step,  $\Delta t$ , ranged between 2.50 and 14.05 min, depending on the total hydrograph duration,  $t_f$ , and on the range of the applied flow rate,  $Q$ . The value of  $\Delta Q$  was chosen on the basis of instrument accuracy, which was within  $\pm 0.1$  l/s, and the value of the time

step was derived with the relationship  $\Delta t/t_p = \Delta Q/(Q_{max} - Q_{min})$ . Figure 5.2 shows the characteristics of the flood hydrograph flowing over the sediment bed during each test. At the beginning of each experiment, the flume was slowly filled at a low rate. Once the flow reached conditions close to or just above threshold for grain entrainment (i.e. few single grains could be observed rolling on the bed surface), the experiment started.

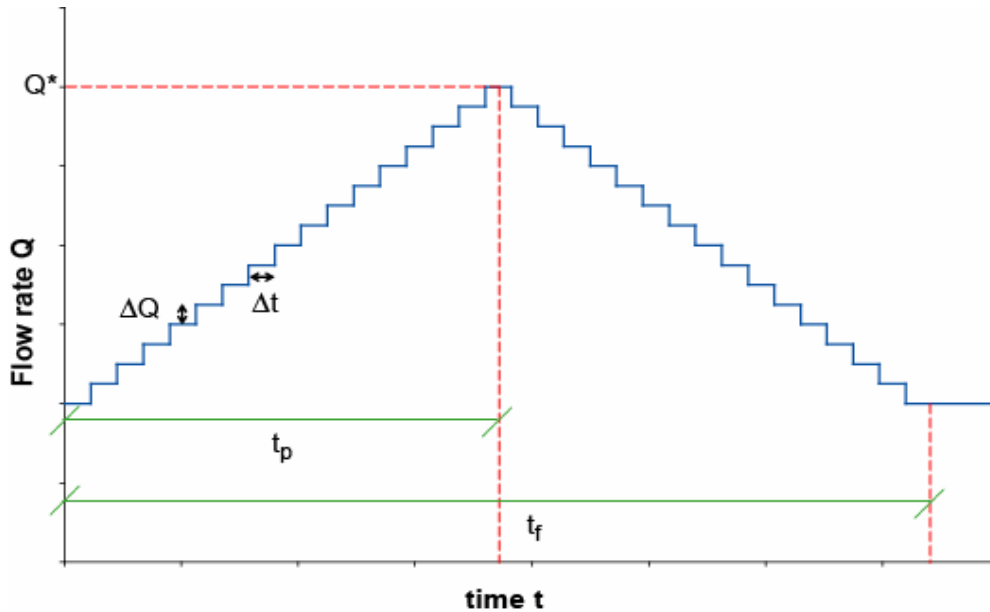


Figure 5.2 - Flood hydrograph applied for each test.

Two types of test series were performed, with 5 tests carried out for each series. The initial bed slope was set to  $S_0 = 3\%$  for series 1 - 2, and  $S_0 = 4\%$  for series 3 - 4. During A-type tests, experiments were run for  $t_f$  ranging from 2 to 7.5 h, while the minimum and maximum values of the flow rate were not changed (i.e.  $Q_{min} = 6$  l/s and  $Q_{max} = 16$  l/s for  $S_0 = 3\%$ ;  $Q_{min} = 4$  l/s and  $Q_{max} = 12$  l/s for  $S_0 = 4\%$ ). During B-type tests, the length of the experiment,  $t_f$ , was set to a constant value, and the peak value of the flood hydrograph,  $Q_{max}$ , was varied between 12 and 20 l/s for  $S_0 = 3\%$  and between 8 and 16 l/s for  $S_0 = 4\%$ . In both A and B-type tests, the recession part of the flood hydrograph had the same length as the rising limb, i.e.  $t_f/t_p = 2$  (where  $t_p$  is the time at which the flood peak occurs), resulting in symmetrical triangular-shaped flood hydrographs. The main parameters for both groups of series 1 - 2 ( $S_0 = 3\%$ ) and series 3 - 4 ( $S_0 = 4\%$ ) tests are presented in Table 5.1.

**Table 5.1 - Experimental parameters for  $S_0 = 3\%$  (series 1 and 2, 1S) and  $S_0 = 4\%$  (series 3 and 4, 3S). Series 1S and 3S represent steady flow (at peak discharge) tests**

Series #	Series Type	Test #	$Q_{\min}$ (l/s)	$Q_{\max}$ (l/s)	$t_f$ (h)	$\Delta t$ (min)	$t_f/t_p$
1	A	1 ÷ 5	6.0	16.0	2.50 ÷ 7.50	4.75 ÷ 14.05	2
2	B	6 ÷ 10	6.0	12.0 ÷ 20.0	2.50	7.50 ÷ 2.50	2
3	A	11 ÷ 15	4.0	12.0	2.00 ÷ 6.00	3.75 ÷ 11.25	2
4	B	16 ÷ 20	4.0	8.0 ÷ 16.0	2.00	11.25 ÷ 2.90	2
1S	steady	1a ÷ 5a	-	8.0 ÷ 16.0	-	-	-
3S	steady	6a ÷ 10a	-	5.0 ÷ 12.0	-	-	-

During the tests, simultaneous measurements of water and bed surface profiles were performed along the centerline at varying time intervals, depending on the test type and the phase of the experiment (i.e. increasing or decreasing part of the flood hydrograph). The spatial resolution of measurements,  $\Delta x$ , was approximately 2.4 mm, with the measuring equipment mounted on a carriage moving on rails along the flume. A laser profiler was used to record the water surface level, while a counterweighted point gauge attached to a potentiometer device was used to measure bed profiles. The light of the laser was reflected by a thin black sheet, 4 cm-wide and 8 cm-long, attached to the carriage, which gently floated on the free surface with no significant effect on the local flow field. The latter instrument was calibrated to measure bed elevations to within  $\pm 0.5$  mm, and was equipped with a 25 mm diameter cogwheel to minimize any sediment-bed disturbance while carrying out the measurements. These techniques were adopted as other instruments tested for measuring bed elevations, either acoustic or laser-based devices, were strongly affected by the turbulence due to the plunging jet over the scour hole. The movement of the grains generated by the two counter-rotating eddies (rollers), upstream and downstream of the diffuse jet, also produced significant disturbance, resulting in highly scattered point measurements. Data were acquired automatically as the carriage was moved along the test section at the selected times. A schematic of the measuring design is shown in Figure 5.3. At the end of each run, 25 profiles of both water and bed surfaces were obtained that described the time

development of these surfaces during the scouring process by the simulated flood events.

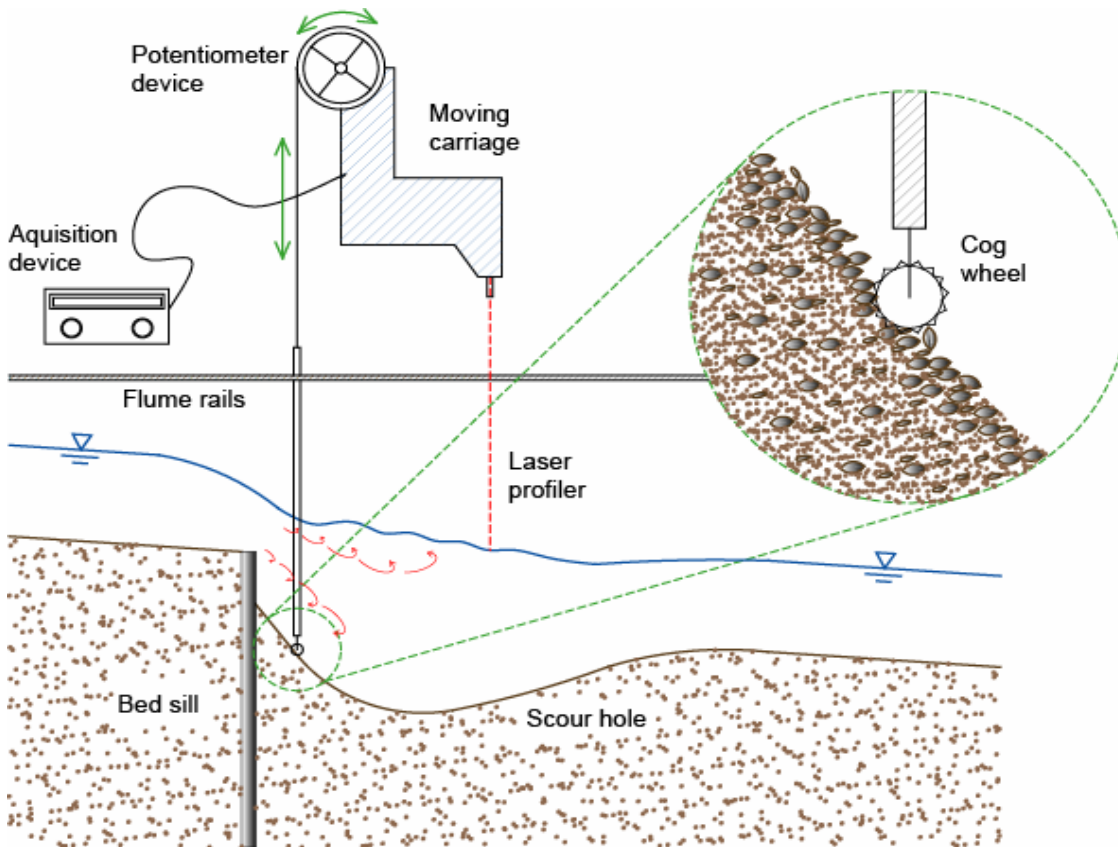


Figure 5.3 - Schematic of the measuring devices.

## 5.4 RESULTS

### 5.4.1 Steady flow tests

Two series of experiments were also carried out for steady flow conditions. Series 1S tests were performed with  $S_0 = 3\%$  and  $Q$  ranging between 8 and 16 l/s. In series 3S,  $S_0 = 4\%$  and  $Q = 5 - 12$  l/s (see Table 5.1). Bed and water-surface profiles were recorded with the same procedure described in the previous section. In order to guarantee that long-term equilibrium conditions were attained, the test durations were set on the basis of direct observations to be conservative with respect to the time needed to achieve complete scour development (i.e. when scour depths no longer increased and net sediment transport became zero). The maximum scour depth occurring at the  $k$ -th

sill,  $y_{s,k}(t)$ , at time  $t$  was obtained from the measured bed profiles and scaled with the maximum scour depth at equilibrium,  $y_s$ , which was the same for both sills. Time was scaled with the morphological time,  $T_{s,k}$ , where  $S_{eq}$  was determined from the measured profiles, and  $Q_s$  was evaluated based on the Meyer-Peter-Müller equation. The dimensionless plot displayed in Figure 5.4 shows the agreement of the measured data (with a mean relative error  $\varepsilon_{mean} = 14.1\%$ ), with the relationship by *Gaudio and Marion* [2003] presented in CHAPTER 2, here re-proposed with the following expression:

$$\frac{y_{s,k}(t)}{y_s} = 1 - \exp\left(-0.41 \frac{t}{T_{s,k}}\right) \quad (5.3)$$

This result confirms that the morphological time given by Eq. (5.1a) can be assumed as a reasonable temporal scale for the ranges of hydraulic conditions and geometrical and sediment properties presented in this work, if stationary flows are applied.

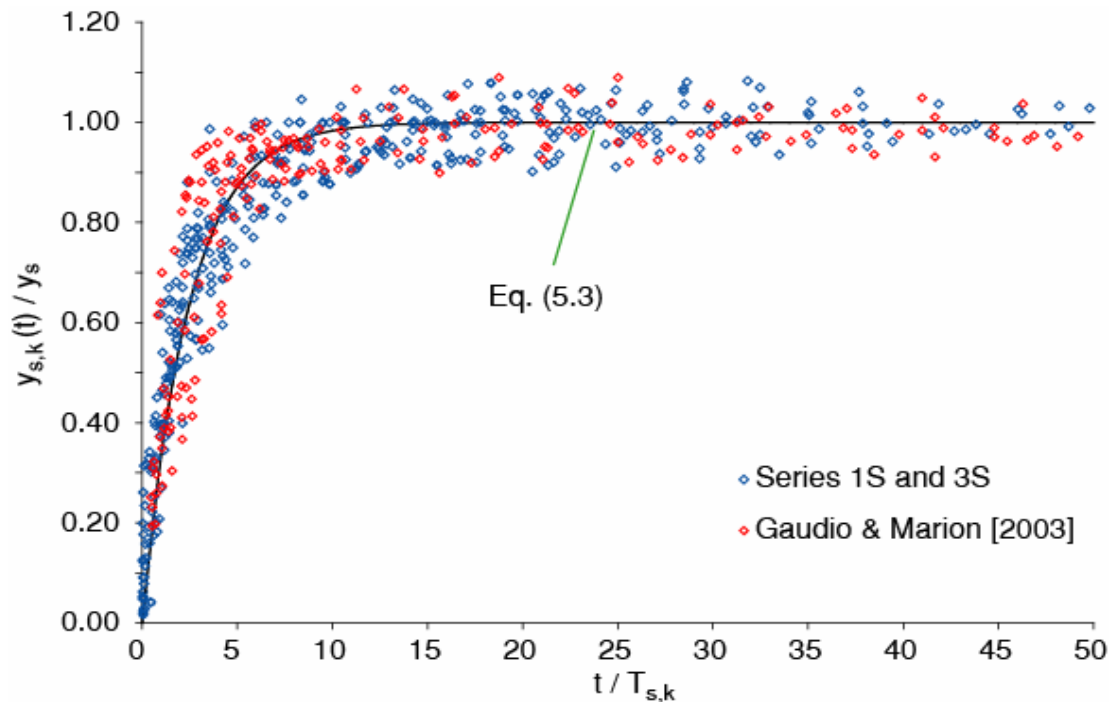


Figure 5.4 - Comparison of steady flow data with expression and data of Gaudio and Marion [2003].

### 5.4.2 Scaling of time and scour depth for unsteady flows

In terms of water resources management, the severity of a flood is a function of the flood peak, volume, duration, and shape of its hydrograph, which together represent a stochastic event whose properties can be statistically described [Yue *et al.*, 2002] and predicted through probabilistic models, such as those based on the instantaneous unit hydrograph [Hjelmfelt and Wang, 1994]. For the purpose of this study, triangular-shaped flood hydrographs were simulated in order to investigate the effects of hydrograph form on scour development.

It is stressed here that the morphological time  $T_{s,k}$  can not be defined as the temporal scale for unsteady flow experiments, with  $T_{s,k}$  a function of time given by:

$$T_{s,k} = \frac{V_{g,up}(Q(t)) + V_{g,k}(S_{eq}(Q(t)))}{Q'_s(Q(t))} = f(t) \quad (5.4)$$

The maximum scour depth at the end of the test,  $y_{s,k}(t_f)$ , is also not a reasonable length scale for scour depths. Depths and times are therefore scaled, respectively, with the potential maximum scour depth and the morphological time,  $y_s^*$  and  $T_{s,1}^*$ , associated with the flow rate at the peak of the flood hydrograph,  $Q^* = Q_{max}$ .  $T_{s,1}^*$  is computed by using only the volume eroded within the first and second sills ( $V_{g,up} = 0$ ), i.e.  $T_{s,1}^* = T_{s,1}(Q^*)$ , which is the morphological time associated with the first sill of the experiments. The use of  $T_{s,1}^*$  for both sills at this stage of analysis enables scour development for the two sills to be directly compared in the plots of Figure 5.5 to Figure 5.8. Results are presented in dimensionless form following this choice.

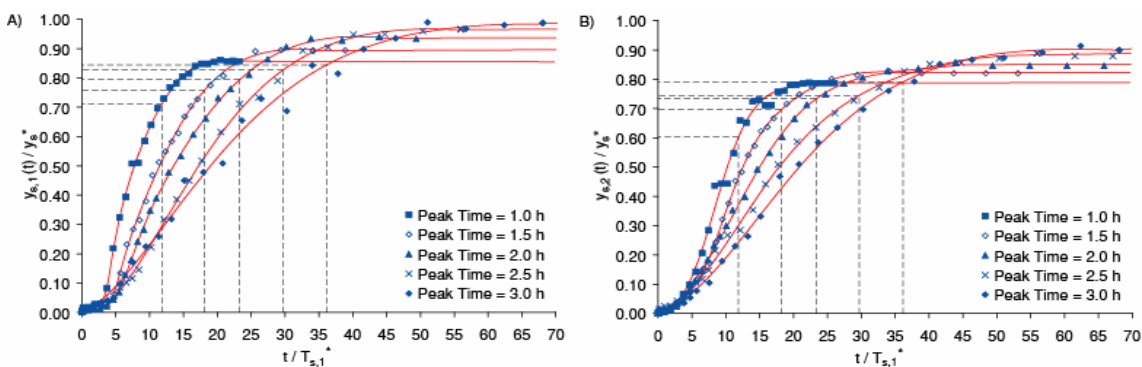


Figure 5.5 - Dimensionless scour development for different durations of the flood hydrograph ( $S_0 = 4\%$ , series 3). A) Scour downstream of the first sill; B) Scour downstream of the second sill.

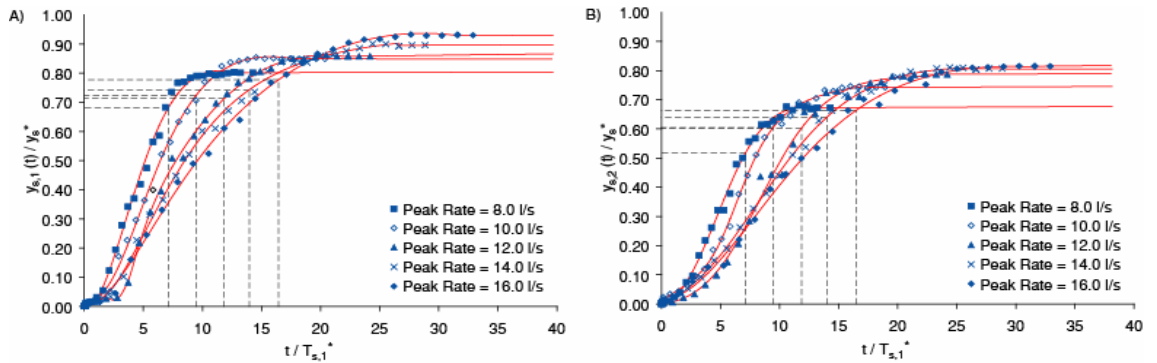


Figure 5.6 - Dimensionless scour development for different flood peak magnitudes ( $S_0 = 4\%$ , series 4). A) Scour downstream of the first sill; B) Scour downstream of the second sill.

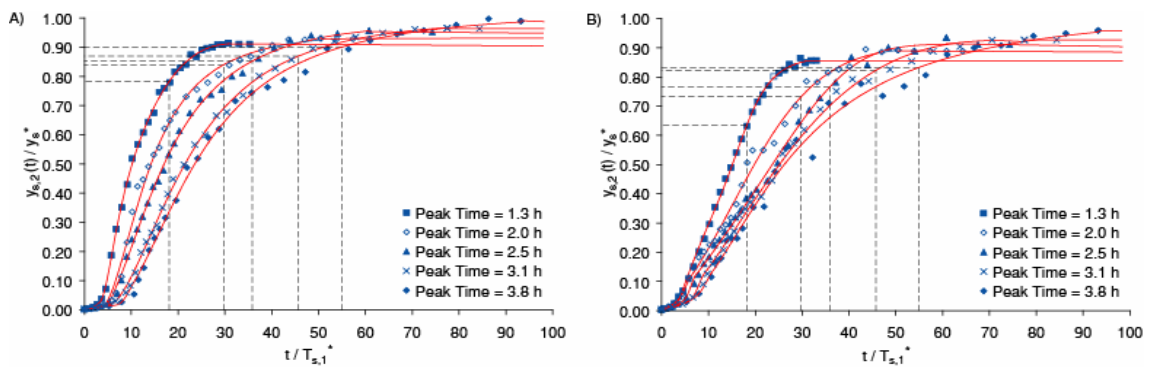


Figure 5.7 - Dimensionless scour development for different durations of the flood hydrograph ( $S_0 = 3\%$ , series 1). A) Scour downstream of the first sill; B) Scour downstream of the second sill.

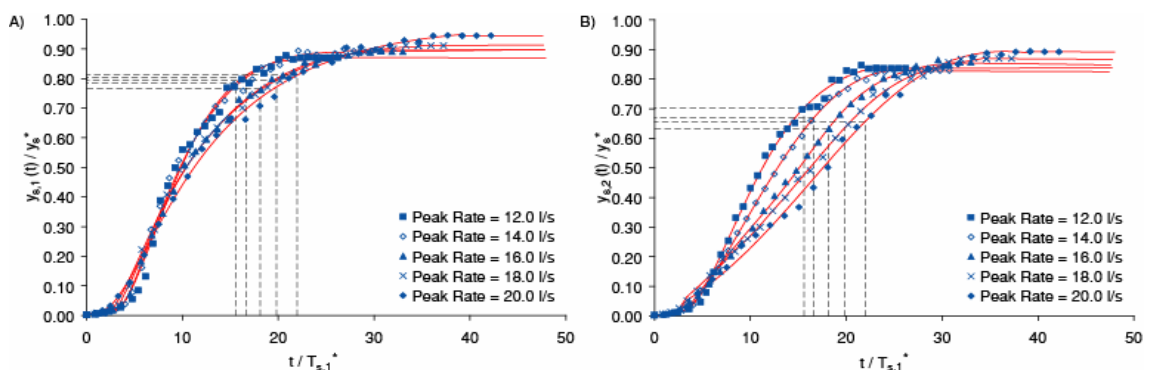


Figure 5.8 - Dimensionless scour development for different flood peak magnitudes ( $S_0 = 3\%$ , series 2). A) Scour downstream of the first sill; B) Scour downstream of the second sill.

### 5.4.3 Scour evolution for unsteady flows

Figure 5.5A and Figure 5.5B show the development of the scour downstream of the first and second sills, respectively, for different durations of the flood hydrograph, and with the initial bed slope  $S_0 = 4\%$  (series 3). Data were fitted with rational polynomial equations, with coefficients of determination,  $R^2$ , in the range 0.90 - 0.98. All fitted curves presented a similar “S” shaped pattern, and three temporal stages could be clearly identified: an initial rapid scouring phase, from the beginning of the test to approximately the peak time (dashed lines); a decelerating scouring phase, up to  $t = 1.5 - 1.8 t_p$ ; and a final stage, during which the scour depth did not further increase. Similar behaviors can be observed when plotting scour development with time for different flood-peak magnitudes (series 4, see Figure 5.6). In these tests the final value of the maximum scour depth,  $y_{s,k}(t_f)$ , ranged between 70% and 98% of the maximum scour depth associated with the peak rate in steady flow conditions,  $y_s^*$ . This percentage increased with the ratio  $t_f/T_{s,1}^*$ , i.e. the scour depth attained values close to the potential depth either for longer flood hydrograph durations or for smaller values of the morphological time  $T_{s,1}^*$  relevant to the peak flow rate. This implies that the concept of flash flood, as defined above, is dependent on both the characteristics of the flood event itself and the morphological and geometrical characteristics of the stream reach.

Figure 5.7 and Figure 5.8 show the scour development for different durations and peak magnitudes, respectively, of the flood hydrograph, for the tests of  $S_0 = 3\%$  (series 1 and 2). It is noted that in all of the experiments the sediment bed downstream of the first sill always experienced more severe scouring when compared with the subsequent structure, even though the sills were uniformly spaced, and the same equilibrium scour depths can be predicted for a given water discharge. This was expected since scour development takes longer for sills placed further downstream in a sequence. In this regard, for steady flows,  $T_{s,2} = 2T_{s,1}$  according to Eqs. (5.1a) and (5.1b) in case of no erosion in the upstream reach ( $V_{g,up} = 0$ ). The ratio of length of the flood hydrograph to the morphological time influences the degree of this effect, since the difference between the final maximum depths downstream of the first and second sills reduced for the higher values of  $t_f/T_{s,1}^*$ , as can be seen, for example, in the curves in Figure 5.5 and Figure 5.7.



## 5.5 HYDROLOGICAL AND MORPHOLOGICAL TIME SCALES

### 5.5.1 A revised dimensional analysis

For a wide rectangular channel of constant width, the maximum depth,  $y_{s,k}(t_f)$ , of the scour hole downstream of the  $k$ -th sill (in a sequence of uniformly spaced bed sills) that is produced by a symmetrical triangular-shaped flood hydrograph, can be expressed:

$$y_{s,k}(t_f) = f_y \left( g, \nu, \rho_w, \rho_s', q^*, q_{s,in}, h_{u,0}^*, h_{u,eq}^*, D, S_0, S_{eq}^*, L, k, A_{g,up}, T_{hyd} \right) \quad (5.5)$$

where  $g$ ,  $\nu$ ,  $\rho_w$ ,  $\rho_s'$ ,  $D$  and  $L$  follow the usual notation introduced in the previous chapters;  $q^*$  and  $q_{s,in}$  are the peak flow rate and the incoming sediment supply per unit width;  $h_{u,0}^*$  and  $h_{u,eq}^*$  are the initial and final normal depths;  $S_0$  and  $S_{eq}^*$  are the initial and final bed slopes; and  $A_{g,up} = V_{g,up}/B$  is the upstream eroded volume per unit width. The star superscript stands for the quantities associated to the maximum flow rate occurring at the sill cross-section,  $q_{max} = q^*$ . The hydrological time  $T_{hyd}$  is defined as a characteristic duration of the flood hydrograph, here identified with the time of the flood peak, i.e.  $T_{hyd} = t_p$ . It is stressed here that, while  $L$  was correctly deleted when deriving the analysis for steady-state scours (at the equilibrium stage  $L$  and  $S_0$  are meaningful only combined together into the morphological jump,  $a_1$ , and the final value of  $y_s$  does not depend on the temporal development of the scour), in case of unsteady flow,  $L$  must be taken into account as it affects the total amount of eroded sediment,  $V_{s,k}$ , and thereafter the time required for the scour to develop. If the spacing between sills is large enough for the scour development not to be limited by the proximity of the subsequent sill, i.e. no interference occurs,  $L$  in Eq. (5.5) can be replaced by the morphological time associated with a steady peak rate and relevant to the  $k$ -th scour,  $T_{s,k}^*$ , i.e. from Eqs. (1) to (3) it follows:

$$T_{s,k}^* = \frac{A_{s,up} + k \cdot 0.5 \cdot [S_0 - S_{eq}^*] L^2}{q_s^* (S_0, h_{u,0}^*, g, \Delta, D) - q_{s,in}} \quad (5.6a)$$

or

$$T_{s,k}^* = f_1 \left( g, \rho_w, \rho_s', q_{s,in}, h_{u,0}^*, D, S_{eq}^*, a_1^*, L, k, A_{s,up} \right) \quad (5.6b)$$

where the sediment transport capacity of the flow,  $q_s^*$ , can be estimated with a sediment transport formula for uniform flow, according to Eq. (2.3), and  $a_1^* = (S_0 - S_{eq}^*)L$ , the morphological jump relevant to the peak rate, is introduced instead of  $S_0$ . A uniform flow depth resistance formula (e.g. the Gauckler-Strickler/Manning formula) and a uniform sediment transport capacity formula can be reasonably used to link  $S_{eq}^*$ ,  $h_{u,0}^*$  and  $h_{u,eq}^*$  to the other variables present in Eq. (5.5) and these can then be removed from the original list. Both  $k$  and  $V_{g,up}$  are assumed to affect the scour process only for the definition of the morphological time and therein can be removed from the group of the independent parameters of Eq. (5.5). In the case of no upstream sediment feed ( $q_{s,in} = 0$ ), the application of the Buckingham's  $\pi$ -theorem leads to identification of the following non-dimensional groups from Eq. (5.5):

$$\frac{y_{s,k}(t_f)}{H_s^*} = \Phi_{y,1} \left( \frac{q^*}{v}, \Delta, \frac{a_1^*}{H_s^*}, \frac{H_s^*}{\Delta D}, \frac{T_{hyd}}{T_{s,k}^*}, \frac{q T_{s,k}^*}{(H_s^*)^2} \right) \quad (5.7)$$

where  $H_s^*$  is the specific flow energy at the sill cross-section in equilibrium conditions.  $H_s^*$  is essentially a function of  $q^*$ . According to what discussed in CHAPTER 3,  $H_s^* = 1.5[(q^*)^2/g]^{1/3}$  for subcritical and critical flows (of Froude number  $F_R \leq 1$ ), and  $H_s^* = [h_{u,eq}^* + (v^*)^2/2g]$  for supercritical flows (of  $F_R > 1$ ), where  $v^* = q^*/h_{u,eq}^*$  is mean flow velocity. As for steady flows, assuming a weak dependence of scour depth on Reynolds number ( $q^*/v$ ) in conditions of fully developed turbulent flow, and taking the relative submerged grain density to be constant and equal to approximately 1.63 leads to:

$$\frac{y_{s,k}(t_f)}{H_s^*} = \Phi_{y,2} \left( \frac{a_1^*}{H_s^*}, \frac{H_s^*}{\Delta D}, \frac{T_{hyd}}{T_{s,k}^*}, \frac{q T_{s,k}^*}{(H_s^*)^2} \right) \quad (5.8)$$

As discussed in CHAPTER 2, the dimensionless maximum scour depth at equilibrium for steady flows is dependent on only the first two terms of the right-hand side of Eq. (5.8), i.e. the final value of scour depth is the same downstream of each sill

in the sequence, with no regard to the time required for the scour hole to develop. In turn, the formulation proposed for clear-water conditions, uniform sediments and non-interfering sills can be rewritten for the peak flow rate:

$$\frac{y_s^*}{H_s^*} = \Phi_y \left( \frac{a_1^*}{H_s^*}, \frac{H_s^*}{\Delta D} \right) \quad (5.9)$$

The analytical form of Eq. (5.8) is a growing function with  $T_{hyd}/T_{s,k}^*$ , with  $y_{s,k}(t_f)/H_s^*$  approaching  $y_s^*/H_s^*$  as  $T_{hyd}/T_{s,k}^*$  tends to infinity. A possible form of Eq. (5.8) is found by splitting  $\Phi_{y,2}$  into a product of functions as:

$$\frac{y_{s,k}(t_f)}{H_s^*} = \Phi_y \left( \frac{a_1^*}{H_s^*}, \frac{H_s^*}{\Delta D} \right) \cdot \Phi_\Psi \left( \frac{T_{hyd}}{T_{s,k}^*}, \frac{qT_{s,k}^*}{(H_s^*)^2} \right) \quad (5.10)$$

which, using Eq. (5.9), leads to:

$$\frac{y_{s,k}(t_f)}{y_s^*} = \Phi_\Psi \left( \frac{T_{hyd}}{T_{s,k}^*}, \frac{qT_{s,k}^*}{(H_s^*)^2} \right) = \Phi_\Psi (\Psi_1, \Psi_2) \quad (5.11)$$

The analytical form of Eq. (5.9) is the same retrieved for steady flow conditions. It is stressed that  $y_s^*$  is the maximum potential scour depth which would develop under steady flow and its value is the same for the scour downstream of each sill in a sequence of uniformly spaced bed sills. The definition of Eq. (5.8) and thereby Eq. (5.11) is the main purpose of the present study. The data present in Table 5.2 have been used to validate the assumptions leading to Eq. (5.10) and to find an analytical expression for Eq. (5.11), where, as indicated in Eq. (5.6a),  $T_{s,k}^* = kT_{s,1}^*$  has been adopted for the present normalization, being  $V_{g,up} = 0$ .

### 5.5.2 Statistical analysis of data

Initial inspection of data indicated a high correlation of the ratio  $y_{s,k}(t_f)/H_s^*$  with the dimensionless parameter  $\Psi_1$  over the entire range of the second parameter,  $\Psi_2$ , showing an exponentially-damped trend asymptotically approaching unity, although a

weaker correlation was also found between  $y_{s,k}(t_f)/y_s^*$  and  $\Psi_2$ . Data were then organized by grouping together  $\Psi_1$  and  $\Psi_2$ , and the best data fit was sought within the family of curves described by the following parametric expression:

$$\frac{y_{s,k}(t_f)}{y_s^*} = 1 - w_1 \cdot \exp(-w_2 \cdot \Psi_3) \quad (5.12a)$$

where

$$\Psi_3 = \Psi_1 \cdot (\Psi_2)^w \quad (5.12b)$$

in which  $w_1$  and  $w_2$  are calibration coefficients and the exponent  $w$  was free to vary. Data were tested with  $w$  varying in the range  $-0.5 \div 2.0$  and fitted according to (5.12a). The optimum value of  $w$  was defined as the value that gave the maximum value of the coefficient of determination,  $R^2$ , and the minimum value of the mean relative error,  $\varepsilon_{mean}$ . Figure 5.9 shows that the required conditions are achieved for  $w \approx 0.1$ . The ratio between the final scour depth,  $y_{s,k}(t_f)$ , and the equilibrium steady-state scour depth,  $y_s^*$ , was then considered to be affected only by the ratio between the hydrological time and the morphological time,  $T_{hyd}/T_{s,k}^*$ , with no significant dependence on  $\Psi_2$ .

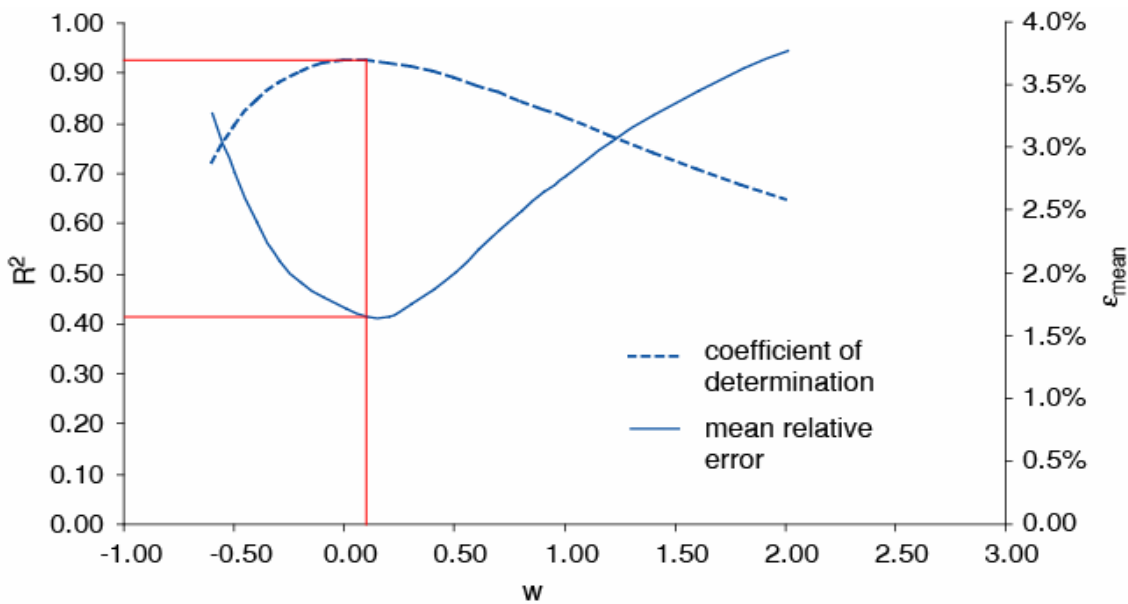


Figure 5.9 - Optimum value of  $w$ .

The experimental data of Table 5.2 are plotted in Figure 5.10, with  $T_{s,k}^*$  and  $y_s^*$  defined by the steady-state tests. The dimensionless data are well approximated by:

$$\frac{y_{s,k}(t_f)}{y_s^*} = 1 - 0.44 \cdot \exp\left(-0.11 \frac{T_{hyd}}{T_{s,k}^*}\right) \quad (5.13)$$

which is valid in the range  $3.2 < T_{hyd}/T_{s,k}^* < 51.8$  with a coefficient of determination  $R^2 = 0.93$ . From Figure 5.10, the value  $T_{hyd}/T_{s,k}^* = 13.6$ , giving a final scour depth 10% smaller than the equilibrium value at the peak flow rate, can be assumed as a reasonable upper threshold for the definition of a flash flood, with the scour depth approximately attaining the equilibrium value for the peak flow rate for flood events with higher ratios of  $T_{hyd}/T_{s,k}^*$ .

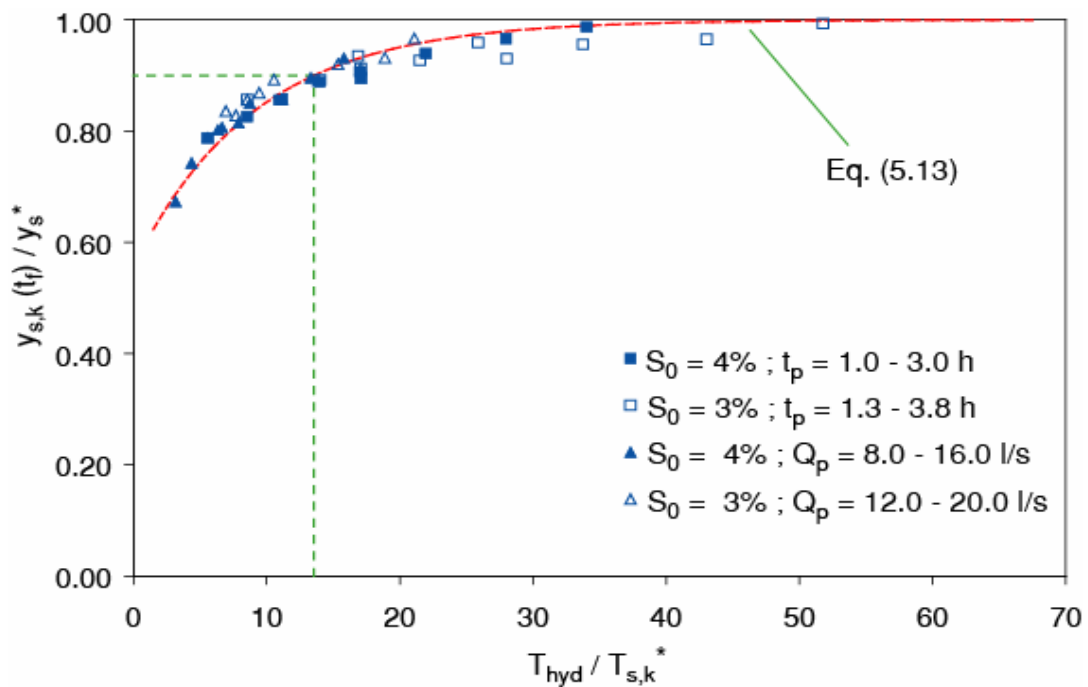


Figure 5.10 - Dimensionless scour depth for sills 1 and 2 versus the ratio between the hydrological time and the equivalent morphological time.

**Table 5.2 - Experimental data: scour depths at the peak flow and flood completion (\*) for each sill; hydrological and morphological times**

Test #	$y_{s,1}(t_p)$ (m)	$y_{s,2}(t_p)$ (m)	$y_{s,1}(t_f)$ (m)	$y_{s,2}(t_f)$ (m)	$T_{hyd}$ (min)	$T_{s,1}^*$ (min)	$T_{s,2}^*$ (min)
1	0.124	0.100	0.144	0.135	75	4.39	8.79
2	0.133	0.116	0.147	0.141	122	4.35	8.70
3	0.134	0.120	0.150	0.147	150	4.44	8.89
4	0.138	0.130	0.153	0.147	188	4.36	8.72
5	0.143	0.132	0.157	0.152	225	4.35	8.69
6	0.104	0.091	0.115	0.108	75	6.49	12.98
7	0.120	0.098	0.134	0.121	75	5.21	10.41
8	0.124	0.100	0.144	0.135	75	4.39	8.79
9	0.136	0.106	0.156	0.145	75	3.81	7.63
10	0.146	0.115	0.170	0.157	75	3.32	6.64
11	0.166	0.134	0.200	0.176	60	5.38	10.75
12	0.178	0.156	0.210	0.185	90	5.27	10.54
13	0.184	0.162	0.217	0.189	120	5.47	10.93
14	0.193	0.166	0.225	0.198	150	5.36	10.72
15	0.198	0.177	0.231	0.203	180	5.29	10.58
16	0.119	0.087	0.140	0.112	60	9.45	18.91
17	0.151	0.121	0.177	0.148	60	6.87	13.75
18	0.166	0.134	0.200	0.176	60	5.38	10.75
19	0.185	0.152	0.223	0.192	60	4.51	9.01
20	0.204	0.167	0.245	0.205	60	3.80	7.60
1a	-	-	0.096	0.087	$\infty$	13.31	26.62
2a	-	-	0.116	0.114	$\infty$	8.76	17.52
3a	-	-	0.129	0.131	$\infty$	6.40	12.80
4a	-	-	0.140	0.140	$\infty$	5.27	10.54
5a	-	-	0.158	0.152	$\infty$	4.48	8.96
6a	-	-	0.081	0.114	$\infty$	25.31	50.62
7a	-	-	0.134	0.116	$\infty$	15.82	31.64
8a	-	-	0.174	0.167	$\infty$	9.43	18.86
9a	-	-	0.209	0.200	$\infty$	6.85	13.70
10a	-	-	0.233	0.223	$\infty$	5.54	11.08

(\*) For tests 1a - 10a (steady flow) scour depths are the values measured at the equilibrium stage

## 5.6 APPLICATION TO A CASE STUDY

The study area is located in the upper part of the Piave River (Eastern Alps, Italy), downstream of the Comelico reservoir (of capacity  $V_R = 1.4 \cdot 10^6 \text{ m}^3$ ). The stream reach is 8 km-long before flowing into the artificial lake of the Pieve di Cadore reservoir ( $V_R = 64.3 \cdot 10^6 \text{ m}^3$ ). The limited capacity of the upstream reservoir compared to the catchment surface ( $S_C = 372 \text{ km}^2$ ) requires frequent removal of sediments through flushing operations. Downstream of the Comelico dam, the thalweg elevation increases a few meters above the original bed after the sediment release, which is then partially eroded by the subsequent low water flows. The thickness of the sediment layer rapidly decreases with distance from the dam and, in the proximity of the confluence with the Ansiei river, almost all of the deposited sediments are washed out by the incoming water. The Ansiei river, whose catchment surface is about  $S_C = 200 \text{ km}^2$ , is intercepted by the Santa Caterina reservoir ( $V_R = 6.7 \cdot 10^6 \text{ m}^3$ ) and flows into the Piave river about 3.5 km downstream of the Comelico dam. Since the Ansiei river is not affected by flushing operations, the stream flow is characterized by clear water conditions and the sediment bed constitutes an armored layer of coarse material.

Information on cross-section geometries, bed elevations and the hydrological regime were collected and granulometric sampling was carried out [Giordan, 2006] in order to simulate the flushing operations performed in the alpine reservoir, along with the morphological evolution of the stream reach. The simulation was run over a period of 20 years, assuming a hypothetical hydrological regime with periodic flood events and with flushing operations occurring every two years [Fasolato *et al.*, 2007]. Results showed a slight degradation of the bed in the upper part of the stream reach. Downstream of the confluence, the channel was deeply incised, mainly by the clear water flows of the Ansiei river. The sediment removed from the reach bottom and delivered to the downstream artificial basin corresponds to approximately 15 - 20% of the annual sedimentation load of the reservoir, which causes progressive reduction of its storage capacity. Stabilizing the channel with bed sills represents a possible strategy for mitigating this loss of storage.

Based on the collected data, the stream reach can be approximated as a rectangular channel with the following characteristics: average width  $B = 30 \text{ m}$ , initial bed slope  $S_0 = 1.5\%$ , median sediment size  $D_{50} = 25 \text{ mm}$ , and grain size for which 90%

by weight of the sediment is finer  $D_{90} = 85$  mm. The design peak discharge is  $Q^* = 150$  m<sup>3</sup>/s. Assuming a uniformly-spaced distribution of bed sills with  $L = 100$  m, and clear-water conditions during the flood event, which represents the most severe condition for scouring, the percentage of scouring downstream of any bed sill with respect to the maximum potential (equilibrium at peak flow) scour depth is dependent on the duration of the flood event, which can be controlled by managing the release of water through the gates of the dam. The equilibrium bed slope,  $S_{eq}^*$ , which is used in Eq. (5.1b) to estimate the potential volume eroded between two subsequent sills, can be calculated using:

$$\theta_c = \frac{S_{eq}^* \cdot h_{u,eq}^*}{\Delta D_{90}} \quad (5.14a)$$

$$Q^* = B \cdot \frac{1}{n} \cdot (h_{u,eq}^*)^{5/3} \cdot (S_{eq}^*)^{1/2} \quad (5.14b)$$

An appropriate sediment transport formula, e.g. the Meyer-Peter-Müller relation for bed load, is used for estimating the sediment transport capacity of the flow, i.e.:

$$Q'_s = Q_s = B \cdot 8 \cdot (\theta - \theta_c)^{3/2} \sqrt{g \Delta D_{50}^3} \quad (5.15)$$

where  $\theta$  is the dimensionless shear stress relevant to the peak flow rate and the initial bed slope. Once all parameters are given, the morphological time,  $T_{s,k}^* = T_{s,k}(t_p)$ , is dependent only on the peak flow rate  $Q^*$ , according to Eq. (5.4) and the associated text. In Figure 5.11, the ratio  $y_{s,1}(t_f)/y_s^*$  relevant to the first sill, which experiences the most severe scouring, is plotted as a function of the peak flow rate, for different durations of the flood hydrograph, ranging from 6 hours to 2 days. For a peak flow rate of 150 m<sup>3</sup>/s, it can be observed that for the shortest flood, corresponding to  $T_{hyd}/T_{s,1}^* = 3.9$ , the scour depth achieves about 70% of its potential value, while scouring fully develops for flood events lasting more than 2 days, for which  $T_{hyd}/T_{s,1}^* > 30$ . Using the present methodology, bed sills can thereby be correctly designed to avoid structure failure by knowing the hydrological regime of the stream reach, and taking into account that the predictive results for the first sill are conservative when applied to the subsequent sills.



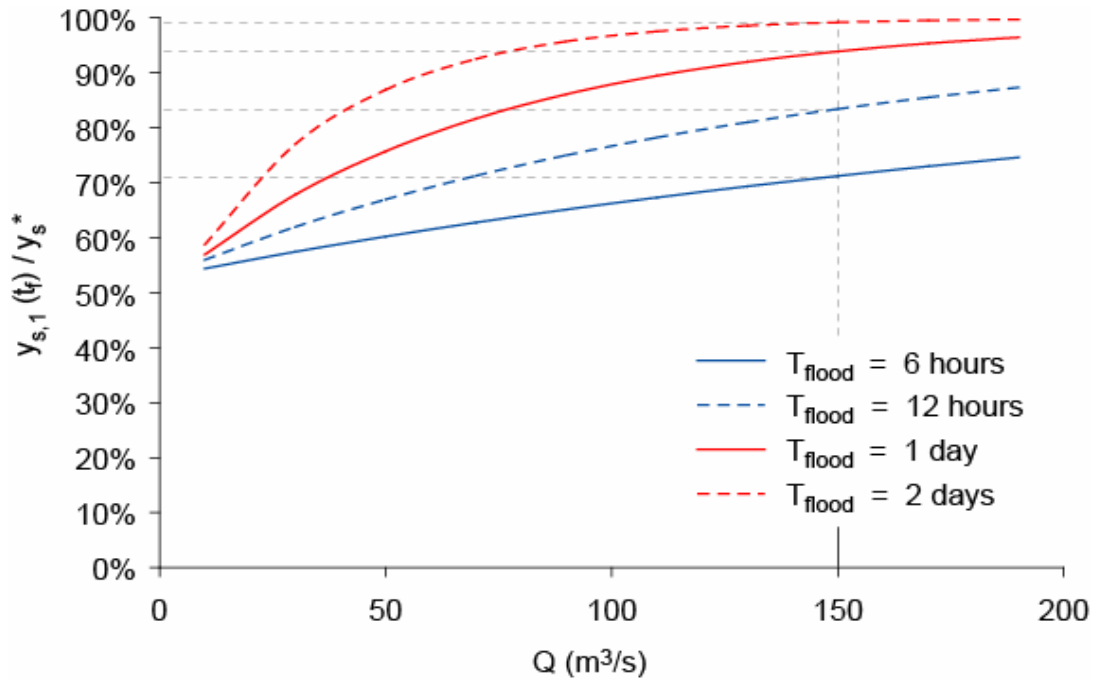


Figure 5.11 - Case study: percentage of scouring by flood events of different durations and peak flow rates.

## 5.7 CONCLUSIONS

This study has presented new experimental data on the temporal development of scour holes downstream of bed sills placed in steep gravel-bed streams when unsteady flows are considered. Initial examination of the data indicated that hydrograph shapes exist for which the local scour depth does not attain its potential depth, i.e. the maximum equilibrium scour depth associated with the peak rate of the flood event. Such flow hydrographs are identified herein as “flash floods”. The temporal trends of the scour development for these floods showed that scour continued deepening after the occurrence of the flood peak, though with a lower rate, and attained a final depth before the end of the flood. The percentage of the scouring in the case of these floods compared with the scouring occurring for steady “peak-discharge” flows varied between 70% and 98% for the range of the experimental conditions tested.

The results from steady-flow tests carried out in this study confirm the previous approach of *Gaudio and Marion* [2003], where the morphological time  $T_{s,k}$  was defined as the temporal scale for scour development. This scale could not be generalized to the

case of unsteady flows as  $T_{s,k}$  is a function of time that is dependent on the characteristics of the flood hydrograph. The morphological time relevant to the peak rate,  $T_{s,k}^*$ , was then introduced as a reasonable temporal scale for the simplified case of the triangular-shaped flood hydrographs presented in this paper. The use of this scale, however, did not allow the temporal scour-development trends to collapse along a unique curve. Instead, revising the original dimensional analysis by *Gaudio et al.* [2000], it was found that the ratio of the final scour depth to the maximum potential (equilibrium at peak flow) scour depth,  $y_{s,k}(t_f)/y_s^*$ , could be expressed as a function of the temporal ratio  $T_{hyd}/T_{s,k}^*$ , where a characteristic time for the flood hydrograph  $T_{hyd}$  is identified here with the peak time and  $T_s^*$  is the morphological time for the first of the series of sills. Data from twenty tests were plotted in dimensionless form showing a reasonable correspondence with this theoretical approach relating  $y_{s,k}(t_f)/y_s^*$  to  $T_{hyd}/T_{s,k}^*$ . The value  $T_{hyd}/T_{s,k}^* = 13.6$ , for which the scouring process was found to achieve 90% of its potential, was identified as a conservative threshold to provide a quantitative definition of what constitutes a flash flood (of reduced scour). This suggests that the flash flood nature of an event is dependent on both the characteristics of the flood event itself and the morphological and geometrical characteristics of the stream reach.

A case study, based on numerical simulations previously developed [*Fasolato et al.*, 2007] confirms the potential of a sequence of bed sills as a technique for mitigating reservoir sedimentation. The application shows that bed sills can be properly designed to avoid structure failure once the durations of the site flood hydrographs can be predicted.

---

## Notations

$A$	dimension matrix.
$A_F, A_{F'}$	area in the original and transformed Cartesian coordinates, $[L^2]$ .
$A_s, A_{s'}$	total and net local scour volume per unit width, $[L^2]$ .
$A_{s,nu}, A'_{s,nu}$	total and net local scour volume per unit width for non-uniform sediments, $[L^2]$ .
$A_{s,up}$	volume of sediment per unit width eroded upstream of the sequence of sills, $[L^2]$ .
$B$	channel (flume) width, $[L]$ .
$C_D$	friction (drag) coefficient.
$C_d$	diffusion coefficient of jets.
$C_u$	uniformity coefficient of sediments.
$D$	representative grain size of sediments, $[L]$ .
$D_m$	mean grain size of sediments, $[L]$ .
$D_s$	equivalent grain size of sediments, based on bed friction produced by non-uniform sediments, $[L]$ .
$D_x$	grain size for which $x\%$ (in weight) of sediments is smaller, $[L]$ .
$E_H$	$= S_0L$ potential energy which must be dissipated along the distance $L$ , $[L]$ .
$F, F'$	figures in the original and transformed Cartesian coordinates.
$F_1, F_2$	hydrostatic forces upstream and downstream of a control volume $[ML/T^2]$ .
$F_R$	Froude number.
$F_{R,jet}$	Froude number relevant to the jet characteristics.
$F_{R,jet}^*$	densimetric Froude Number relevant to the jet characteristics.
$G(y_s, x)$	shape function describing the shear stress exerted by diffusive jets for non horizontal boundary.
$H_s$	specific flow energy over the sill for steady flows, $[L]$ .
$H_s^*$	specific flow energy over the sill relevant to peak rate for unsteady flows, $[L]$ .
$K_1, K_2, K_3$	local scour hole shape coefficients.
$K_A$	bridge scour parameter for pier alignment.
$K_C$	bridge scour parameter for channel geometry.
$K_D$	bridge scour parameter for relative sediment size.
$K_{h-b}$	bridge scour parameter for relative size of flow depth and pier width, $[L]$ .
$K_S$	bridge scour parameter for bridge pier shape.
$K_q$	bridge scour parameter for flow intensity.
$L_1, L_2, L_3$	longitudinal distance between sills in the experiments, $[L]$ .
$L, L'$	longitudinal distance between sills in a sequence of uniformly spaced bed sills, $[L]$ .
$L_{lim}$	longitudinal distance between sills over which scour similarity occurs, $[L]$ .
$N$	number of tests.

---

$Q$	flow rate, [L <sup>3</sup> /T].
$Q^*, Q_{max}$	peak flow rate, [L <sup>3</sup> /T].
$Q_s$	sediment transport capacity of the flow, [L <sup>3</sup> /T].
$Q'_s$	net sediment transport, [L <sup>3</sup> /T].
$Q_{s,in}$	upstream sediment supply, [L <sup>3</sup> /T].
$R_E$	Reynolds number.
$R_E^*$	grain Reynolds Number.
$R_{E,jet}$	Reynolds number relevant to the jet characteristics.
$R_{wall}$	jet diffusion boundary parameter accounting for molecular and turbulent viscosity.
$S_0$	initial bed slope.
$S_{eq}$	equilibrium bed slope for steady flows.
$S_{eq}^*$	equilibrium bed slope relevant to peak rate for unsteady flows.
$S_{eq,i}$	measured equilibrium bed slope at each reach.
$SI$	sorting index.
$T_{hyd}$	hydrological time, [T].
$T_s$	morphological time for steady flows, [T].
$T_{s,1}, T_{s,2}$	first and second sill morphological time for steady flows, [T].
$T_{s,k}$	$k$ -th sill morphological time for steady flows, [T].
$T_{s,1}^*, T_{s,2}^*$	first and second sill morphological time relevant to the peak rate for unsteady flows, [T].
$T_{s,k}^*$	$k$ -th sill morphological time relevant to the peak rate for unsteady flows, [T].
$T_R$	return period for extreme flood events, [T].
$U_0$	mean flow velocity downstream of hydraulic structures, [L/T].
$U_c$	mean critical flow velocity, [L/T].
$U_{jet}$	velocity of jet entering the water at hydraulic structures, [L/T].
$V_{g,i}$	volume of sediment eroded between the $i$ -th sill and the subsequent one, [L <sup>3</sup> ].
$V_{g,k}$	volume of sediment eroded between the first and the $k$ -th sill, [L <sup>3</sup> ].
$V_{g,up}$	volume of sediment eroded upstream of the sequence of sills, [L <sup>3</sup> ].
$V_R$	reservoir capacity, [L <sup>3</sup> ].
$V_s, V'_s$	total and net local scour volume, [L <sup>3</sup> ].
$X, Y$	Cartesian coordinates, [L].
$X', Y'$	transformed Cartesian coordinates, [L]
$\tilde{X}, \tilde{Y}$	dimensionless scale factor for scour hole profiles.
$Z$	product of power of physical variables in dimensional analysis.
$a_1$	morphological jump for steady flows, [L].
$a_1^*$	morphological jump relevant to peak rate for unsteady flows, [L].
$a_D$	drop between the crest of the structure and the bottom of the bed level, [L].
$a_H$	head drop from upstream to downstream water levels at hydraulic structures, [L].

---

$b_A, b_P$	width of bridge abutment/pier, [L].
$c_H$	empirical coefficient for horizontal two-dimensional jets.
$c_V$	empirical coefficient for vertical two-dimensional jets.
$d$	coefficient for sediment transport formulae based on Shields' mobility parameter.
$e$	exponent for sediment transport formulae based on Shields' mobility parameter.
$f_1, f_2$	local scour shape functions.
$f_x, f_y$	local scour length and depth functions.
$f_z$	generic function of the physical variables $z_i$ .
$f_{\pi}, f_{\pi,1}$	generic function of the dimensionless parameters $\pi_i$ .
$g$	acceleration due to gravity, [L/T <sup>2</sup> ].
$h_0$	tailwater depth downstream of hydraulic structures, [L].
$h_{jet}$	thickness of the jet entering the water depth at hydraulic structures, [L].
$h_{u,0}^*$	initial normal depth relevant to peak rate for unsteady flows, [L].
$h_{u,eq}$	equilibrium normal depth for steady flows, [L].
$h_{u,eq}^*$	equilibrium normal depth relevant to peak rate for unsteady flows, [L].
$k$	integer indicating the position from upstream of a sill along a sequence of uniformly spaced bed sills.
$k_c$	scour coefficient depending on the material properties forming the scour hole.
$k_{ij}$	physical variable exponents depending on dimension coefficients $\alpha_{ij}$ .
$l_A, l_P$	length of bridge abutment/pier, [L].
$l_a$	length of bed protection (apron) downstream of hydraulic structures, [L].
$l_d$	longitudinal distance from the sill at the point of the deepest scouring, [L].
$l_{jet}$	diffusion length of jets at the equilibrium stage, [L].
$l_s$	scour hole length, [L].
$l_{s,nu}$	scour hole length for non-uniform sediments, [L].
$m$	number of scour holes.
$n$	Manning's roughness coefficient, [T/L <sup>1/3</sup> ].
$p$	= $(s - r)$ number of independent dimensionless parameters, $\pi_i$ , in dimensional analysis.
$q$	flow rate per unit width, [L <sup>2</sup> /T].
$q^*, q_{max}$	peak flow rate per unit width, [L <sup>2</sup> /T].
$q_s$	sediment transport capacity per unit width, [L <sup>2</sup> /T].
$q_s^*$	sediment transport capacity per unit width relevant to peak rate for unsteady flows, [L <sup>2</sup> /T].
$q_s'$	= $(q_s - q_{s,in})$ net sediment transport capacity per unit width, [L <sup>2</sup> /T].
$q_{s,in}$	upstream sediment supply per unit width, [L <sup>2</sup> /T].
$r$	number of independent fundamental physical dimensions, $\Omega_i$ , in dimensional analysis.

---

$s$	number of physical variables, $z_i$ , in dimensional analysis.
$t$	time, [T].
$t_\xi$	characteristic time at which $y_s(t) = y_\xi$ , [T].
$t_f$	total duration of the flood hydrograph, [T].
$t_p$	time at which the flood peak occurs, [T].
$u(x)$	maximum velocity of diffusive jets, [L].
$u(x,y)$	velocity flow-field of diffusive jets, [L].
$u^*$	shear velocity, [L/T].
$u_c^*$	critical shear velocity, [L/T].
$v$	mean flow velocity, [L/T].
$v^*$	mean flow velocity relevant to peak rate for unsteady flows, [L/T].
$v_x, v_y$	components of the velocity of the jet, [L/T].
$w$	parametric coefficient for dimensionless temporal parameters accounting for unsteady flow conditions.
$w_1, w_2$	calibration coefficients for dimensionless temporal parameters accounting for unsteady flow conditions.
$x, y, y'$	total and net scour hole coordinates, [L].
$x^*, y^*$	dimensionless scour hole coordinates.
$\tilde{x}, \tilde{y}$	dimensional scale factor for scour hole profiles, [L].
$y_s$	maximum scour depth with respect to the initial bed for steady flows, [L].
$y_s'$	maximum scour depth with respect to the equilibrium bed for steady flows, [L].
$y_s^*$	maximum scour depth with respect to the initial bed relevant to the peak rate for unsteady flows, [L].
$y_s(t)$	maximum scour depth with respect to the initial bed at the time $t$ , [L].
$y_{s,1}(t), y_{s,2}(t)$	first and second sill maximum scour depth at the time $t$ , [L].
$y_{s,1}(t_f), y_{s,2}(t_f)$	first and second maximum scour depth at the completion of the flood, [L].
$y_{s,k}(t)$	$k$ -th sill maximum scour depth at the time $t$ , [L].
$y_{s,k}(t_f)$	$k$ -th sill maximum scour depth at the completion of the flood, [L].
$y_{s,i}$	maximum scour depth with respect to the initial bed for interfering sills, [L].
$y'_{s,i}$	maximum scour depth with respect to the equilibrium bed for interfering sills, [L].
$y_{s,nu}$	maximum scour depth with respect to the initial bed for non-uniform sediments, [L].
$y'_{s,nu}$	maximum scour depth with respect to the equilibrium bed for non-uniform sediments, [L].
$y_{se}$	maximum scour depth occurring at standard-geometry structures, [L].
$y_\xi$	characteristic length scale for time development of scouring, [L].
$z_i$	generic physical variables in dimensional analysis.

---

$\Delta$	relative submerged density of sediments.
$\Phi_1, \Phi_2, \Phi_3$	dimensionless function depending on the drop ratio.
$\Phi_L$	dimensionless function accounting for geometric interference.
$\Phi_{SI}$	dimensionless function accounting for sediment gradation.
$\Phi_T$	dimensionless function accounting for time development for steady flows.
$\Phi_x, \Phi_y, \Phi_{xy}$	dimensionless maximum scour length, depth, and length to depth ratio.
$\Phi_\Psi$	dimensionless function accounting for unsteady flow conditions.
$\Psi_1, \Psi_2, \Psi_3$	dimensionless temporal parameters accounting for unsteady flow conditions.
$\Omega_i$	fundamental physical unit in dimensional analysis.
$\alpha$	exponent of the power-law representation for an incomplete self-similarity.
$\alpha_{A,d}, \alpha_{A,u}$	downstream and upstream angle of the wing-walls at abutments.
$\alpha_{i,j}$	coefficients of the dimension matrix $A$ .
$\alpha_x, \alpha_y$	calibration coefficients for the effect of sediment gradation on scour length and depth.
$\beta_{A,n}, \beta_{A,s}$	nose and side slope angle at abutments.
$\beta_i$	physical unit exponents in dimensional analysis.
$\beta_x, \beta_y$	calibration coefficients for the effect of geometrical interference on scour length and depth.
$\gamma_s$	specific weight of sediments, [F/L <sup>3</sup> ].
$\gamma_s'$	specific submerged weight of sediments, [F/L <sup>3</sup> ].
$\gamma_w$	specific weight of water, [F/L <sup>3</sup> ].
$\gamma_x, \gamma_y$	calibration coefficients for the temporal development of scour length and depth.
$\delta(x)$	thickness of diffusive jets, [L].
$\varepsilon_{max}$	max relative error.
$\varepsilon_{mean}$	mean relative error.
$\varepsilon_{Seq}$	$= 1/N \cdot \sum_i  S_{eq,i} - S_{eq}  / S_{eq}$ , mean relative error for measured equilibrium bed slopes.
$\zeta$	calibration coefficient of velocity scale for jet diffusion.
$\eta$	calibration coefficient of thickness scale for jet diffusion.
$\theta$	Shields' mobility parameter .
$\theta_c$	critical Shields' mobility parameter .
$\lambda_i$	exponents of physical variables in dimensional analysis.
$\lambda_{a1}$	dimension exponent for morphological jump.
$\lambda_D$	dimension exponent for grain size.
$\lambda_g$	dimension exponent for gravity.
$\lambda_q$	dimension exponent for flow rate.
$\lambda_y$	dimension exponent for scour depth.
$\lambda_\nu$	dimension exponent for kinematic viscosity.
$\lambda_{\rho s}$	dimension exponent for density of sediments.

---

$\lambda_{\rho_w}$	dimension exponent for density of water.
$\nu$	kinematic viscosity of water, [L <sup>2</sup> /T].
$\xi$	calibration coefficient for time development of scouring.
$\xi_c$	Egiazaroff (critical shear stress) coefficient for non-uniform sediments.
$\pi_i$	generic dimensionless parameters in dimensional analysis.
$\pi_{a1}$	dimensionless parameter accounting for morphological jump.
$\pi_D$	dimensionless parameter accounting for grain size.
$\pi_y$	dimensionless parameter accounting for scour depth.
$\pi_\nu$	dimensionless parameter accounting for kinematic viscosity.
$\pi_\rho$	dimensionless parameter accounting for density of sediments.
$\rho(Z), \rho(z_i)$	numerical values of physical variables in dimensional analysis.
$\rho_s$	density of sediments, [M/L <sup>3</sup> ].
$\rho_s'$	= ( $\rho_s - \rho_w$ ) submerged density of sediments, [M/L <sup>3</sup> ].
$\rho_w$	density of water, [M/L <sup>3</sup> ].
$\sigma_g$	geometric standard deviation for log-normal distribution.
$\sigma_u$	standard deviation for vertical distribution of velocities, [L/T].
$\tau_c$	critical shear stress for flat sediment beds, [F/L <sup>2</sup> ].
$\tau_{jet}$	shear stress exerted by diffusive jets, [F/L <sup>2</sup> ].
$\varphi_{jet}$	angle of jet impact to the horizontal plane.
$\varphi_{scour}$	angle of the downstream side of the scour hole to the horizontal plane.
$\varphi_{sed}$	angle of repose of sediments.
$\varphi_{stuct}$	angle of the downstream side of the structure to the horizontal plane.
$\chi$	= ( $\eta - \zeta$ ), calibration coefficient of scaling for jet diffusion.
$\psi$	global calibration coefficient of scaling for jet diffusion.
$\omega$	coefficient taking into account the relative turbulence intensity.
$\omega_i, \omega_Z$	fundamental and derived physical units in dimensional analysis.



---

## References

- Adduce, C., and G. Sciortino, (2006), Scour due to a horizontal turbulent jet: Numerical and experimental investigation, *J. Hydraul. Res.*, 44(5), 663-673.
- Aderibigbe, O., and N. Rajaratnam (1998), Effect of sediment gradation on erosion by plane turbulent wall jets, *J. Hydraul. Eng.*, 124(10), 1034-1042.
- Akashi, N., and T. Saitou, (1986). Influence of water surface on scour from vertical submerged jets, *J. Hydrosc. Hydr. Eng.*, 55-69.
- Andrews, E. D., and Parker, G. (1987), Formation of a coarse surface layer as the response to gravel mobility, in *Sediment Transport in Gravel Bed Rivers*, edited by C. R. Thorne, J. C. Bathurst, R. D. Hey, pp. 269-325, John Wiley, Hoboken, N. J.
- Ashida, K., and M. Michiue (1971), An investigation of river bed degradation downstream of a dam, *Proc. 14<sup>th</sup> Int. Association of Hydraulic Research Congress*, IAHR, Paris, France, 31 July - 3 Sept.
- Albertson, M. L., Y. B. Dai, R. A. Jensen, and H. Rouse (1950), Diffusion of submerged jets, *Trans. Am. Soc. Civ. Eng.*, 115(2409), 639-697.
- Altinbilek, H. D., and Y. Basmaci, (1973), Localized scour at downstream of outlet structures, *Proc. 11<sup>th</sup> Int. Congress on Large Dams*, ICOLD, Madrid, Spain, 11-15 June.
- Armanini, A. (2005), *Principi di idraulica fluviale*, 207pp., BIOS, Cosenza, Italy (in Italian).
- Barenblatt, G.I. (1996), *Scaling, Self-Similarity, and Intermediate Asymptotics*, 386pp., Cambridge University Press, Cambridge, UK.

- 
- Beltaos, S., and N. Rajaratnam, (1973), Plane turbulent impinging jets, *J. Hydraul. Res.*, *1*(1), 29-59.
- Bennett, S. J., C. V. Alonso, S. N. Prasad, and M. J. M. Romkens, (2000), Experiments on headcut growth migration in concentrated flows typical of upland areas, *Water Resour. Res.*, *36*(7), 1911-1922, doi: 10.1029/2000WR900067.
- Bormann, N., and P. Y. Julien (1991), Scour downstream of grade-control structures, *J. Hydraul. Eng.*, *117*(5), 579-594.
- Breusers, H. N. C (1967), Time scale of two-dimensional local scour, *Proc. 12<sup>th</sup> Int. Ass. of Hydraul. Eng. and Res. Congress*, IAHR, Fort Collins, Colorado, 11-14 Sept.
- Breusers, H. N. C, and A. J. Raudkivi (1991), *Scouring. Hydraulic Structures Design Manual*, 143pp., A. A. Balkema, Brookfield, Vt.
- Buckingham, E. (1914), On physically similar systems; illustrations of the use of dimensional equations, *Phys. Rev.*, *4*, 345-376.
- Cardoso A. H., and R. Bettess (1999), Effects of time and channel geometry on scour at bridge abutments, *J. Hydraul. Eng.*, *125*(4), 388-399.
- Chatterjee, S. S., and S. N. Ghosh, (1980). Submerged horizontal jet over erodible bed, *J. Hydraul. Div.*, *106*(11), 1765-1782.
- Chatterjee S. S., S. N. Ghosh, and M. Chatterjee (1994), Local scour due to submerged horizontal jets, *J. Hydraul. Eng.*, *120*(8), 973-992.
- Chin, A. (1999), The morphologic structure of step-pools in mountain streams, *Geomorphology*, *27*, 191-204.
- Coleman, S. E., C. S. Lauchlan, and B.W. Melville (2003), Clear-water scour development at bridge abutments, *J. Hydraul. Res.*, *41*(5), 521-531.

- 
- Comiti, F. (2003), Local scouring in natural and artificial step-pool systems, Ph.D. Thesis, 210pp., University of Padua, Padua, Italy.
- Comiti, F., M. A. Lenzi, and A. Marion (2001), Interference of erosion-control structure in mountain streams, *Proc. 3<sup>rd</sup> Int. Symposium on Environmental Hydraulics*, IAHR, Tempe, Ariz., 5-8 Dec.
- D'Agostino, V. (1994), Indagine sullo scavo a valle di opere trasversali tramite modello a fondo mobile, *Energ. Elettr.*, 71(2), 37-51 (in Italian).
- Dey S. H., and R. V. Barbhuiya (2005), Time Variation of Scour at Abutments, *J. Hydraul. Eng.*, 131(1), 11-23.
- Dey S. H., and R. V. Raikar (2007), Scour below a High Vertical Drop, *J. Hydraul. Eng.*, 133(5), 564-568.
- Dey, S., and A. Sarkar (2006), Scour downstream of an apron due to submerged horizontal jets, *J. Hydraul. Eng.*, 132(3), 246-257.
- Dey, S., and B. Westrich (2003), Hydraulics of submerged jet subject to change in cohesive bed geometry, *J. Hydraul. Eng.*, 129(1), 44-53.
- De Vries (1975), A morphological time scale for rivers, *Proc. 16<sup>th</sup> Int. Ass. of Hydraul. Eng. and Res. Congress*, IAHR, Sao Paulo, Brazil, 27 July - 3 Aug.
- Farhoudi, J. and K. V. H. Smith, (1982), Time scale for scour downstream of hydraulic jump. *J. Hydraul. Div.*, 108(10), 1147-1162.
- Farhoudi, J., and K.V.H. Smith (1985), Local scour profiles downstream of hydraulic jump, *J. Hydraul. Res.*, 23(4), 343-358.
- Fasolato, G., P. Ronco, and Y. Jia (2007), Studies on sediment transport and morphodynamic evolution of a river due to sediment flushing operations of an

- 
- alpine reservoir, *Proc. 32<sup>nd</sup> Int. Association of Hydraulic Research Congress*, IAHR, Venice, Italy, 1-6 July.
- Gaudio, R., A. Marion, and V. Bovolin (2000), Morphological effects of bed sills in degrading rivers, *J. Hydraul. Res.*, 38(2), 89-96.
- Gaudio, R., and A. Marion (2003), Time evolution of scouring downstream of bed sills, *J. Hydraul. Res.*, 41(3), 271-284.
- Giacometti, L. (2000), Indagine sperimentale sullo scavo a valle di opera trasversali in alvei a media e alta pendenza, Ph.D. Thesis, 190pp., University of Padua, Padua, Italy (in Italian).
- Giordan, G. (2006), Osservazione della dinamica dei sedimenti su un corso d'acqua alpino: il Piave tra la diga di Comelico e la confluenza con il torrente Ansiei, M.S. Thesis, 99pp., University of Padua, Padua, Italy (in Italian)
- Habib, E., M. Mossa, and A. Petrillo (1994), Scour downstream of hydraulic jump, *Proc. Modelling, Testing & Monitoring for Hydro PowerPlants Conference*, Hydropower and Dams, Budapest, Hungary, 11-13 July.
- Hassan, N. M. K., and R. Narayanan, (1985). Local scour downstream of an apron, *J. Hydraul. Eng.*, 111(11), 1371-1385.
- Hjelmfelt A., and M. Wang (1994), General stochastic unit hydrograph, *J. Irrig. and Drain. Eng.*, 41(3), 271-284.
- Hoffmans, G. J. C. M. (1998), Jet scour in equilibrium phase, *J. Hydraul. Eng.*, 124(4), 430-437.
- Hoffmans, G. J. C. M., and K. W. Pilarczyk (1995), Local scour downstream of hydraulic structures, *J. Hydraul. Eng.*, 121(4), 326-339.

- 
- Hoffmans, G. J. C. M., and H. J. Verheij (1997), *Scour Manual*, 205pp., A. A. Balkema, Brookfield, Vt.
- Hogg, A. J., H. E. Huppert, and W. B. Dade (1997), Erosion by planar turbulent jet, *J. Fluid. Mech.*, 338, 317-340.
- Jia Y., S. N. Kitamura, and S. S. Y. Yang (2001), Simulation of scour process in plunging pool of loose bed-material, *J. Hydraul. Eng.*, 127(3), 219-229.
- Kobus, H., P. Leister, and B. Westrich (1979), Flow field and scouring effects of steady and pulsating jets impinging on a movable bed. *J. Hydraul. Res.*, 17, 175-192.
- Lambe, T.W., and R.V. Whitman (1969), *Soil Mechanics*, 576pp. JohnWiley, Hoboken, N. J.
- Lenzi, M. A. (2001), Step-pool evolution in the Rio Cordon, Northeastern Italy, *Earth Surf. Process. Landforms*, 26, 991–1008.
- Lenzi M. A. (2002), Stream bed stabilization using boulder check dams that mimic step-pool morphology features in Northern Italy, *Geomorphology*, 45, 243-260.
- Lenzi M. A, and F. Comiti (2003), Local scouring and morphological adjustments in steep channels with check-dam sequences, *Geomorphology*, 55, 97-109.
- Lenzi, M. A., A. Marion, F. Comiti, and R. Gaudio (2002), Local scouring in low and high gradient streams at bed sills, *J. Hydraul. Res.*, 40(6), 731-739.
- Lenzi, M. A., A. Marion, and F. Comiti (2003a), Local scouring at grade-control structures in alluvional mountain rivers, *Water Resour. Res.*, 39(7), 1176, doi:10.1029/2002WR001815.
- Lenzi, M. A., A. Marion, and F. Comiti (2003b), Interference processes on scouring at bed sills, *Earth Surf. Process. Landforms*, 28(1), 99-110.

- 
- Lunardi S. (2002), Indagine sperimentale presso il torrente Cordevole sullo scavo a valle di soglie di fondo: aspetti sedimentologici e geometrici, M.S. Thesis, University of Padua, Padua (in Italian).
- Marion, A., R. Gaudio, and V. Bovolin (1998), Scour downstream of bed sills, *Res. Rep. TR70*, HR Wallingford, Wallingford, UK.
- Marion, A., M. A. Lenzi, and F. Comiti (2004), Prediction of scour depth with geometrical interference in high gradient streams, *Earth Surf. Process. Landforms*, 29, 983-993.
- Martin Vide J. P., and A. Andreatta (2006), Disturbance caused by bed sills on the slopes of steep streams, *J. Hydraul. Eng.*, 132(11), 1186-1194.
- Mason, P. J. (1989), Effects of air entrainment on plunge pool scour, *J. Hydraul. Eng.*, 115(3), 385-399.
- Mason, P. J., and K. Arumugam (1985), Free jet scour below dams and flip buckets, *J. Hydraul. Eng.*, 111(2), 220-235.
- Meftah, M. B., and M. Mossa (2006), Scour holes downstream of bed sills in low-gradient channels, *J. Hydraul. Res.*, 44(4), 497-509.
- Melville, B. W. (1992), Local scour at bridge abutments, *J. Hydraul. Eng.*, 118(4), 615-631.
- Melville, B. W. (1995), Bridge abutment scour in compound channels, *J. Hydraul. Eng.*, 121(12), 863-868.
- Melville, B. W., (1997). Pier and abutment scour: integrated approach, *J. Hydraul. Eng.*, 123(2), 125-136.
- Melville, B. W., and Y. M. Chiew (1999), Time scale for local scour at bridge piers, *J. Hydraul. Eng.*, 125(1), 59-65.

- 
- Melville, B. W., and Sutherland, A. I. (1988), Design method for local scour at bridge piers. *J. Hydraul. Eng.*, 114(10), 1210-1226.
- Meyer-Peter, E. and R. Muller (1948), Formulas for bed load transport. *Proc. 2<sup>nd</sup> Int. Ass. of Hydraul. Eng. and Res. Congress*, IAHR, Stockholm, Sweden.
- Mohamed, M. S., and J. A. McCorquodale, (1992), Short term local scour, *J. Hydraul. Res.*, 30(5), 685-699.
- Morris, G. L., and J. Fan (1998), *Reservoir Sedimentation Handbook*, 746pp., McGraw-Hill, New York.
- Proffitt, G. T., and A. J. Sutherland (1983), Transport of non-uniform sediments, *J. Hydraul. Res.*, 21(1), 33-43.
- Rajaratnam, N. (1976), *Turbulent jets*, 304pp., Elsevier Scientific Publishing Co., Amsterdam and New York.
- Rajaratnam, N. (1981), Erosion by plane turbulent jets, *J. Hydraul. Res.*, 19(4), 339-358.
- Raudkivi, A. I. (1986), Functional trends of scour at bridge piers, *J. Hydraul. Eng.*, 112(1), 1-13.
- Sarkar, A., and S. Dey (2004), Review on local scour due to jets, *Int. J. Sediment Res.*, 19(3), 210-238.
- Sarkar, A., and S. Dey (2005), Scour hole downstream of aprons caused by sluices, *Water Management*, 158(2), 55-64.
- Schlichting, H. (1979), *Boundary-layer theory*, 817pp., McGraw-Hill, New York.
- Struiksmma, N., K. W. Olsen, C. Flokstra, and H. J. De Vriend (1985), Bed deformation in curved alluvial channels, *J. Hydraul. Res.*, 23(1), 57-79.
- Schoklitsch, A. (1932), Kolkbildung unter Überfall-strahlen. Die Wasserwirtschaft.

- 
- Schoklitsch, A. (1932), Prevention of scour and energy Dissipation. Translated from German by E. F. Wilsey, USBR.
- Shields, A. (1936), Application of the similarity principles and turbulence research to bedload movement, *Res. Rep. No. 167*, California Institute of Technology, Pasadena, (translated from German).
- Shvidchenko, A. B., and G. Pender (2000), Flume study of the effect of relative depth on incipient motion of coarse sediments, *Water Resour. Res.*, 36(2), 619–628, doi:10.1029/1999WR900312.
- Stein, O. R., and P. Y. Julien (1994), Sediment concentration below free overfall, *J. of Hydraul. Eng.*, 120(9), 1044-1053.
- Stein, O. R., P. Y. Julien, and C. V. Alonso (1993), Mechanics of jet scour downstream of a headcut, *J. Hydraul. Res.*, 31(6), 723-738.
- Surian, N. (1999), Channel changes due to river regulation: the case of the Piave River, Italy, *Earth Surf. Process. Landforms*, 24, 1135-1151.
- Van der Meulen, T., and H. J. Vinjé (1975), Three-dimensional local scour in non-cohesive sediments, *Proc. 16th Int. Ass. of Hydraul. Eng. and Res. Congress*, IAHR, Sao Paulo, Brazil, 27 Jul. - 3 Aug.
- Whittaker, J. G. (1987), Sediment transport in step-pool streams, in *Sediment Transport in Gravel Bed Rivers*, edited by C. R. Thorne, J. C. Bathurst, R. D. Hey, pp. 545-570, John Wiley, Hoboken, N. J.
- Whittaker, J. G., and M. N. R. Jaeggi (1982), Origin of step-pool systems in mountain streams, *J. of Hydraul. Div.*, 108(HY6), 758-773.
- Whittaker, J. G., and A. Schleiss (1984), Scour related to energy dissipators for high head structures, Mitt. Nr. 73 VAW/ETH, Zurich.



- 
- Wilcock, P. R., and J. C. Crowe (2003), Surface-based transport model for mixed-size sediment, *J. Hydraul. Eng.*, 129(2), 120-128.
- Wohl, E. E., S. Madsen, and L. MacDonald (1997), Characteristics of log and clast bed-steps in step-pool streams of northwestern Montana, USA, *Geomorphology*, 20, 1-10.
- Yen, C. L. (1987), Discussion on “Free jet scour below dams and flip buckets” by Mason and Arumugam, *J. Hydraul. Eng.*, 113(9), 1200-1202.
- Yue S., T. B. M. J. Ourada, B. Bobée, P. Legendre, and P. Bruneau (2002), Approach for describing statistical properties of flood hydrograph, *J. Hydrol. Eng.*, 7(2), 147-153.
- Yuen, E. M. (1984). Clear water scour by high velocity jets, M.S. Thesis, University of Windsor, Windsor, Ontario.